ROZPRAWA DOKTORSKA

Droplet microfluidic systems for formation and studies of lipid bilayers

Magdalena Anna Czekalska

Advisor: Prof. dr hab. Piotr Garstecki

The dissertation was prepared within the International PhD Studies at the
Institute of Physical Chemistry of the Polish Academy of Sciences
ul. Kasprzaka 44/52, 01-224 Warsaw

Warsaw, April 2019

Acknowledgements

I would like to acknowledge the supervisor of my doctoral studies – prof. Piotr Garstecki – for giving me the opportunity to work in his laboratory, for providing necessary means to conduct my research and for advice.

I am very grateful to researchers who were my co-workers during my doctoral projects:

- Tomasz Kamiński for his input and help with the experiments in all the projects,
- Sławek Jakieła for developing software for automated systems,
- Michał Horka for developing the model of electric circuit,
- Karol Makuch for analyzing the diffusion data.

I would like to thank foreign collaborators:

- prof. Hagan Bayley and dr Tanuj Sapra from Oxford University and other members of Chemical Biology group (especially dr Gokce Su Pulcu and Ellina Mikhailova) for hosting me in the laboratory and for training on to the techniques of droplet interface bilayers, electrophysiology and alpha-hemolysin purification,
- prof. Tuomas Knowles and members of his group from University of Cambridge for hosting me during the final year of my doctoral studies.

Many thanks to the current and former members of the Group of Microfluidics and Complex Fluids and the Department of Soft Condensed Matter for their help with my research and interesting scientific discussions and comments. I especially thank Laci Derzsi, Justyna Gruszka, Joanna Smyda, Olgierd Cybulski, Paweł Jankowski, Jan Guzowski, Witold Postek, Łukasz Kozoń, Adam Opalski, Patryk Adamczuk, Karol Patyrak, Piotr Pawlicki and Bogdan Dąbrowski.

Składam najserdeczniejsze podziękowania dla mojego Narzeczonego Tomasza, Rodziców, Babci i Rodzeństwa za wsparcie okazane w czasie studiów doktoranckich.

Acknowledgements for funding

The research presented in this dissertation was supported by the following projects:

1) Author obtained the funds for the preparation of the doctoral dissertation from the National Science Centre within the ETIUDA scholarship on the basis of the decision number 2017/24/T/ST4/00334.

2) Research was co-funded by Starting Grant 279647 *"Microfluidic Combinatorial on Demand Systems: a Platform for High-Throughput Screening in Chemistry and Biotechnology"* financed by European Research Council.

3) Research was co-funded by Symfonia 2014/12/W/NZ6/00454 project "The role of antimicrobial protein-chemerin in skin pathophysiology." within Symfonia 2 Programme of National Science Centre.

4) Research was co-funded by TEAM-TECH/2016-2/10 project *"BacterOMIC - development of systems for comprehensive information on antibiotic susceptibility of bacteria."* within TEAM-TECH Programme of Foundation for Polish Science, co-financed by the European Union within the European Regional Development Fund, through the Innovative Economy Operational Programme.

5) This work was partially performed in the NanoFun laboratories co-financed by the European Regional Development Fund Project POIG.02.02.00-00-025/09.

List of publications and patent applications

Publications related to the topic of the dissertation:

1) **Czekalska MA**, Kaminski TS, Jakiela S, Sapra Tanuj K, Bayley H, Garstecki P. *A droplet microfluidic system for sequential generation of lipid bilayers and transmembrane electrical recordings*, Lab on a Chip, 2015, 15(2), 541-548

2) **Czekalska MA**, Kaminski TS, Jakiela S, Horka M, Garstecki P. *An automated microfluidic system for generation of Droplet Interface Bilayers networks*, Micromachines, 2017, 8(3), 93

3) **Czekalska MA**, Kaminski TS, Makuch K, Garstecki P. *Passive and parallel microfluidic formation of droplet interface bilayers (DIBs) for measurement of leakage of small molecules through artificial phospholipid membranes*, Sensors and Actuators B: Chemical 2019, 286, 258-265

Other publications:

1) Kaminski TS, Jakiela S, **Czekalska MA**, Postek W, Garstecki P, *Automated generation of libraries of nL droplets*, Lab on a Chip, 2012, 12, 3995-4002

Patents and patent applications:

1) **Czekalska MA,** Kamiński TS, Garstecki P. *Microfluidic system, in particular for automated generation of phospholipid bilayers and testing of membrane protein activity.* Finnish Patent (FI 125616) granted on 15 December 2015

2) **Czekalska MA,** Kamiński TS, Garstecki P. *Mikroprzepływowy układ zwłaszcza do automatycznego tworzenia dwuwarstw fosfolipidowych i badania aktywności białek błonowych.* Polish Patent P-405321 granted on 31 October 2016.

3) Kaminski TS, **Czekalska MA**, Garstecki P. S*posób automatycznego tworzenia dwuwarstw fosfolipidowych i/lub badania aktywności białek błonowych i/lub regulacji stężenia białek błonowych.* Polish patent P-405819 granted on 30 November 2016.

4) Kaminski TS, **Czekalska MA**, Garstecki P. *Mikroprzepływowy układ zwłaszcza do automatycznego tworzenia dwuwarstw fosfolipidowych i badania aktywności białek błonowych.* Polish patent P-410696 granted on 31 May 2017.

Contributions

This dissertation comprises the experimental results of four research projects. Three of them ended with per-reviewed publications. I am the first author or co-first author of the three publications:

1) **Czekalska MA**, Kaminski TS, Jakiela S, Sapra K Tanuj, Bayley H, Garstecki P. *A droplet microfluidic system for sequential generation of lipid bilayers and transmembrane electrical recordings*, Lab on a Chip, 2015, 15(2), 541-548

Main contribution: MC and TK together conceived the idea for the project. MC and TK developed the initial version of the system. MC optimized the architecture of microfluidic system and conducted electrophysiological experiments. MC and TK together analyzed and interpreted the results and wrote the manuscript. SJ developed automated system and KTS participated in the design of experiments and writing of manuscript.

2) **Czekalska MA**, Kaminski TS, Jakiela S, Horka M, Garstecki P. *An automated microfluidic system for generation of Droplet Interface Bilayers networks*, Micromachines, 2017, 8(3), 93

Main contribution: MC conceived the idea for the project. MC developed the architecture of microfluidic system and conducted electrophysiological experiments. MC interpreted the results based on model developed by SJ and MH and wrote the manuscript.

3) **Czekalska MA**, Kaminski TS, Makuch K, Garstecki P. *Passive and parallel microfluidic formation of droplet interface bilayers (DIBs) for measurement of leakage of small molecules through artificial phospholipid membranes*, Sensors and Actuators B: Chemical 2019, 286, 258-265

Main contribution: MC conceived the idea for the project and optimized the architecture of microfluidic system with the help from TK. MC conducted the experiments. MC interpreted the results based on model developed by KM and wrote the manuscript.

All results included in this dissertation are presented with the consent of all of the co-authors. All projects were conducted under the guidance of prof. Piotr Garstecki – the supervisor of my doctoral studies.

List of symbols and abbreviations

Ca	capillary number
C_T	capacitance
D	mass diffusivity, diffusion coefficient
I_C	capacitive current
IC_{50}	half maximal inhibitory concentration
K_d	dissociation constant
k_{on}	association rate constant
k_{off}	dissociation rate constant
L	characteristic length scale
P_{open}	probability of open channel
Q_c	flow velocity of continuous phase
Q_d	flow velocity of dispersed phase
Re	Reynolds number
u	velocity of flow
U	characteristic velocity
t	time
V	electric potential or volume
γ	surface tension
μ	dynamic viscosity of the fluid
ρ	density of fluid
τ_{on}	time of inter-event interval
τ_{off}	mean residence time

αHL	alpha-hemolysin
AC	alternating current
AFM	atomic force microscopy
ATP	adenosine triphosphate
BLM	black lipid membranes
CNC	computer numerical control
D	diffusion coefficient
DEP	dielectrophoresis
DHB	droplet hydrogel bilayer
DIB	droplet interface bilayer

DOD	droplets on demand
DOPC	1,2-dioleoyl-*sn*-glycero-3-phosphocholine
DNA	deoxyribonucleic acid
DPhPC	1,2-diphytanoyl-*sn*-glycero-3-phosphocholine
EDTA	ethylenediaminetetraacetic acid
EWOD	electrowetting-on-dielectric
FITC	fluorescein isothiocyanate
γCD	gamma-cyclodextrin
GLUT4	glucose transporter type 4
GUV	giant unilamellar vesicle
HEPES	4-(2-hydroxyethyl)-1-piperazineethanesulfonic acid
I.D.	internal diameter
IVTT	*in vitro* transcription and translation
Kcv	viral potassium channel
kDa	kiloDalton
LUV	large unilamellar vesicle
MIC	minimum inhibitory concentration
MscL	large-conductance mechanosensitive channel
MW	molecular weight
O.D.	outer diameter
PC	polycarbonate
PCR	polymerase chain reaction
PDMS	polydimethylsiloxane
PFT	pore-forming toxin
PTFE	polytetrafluoroethylene
PMMA	poly(methyl methacrylate)
RSD	relative standard deviation
SCR	single channel recording
SDS	sodium dodecyl sulfate
SEBS	poly[styrene-b-(ethylene-co-butylene)-b-styrene]
SLB	supported lipid bilayer
SUV	small unilamellar vesicle
TIRF	total internal reflection microscopy
TRIS.HCl	tris(hydroxymethyl)aminomethane hydrochloride

Streszczenie (Abstract in Polish)

Tworzenie modelowych dwuwarstw lipidowych w warunkach *in vitro* jest kluczowe w prowadzeniu badań nad elementarnymi właściwościami błon biologicznych i białek błonowych. Jednym ze sposobów, który pozwala na uzyskanie stabilnej membrany jest zanurzenie wodnych kropel w oleju zawierającym lipid, a następnie, po utworzeniu monowarstwy lipidowej na powierzchni każdej z kropel, ich zetknięcie. W miejscu zetknięcia się powierzchni dwóch kropli, tworzy się dwuwarstwa lipidowa na styku kropel (ang. *droplet interface bilayer,* DIB). Układ ten, w porównaniu do innych fizycznych modeli dwuwarstw lipidowych, cechuje się wyjątkową stabilnością mechaniczną. Dodatkowo krople są zamkniętymi mikroreaktorami, umożliwiając stosunkowo łątwą kontrolę nad warunkami chemicznymi po każdej z dwóch stron błony lipidowej niezależnie.

Bardzo korzystną strategią tworzenia kropel jest zastosowanie układów mikroprzepływowóch – technologii, kóra jest dynamicznie rozwijana w ciągu ostatnich 25 lat. Miniaturyzacja systemów pozwalających na wysokoprzepustowe prowadzenie badań biologicznych i chemicznych w bardzo małych objętościach płynów, jest możliwa dzięki opracowaniu metod mikroprzepływowych operacji na kroplach o objętości pomiędzy femto- a mikrolitrami.

Projekty badawcze, których wyniki opisuje ta rozprawa doktorska, skupione były na – w wielu aspektach pionierskim – zastosowaniu technik mikroprzepływowych do tworzenia dwuwarstw lipidowych oraz prowadzenia na tych modelowych układach eksperymentów. Celem badań było synergistyczne połączenie zalet prowadzenia badań za pomocą technik mikroprzepływów dwufazowych z unikalnymi właściwościami metody DIB. W projektach uwzględniono zarówno aspekt badań podstawowych, jak i praktyczne zastosowanie prowadzonych prac.

Rozprawa podzielona jest na 7 rozdziałów. W rozdziale 1 zawarty jest przegląd literatury na temat dostępnych metod tworzenia modelowych dwuwarstw lipidowych, ze szczególnym uwzględnieniem wykorzystania technik mikroprzepływowych. Rozdział 2 przedstawia materiały i metody użyte w pracach badawczych. Wyniki zaprezentowane są w rozdziałach 3 – 6 pod kątem podziału na następujące projekty.

Rozdział 3 przedstawia zautomatyzowany system do cyklicznego tworzenia dwuwarstw lipidowych i badania aktywności kanałów białkowych. W prezentowanym układzie mikroprzepływowym proces uzyskiwania stabilnych, funkcjonalnych membran lipidowych był kontrolowany przez programowalne zawory. Wyposażenie układu w elektrody pozwoliło na przeprowadzenie elektrofizjologicznych pomiarów aktywności nanoporów - białka alfa-hemolizyny w obecności jego małocząsteczkowego inhibitora, w celu wyznaczenia kinetyki procesu blokowania białka błonowego.

Rozdział 4 opisuje transmisję sygnału elektrycznego w sieci kropel. Opracowano zautomatyzowany system do tworzenia sieci kropel, połączonych dwuwarstwami lipidowymi. W kroplach na krańcach sieci umieszczone były elektrody pozwalające na pomiar przepływu prądu pomiędzy kolejnymi kroplami. Dodatek różnych stężeń nanoporów alfa-hemolizyny do poszczególnych kropel zapewnił możliwość prowadzenia nieinwazyjnego pomiaru sygnału z dwuwarstwy znajdującej się wewnątrz sieci kropel, bez konieczności umieszczania elektrod w ich wnętrzu. Model obwodu elektrycznego opisujący przepływ prądu w sieci kropel posłużył do interpretacji sygnałów.

W rozdziale 5 opisano rozcieńczanie próbki w zautomatyzowanym systemie. Przedstawiono próbę opracowania systemu, który pozwoli na rozcieńczanie próbek w układzie bezpośrednio przed pomiarem. Zaproponowany system opierał się na precyzyjnym dozowaniu porcji próbek w układzie i ich zautomatyzowanemu rozcieńczaniu.

Rozdział 6 przedstawia mikroprzepływowy system do pasywnego tworzenia membran lipidowych na granicy kropel w tzw. „pułapkach hydrodynamicznych". Istniejące rozwiązania oparte na geometrii kanałów mikroprzepływowych, służące do podziału próbki na krople i ich unieruchomienia, posłużyło do wytwarzania dwuwarstw lipidowych. Dzięki powtarzalności operacji tworzenia błon na granicy kropel o objętości 9 nL i prowadzenia równoległych pomiarów fluorescencji, wyznaczono parametry takie jak przepuszczalność dla małocząsteczkowego barwnika i transport jonów przez kanały białkowe obecne w membranach. Przedstawiono również możliwość przygotowywania rozcieńczeń badanej substancji w kolejnych nanolitrowych kroplach w układzie.

Rozdział 7 zawiera ogólne podsumowanie wyników i wnioski dotyczące dalszych kierunków badań.

Abstract

In vitro formation of model lipid bilayers is an essential part of research on properties of lipid bilayers and membrane proteins. One of the methods to obtain stable lipid bilayers relies on submerging aqueous droplets in an oil phase containing dissolved lipid molecules and upon formation of a monolayer of phospholipids at the surface of droplets, bringing the droplets into contact. Thanks to the self-organization of phospholipid molecules at the interface of aqueous and continuous phase, a lipid bilayer is formed at the point of contact between the droplets (droplet interface bilayer, DIB). In comparison to other models of a lipid bilayer, DIB is characterized by an exceptional mechanical stability. In addition, droplets are separate microreactors, allowing for a control over the chemical composition on both sides of a bilayer.

In the recent 25 years a significant progress was made towards establishing miniaturized high-throughput systems dedicated for biological and chemical research. Microfluidic techniques allowed to develop experimental assays on droplets of volumes ranging from femto- to microliters, which is an attractive strategy to implement in developing experimental systems for formation of artificial lipid bilayers.

This dissertation presents results of development of pioneering microfluidic devices dedicated for formation of lipid bilayers. The main objective was to combine the advantages rising from the use of droplet microfluidic systems with the unique properties of the DIB technology. Research projects were focused both on development of microfluidic devices and on using them for experiments on membrane proteins.

The dissertation is composed of seven Chapters. Chapter 1 contains a literature review on the methods available for formation of artificial lipid bilayers, especially on the use of microfluidic techniques. Chapter 2 describes materials and methods used in the research projects. The results are presented from Chapter 3 through Chapter 6 as follows.

In Chapter 3 I present an automated system for repetitive formation of lipid bilayers and electrophysiological measurements on nanopores. The control over the formation of lipid bilayers in the presented system was achieved with programmable external valves. The electrodes inserted into the system allowed for electrophysiological measurements on activity of nanopores – alpha-hemolysin protein molecules. The kinetics of inhibition of proteins pore with small molecule was determined.

Chapter 4 describes the signal transmission in a network of droplets. An automated droplet microfluidic system was used to generate networks of droplets interconnected with lipid bilayers. Electrodes inserted into the droplets at the edges of a network were used to measure the flow of electric current across several droplets. Various concentrations of alpha-hemolysin nanopores were added to droplets, allowing for measurements of an electric signal from the interior of a network and excluding the direct contact of electrode with a sample. A model of electric circuit describing the flow of electric current in a network of droplets was used to interpret the data.

Chapter 5 focuses on the automated dilution of a sample on-chip. A brief description of an attempt to construct an automated system for dilution of a sample is provided. The proposed system relied on metering of portions of samples on-chip and automated serial dilution.

Chapter 6 details the passive microfluidic device for a formation of lipid membranes in hydrodynamic traps. A system based on geometry of microfluidic channels, capable of splitting the sample into immobilized droplets, was adapted for formation of lipid bilayers. Permeability of lipid bilayers for small molecule dye and the transport of ions through nanopores inserted in the membranes were determined using the microfluidic device in which multiple bilayers were formed in parallel at the interface of 9-nanoliter droplets. The on-chip dilution of a sample in a series of hydrodynamic traps was also demonstrated.

Finally, Chapter 7 summarizes the results and provides an outlook for a future research.

Contents

CHAPTER 1.

Introduction and Literature Review

Chapter 1 introduces general concepts of cell membrane biophysics and complexity of protein interactions with lipid surfaces. We review the available research methods for obtaining model lipid bilayers, starting with the description of traditional techniques dedicated for in vitro formation of artificial lipid bilayers. The chapter then proceeds to describe the benefits of using microfluidic techniques in biological and chemical assays. We focus on the use of microfluidic techniques (with the special emphasis on droplet microfluidics) for obtaining lipid bilayers and review the microsystems for efficient preparation of lipid membranes. Finally, open challenges in the field and solution addressing them are listed.

1.1. Cellular membranes

In the past the cell membranes were regarded as an inert material providing separation from the outside environment and a compartmentalization within cells. Currently lipid membranes are proven to be important and active component engaged in bidirectional interplay with protein molecules. Elucidating mechanisms by which lipid surfaces take part in the control of protein activity has important pharmaceutical implications, since approximately 60% of drugs targets proteins embedded in the membranes [1]. What is also important, all potential drug molecules need to be tested against certain types of membrane proteins in order to avoid undesired side effects. However, the complexity of interactions between cellular membranes and proteins is not trivial to pinpoint using the established biophysical techniques. Moreover, a reproducible, robust *in vitro* preparation of stable model lipid membranes is challenging due to the fragile nature of a nanometer-thick bilayer.

1.1.1. Structure and functions of cell membranes

An around 4-nanometer thick lipid bilayer is the main structural component of membranes present in cells. A variety of lipid molecules that compose membranes in cells (so far more than 40 000 species identified [2]) share the common feature – the presence of hydrophilic headgroup and hydrophobic acyl chain tail/s – that result in self organization in aqueous environment. The cylindrical shape of membrane lipids contributes to the spontaneous self-assembly into a two-layer sheet – a bilayer. The composition of lipid bilayer differs significantly between taxonomic kingdoms. In bacterial plasma membranes, one type of phospholipid predominates and no cholesterol is found. In eukaryotic cells more than a half of lipid mass is constituted of 4 types of phospholipids: phosphatidylcholine, phosphatidylethanolamine, phosphatidylserine and sphingomyelin. At physiological pH phosphatidylserine exhibits negative charge, whereas the rest of above listed types of lipids are not charged [3].

Lipids contribute to around 50% of mass of cell membrane, the rest being mostly proteins. Lipid bilayer provides a support for insertion of proteins, the process often being dependent on the presence of specific lipid molecules. The sequence of amino acids evolved towards the insertion into the hydrophobic core of bilayer – non-polar amino acids dominate in parts that are associated directly with lipid tails in case of integral membrane proteins. Integral membrane proteins completely span across the membrane

adopting either alpha-helix (or helical bundle) or beta-barrel structure. Contrary, peripheral membrane proteins only transiently interact with one of the bilayer leaflets (Figure 1).

All functions of living organisms are orchestrated by proteins. Several major functions in cell physiology can be attributed to membrane proteins:

- Providing a junction between cells,
- Localization of enzymatic activity,
- Recognition of markers (including cell-cell recognition) and transduction of signals,
- Attachment of cytoskeletal elements,
- Facilitation of transport through the membrane.

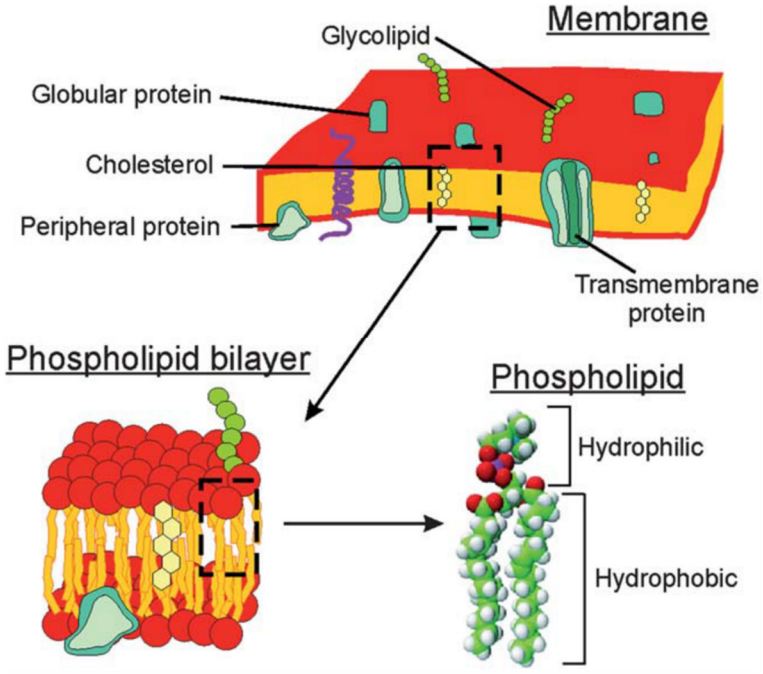

Figure 1 Schematic representation of a cell membrane and its components. Cell membranes are constituted from proteins and other types of molecules e.g. phospholipids, glycolipids, cholesterol. Phospholipids are amphiphilic molecules that self-organize into a bilayer structure in aqueous environment. Figure reproduced from [4].

1.1.2. Transport processes through cell membrane

One of the key functions of plasma membrane in the maintenance of homeostasis is to regulate the movement of substances out from the cell and into its interior. This control is achieved thanks to the semi-permeability – the ability to let only certain types of

molecules to pass freely by diffusion. A factor that characterizes the ease at which a molecule can cross the bilayer is defined as permeability. Typically, small non-polar species can freely permeate through a lipid bilayer as they are soluble in the hydrophobic core of the membrane. A membrane is impermeable to large polar molecules and charged species (ions). The ability to diffuse through a bilayer is an important feature to be considered when testing molecules for a potential medical application, especially when deciding about the administration pathway and possible absorption routes.

A transport by diffusion does not require energy input, but in some instances specialized proteins are needed for a molecule to be able to pass through in a process of facilitated diffusion. A typical example is the transport of glucose through GLUT4 channel that inserts into the membrane after being activated by insulin [5]. A leakage of small molecules can also occur through pores formed in the membrane during stress event e.g. pathogen infection. Bacteria produce pore-forming toxins (PFTs) in order to exert an uncontrolled release of the content of attacked cell [6]. An example of PFT is alpha-hemolysin (αHL) – a toxin produced by *Staphylococcus aureus*, named after the ability to damage human blood cells, including erythrocytes (Figure 2). αHL is expressed and released as water-soluble 33.2 kDa monomers that assemble into 232.4 kDa heptameric pores when binding to a lipid bilayer [7,8]. Well-defined heptameric pores are assembled in a low concentration of protein, whereas less organized structures are formed when the toxin is present in a high concentration. The cell death induced by αHL is a result of uncontrolled release of ions, water and small molecules (including ATP) through nanopores. In *in vitro* experiments αHL perforates artificial model lipid membranes, either by an assembly of monomers or by an insertion of pre-formed heptamers that can be obtained from incubation with deoxycholate micelles. The ability of αHL to accommodate and pass molecules through a channel of a structurally well-characterized protein was a prerequisite to use this nanopore in biotechnology as a biosensor, e.g. for sensing of base pairs of DNA strand in nanopore based DNA sequencing [9–11].

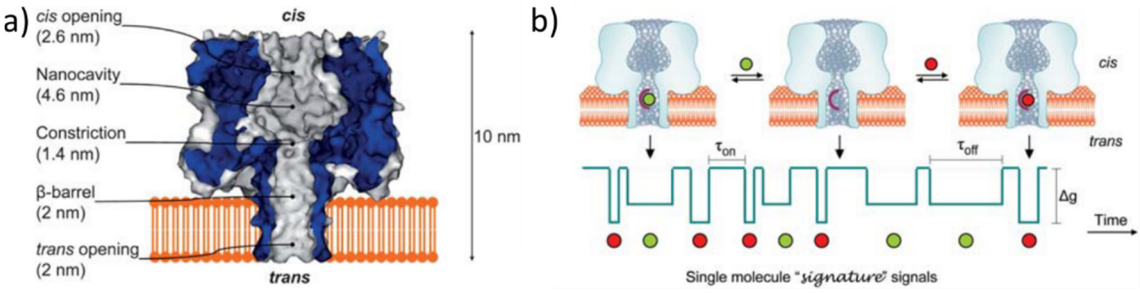

Figure 2 Alpha-hemolysin nanopore. a) A molecular graph of the heptameric alpha-hemolysin pore inserted in the lipid bilayer. The dimensions of the various regions in the lumen of the pore are described. b) Single molecule detection in a protein pore: two different analytes (represented by green and red dots) competitively and reversibly bind within the receptor engineered in the protein pore. The analytes can be identified and quantified based on a characteristic amplitude (Δg) and duration of block of the current passing through a pore (τ_{off}; time of channel being open - τ_{on}). The sides of a bilayer are denoted as cis and trans compartments. Figure reproduced from [12].

In this dissertation the focus is lied on simple and facilitated diffusion processes, however it is important to mention that many vital functions of cells are maintained by active transport that consumes energy for the transport of substances against their gradient.

1.2. Model lipid bilayers

One of the approaches to study the properties of lipid membranes and the interactions between membranes and proteins is to create an artificial lipid bilayer accessible for a variety of experimental techniques. Even though artificial bilayers are very simplified model systems in comparison to natural cell membranes they provide an insight into fundamental properties and allow to test for influence of specific components or conditions. A reproducible and cost-effective method for the generation of lipid bilayers and for measuring electrical currents through channels and pores inserted in them is demanded for the efficient screening of the function of membrane proteins against physical and chemical factors. Several methods to produce lipid membranes *in vitro* were developed so far – in the paragraphs 1.2.1. - 1.2.3. the most important experimental strategies are briefly described.

1.2.1. Lipid vesicles

Lipid vesicles are spherical entities obtained from hydration of lipid film in aqueous buffer (Figure 3a). The size can be controlled depending on the technique of preparation – small unilamellar vesicles (SUVs) are obtained during the sonication of lipid solution and result in liposomes that are 15 - 30 nm in diameter. Large unilamellar vesicles (LUVs,

100 nm – 1 μm diameter) are formed when lipid solution is extruded through porous filters. SUVs and LUVs are similar in sizes to vesicles found in cells and do not comprise the solvent residues in their structure therefore they are good candidates for incorporation of membrane proteins. However, small vesicles are characterized by high curvature elastic free energy and therefore do not maintain the stable size over period longer than approximately 1 day [13]. Additionally, their nanometer dimensions do not allow for the access of electrodes to the inner compartments of vesicles and make experiments on individual membranes challenging, often limiting the experimental techniques to experiments characterizing transport processes in bulk. An alternative to using sub-micron scale vesicles is to produce giant unilamellar vesicles (GUVs) that range in size from 1 to 50 μm in diameter. GUVs are easier to capture individually for microscope imaging than SUVs, however the challenge lies in developing a high-throughput method for fabrication of GUVs that will result in uniform in size and free of solvent vesicles.

1.2.2. Planar lipid bilayers

1.2.2.1. Voltage clamp method

A potent method to characterize lipid bilayers and membrane proteins relies on maintaining a constant voltage of the membrane – this experimental approach is widely known as a voltage clamp method. Ions pass through defects in the membrane as well as through ion channels. In order to keep a voltage stable at an arbitrary set level (recorded by ‘voltage’ electrode), current is applied from ‘current’ electrode to compensate for the leakage of ions. The feedback current is proportional to the membrane conductance with changes detectable at the level as low as few picoamperes, allowing to characterize membrane proteins with the single-molecule resolution. One of the first demonstrations of voltage clamp method was the research on ionic regulation of action potentials performed on the giant squid axon – a nerve cell reaching 1 mm in diameter, able to accommodate inserted electrodes [14]. The recordings of activity of channels at the resolution of single molecule (referred to as single channel recording, SCR) allow to examine voltage dependence, gating behavior, binding of ligands or ion selectivity. A prominent example of application of SCR is the technology of DNA sequencing from recordings of translocation of DNA strands through nanopores [11]. The patch clamp technique is a modification of a voltage clamp method – but it does not require cell membrane to be penetrated with electrodes but relies on the direct contact of a tip of a glass microelectrode with a surface of a small fragment (patch) of a membrane. However,

classical patch clamp method requires skilled manual operation, which limits the throughput in routine drug screening assays. The high demand for screens of protein function has prompted several attempts to increase throughput and to automate the measurements [15]. These methods require the control of protein expression in cells, which can be challenging, and provide limited information (usually to IC_{50} values) on activity of tested molecules usually.

1.2.2.2. Black lipid membrane technique

In order to perform *in vitro* voltage clamp measurements it is necessary to obtain an artificial lipid bilayer that is accessible from both sides for the insertion of electrodes. Formation of mechanically stable bilayers which are also resistant to applied voltage is a challenging task. One of the best established and commonly used by researchers methods was developed in the 1960s. The black lipid membrane (BLM) technique relies on deposition of the lipids dissolved in an organic solvent (e.g. decane or squalene) to an aperture in the Teflon plate that separates two compartments filled with an aqueous solution (Figure 3b, [16]). Lipid molecules self-organize at the interface of water and organic solvent after the lipid solution is manually applied ('painted') to the orifice of a few tens to hundreds of micrometers in diameter. The droplet of solvent, trapped in the hole, gradually thins in the center until two lipid layers meet in the center and form a bilayer. The solvent is stored in a form of annulus that bridges the bilayer with solid support, which is at least an order of magnitude thicker than the membrane. There are several important factors for the stability of the membrane: i) the stability of the annulus – spreading across the plastic barrier, ii) exchange of lipids with the bilayer from the oil pocket, and iii) generation of micelles from oil phase into aqueous phase [17,18]. The presence of solvent residues in the structure of bilayer was eliminated in the modified version of BLM method – developed by Montal and Mueller who lowered polytetrafluoroethylene (PTFE) plate with aperture through the buffer reservoir with a lipid monolayer assembled at the water-air interface, which subsequently covered the plate and the orifice [19]. Additionally, asymmetric bilayers (having different lipid composition in each leaflet) can be obtained using Montal-Mueller approach. The main disadvantages of planar bilayers formed over the aperture are low stability (the rupture is mostly related to small differences in evaporation rate from both aqueous compartments) and laborious manual preparatory technique. However planar bilayers are widely used as

they provide a support for insertion of purified membrane proteins and withstand up to hundreds of mV of applied voltage.

1.2.2.3. Supported lipid bilayers

Producing lipid bilayers on a solid support (supported lipid bilayer, SLB) overcomes the problem of reduced stability (Figure 3c, [20]). The flat bilayers that are spread on a surface can be kept for long period of times and local defects do not exclude the rest of bilayer from experiments, but more importantly SLBs can be subjected to probing with techniques requiring a physical contact of a probe with the sample (e.g. AFM) and to a variety of optical imaging techniques. However, proteins may interact unfavorably with the solid substrate and their mobility and function can be modified or hampered, thus making electrical measurements difficult, especially at the single molecule level.

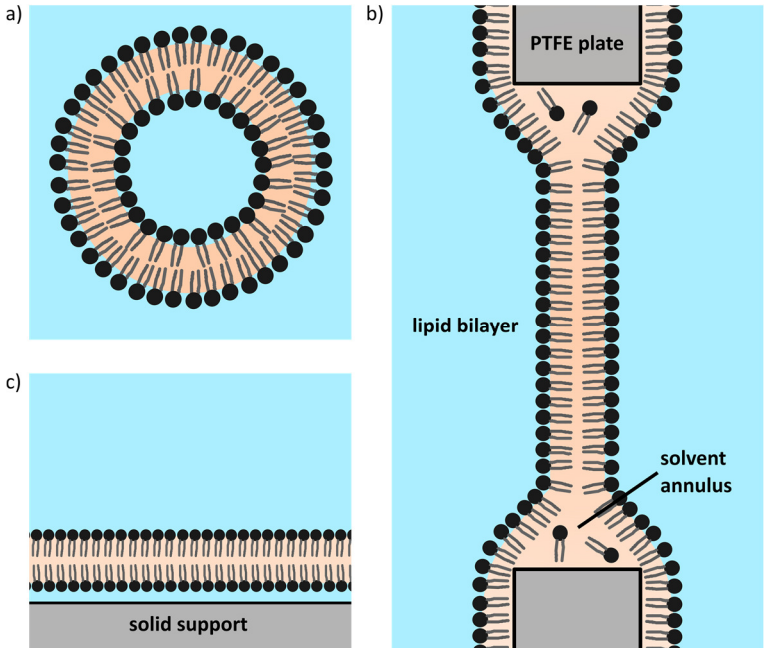

Figure 3 Schematics of various types of a model lipid bilayer. a) Liposome is a spherical lipid structure. Unilamellar lipid vesicles serve as a model of vesicles present in cells. b) Planar black lipid membrane (BLM). Aqueous compartments (blue) are accessible for electric measurements from both sides of a bilayer. c) Supported lipid bilayer - a lipid bilayer is placed on a solid support for an increased stability and accessibility of optical imaging.

1.2.3. Droplet interface bilayers

A convenient method for forming a stable lipid bilayer is by bringing the lipid monolayer-coated interfaces of two aqueous droplets into contact in oil. The original idea of the method was conceived by Tsofina *et al*. and published more than 50 years ago as an alternative to BLM which, at is initial versions, often failed at incorporating proteins into

the structure of bilayer [21]. There was no follow up work on development of the droplet method until 2005, when prof. H. Bayley's and prof. S. Takeuchi's research groups published first demonstrations of experiments with bilayers obtained at the interface of droplets (droplet interface bilayers, DIBs) [22,23].

The principle of the method relies on the self-organization of phospholipid molecules at the interface of aqueous droplet and surrounding oil phase (typically, but not restricted to, hydrocarbons e.g. hexadecane, decane, squalene) (Figure 4). The time required for the full coverage of the surface of droplet with a monolayer of lipids varies between few minutes for immobile droplets suspended in oil down to few milliseconds for droplets flowing in a microfluidic channel or in a capillary [24]. Lipid molecules are delivered to the surface either from being dissolved in continuous phase (*lipid-out* technique) or from liposomes dispersed in droplets (*lipid-in* technique) (Figure 5). Once the droplets are encased in a monolayer of lipids and are brought together, they do not merge but rather form a bilayer at the interface. The molecular mechanism of adhesion of two droplets is explained by changes of the entropy in the system – exclusion of solvent from the structure of acyl chains of lipid molecules. In mechanical equilibrium the surface tension of the bilayer (γ_b) is characterized by the surface tension of monolayers (γ_m) and the contact angle between monolayers: $\gamma_b = 2\gamma_m cos\theta$. Moreover, free energy of bilayer adhesion can be calculated knowing the monolayer tension and contact angle: $\Delta F = 2\gamma_m(cos\theta - 1)$ [25].

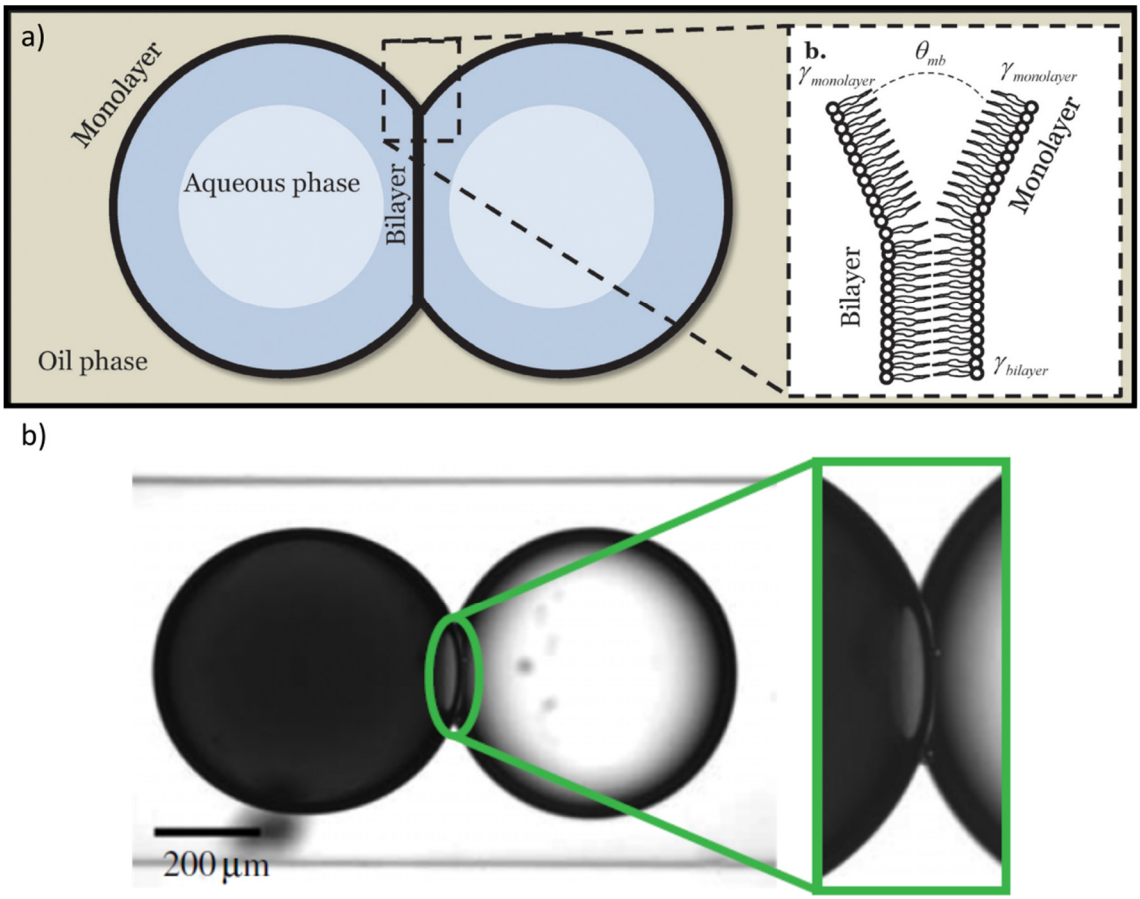

Figure 4 The principle of droplet interface method for formation of model lipid bilayer. a) Schematic representation of the idea of the method in which lipid molecules self-organize at the interface of aqueous and oil phase. When droplets are brought into contact, a lipid bilayer forms at their interface. Figure reproduced from [26] b) Micrographs showing DIB made from 1,2-dioleoyl-*sn*-glycero-3-phosphocholine (DOPC) lipid. Figure reproduced from [27].

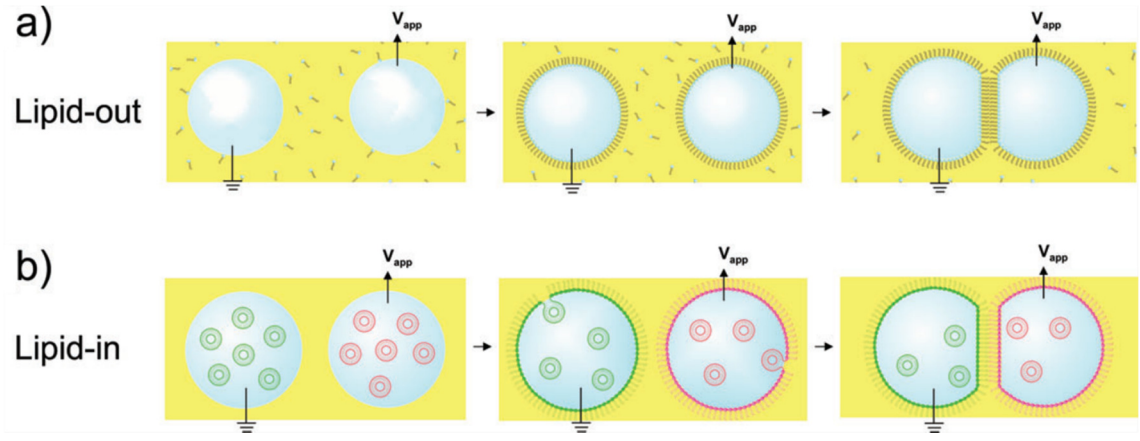

Figure 5 Two methods of droplet interface bilayers preparation. a) Lipid-out: aqueous droplets are submerged in an oil-lipid solution. Droplets are encased with lipid monolayers during the stabilization period. Then they are brought into contact and form a bilayer. b) Lipid-in: aqueous droplets containing lipid vesicles of different composition are kept in an oil reservoir. Vesicles fuse with the oil-water interface of each droplet and form monolayers. The droplets are then brought into contact and an asymmetric bilayer is formed at their interface. Figure reproduced from [22].

Comparing to the classical meta-stable planar bilayer method, DIBs show critical advantage of exceptional stability that supports long-term measurements. There are few differences that contribute to the increased stability of DIB:

- the differences in distribution of interfacial forces,
- lack of annulus in DIB method,
- constant supply of lipids in droplet-based approach,
- low hydrostatic shock associated with submerging droplets in oil (the content of droplet is prevented from evaporation and the control over the droplet volume is more accurate than the control over the volume of compartments in BLM experimental set-up).

Other benefits of DIB include:

- micro-liter consumption of samples (of both the protein and lipid solutions),
- control over the symmetry of the bilayer [28] (phenomena of lipid organization in the bilayer e.g. raft formation or flip-flop can be studied [29]),
- arbitrarily set and controlled droplet content (pH, presence of biomolecules, salt concentration),
- accessibility to various experimental techniques, including electrical interrogation with electrodes inserted into the droplets, and optical imaging of the content of droplet or bilayer,
- ability to easily detach both monolayer leaflets and then re-form the bilayer – a droplet can be transferred from the surface of one droplet to the surface of another droplet, without cross-contamination between the droplet content. A bilayer is successfully formed at each event of the droplet translocation.

1.2.3.1. Applications of droplet interface bilayers in membrane protein research

Many interesting applications that stem from the unique features of DIBs regarding protein-bilayer interactions have been demonstrated. Electrical properties of proteins embedded in DIB match results obtained during characterization in planar bilayer systems. Additionally, potential of more than 150 mV can be applied to DIB similarly as

to a planar bilayer. Protein molecules can be delivered to the bilayer by various means e.g. from proteoliposomes contained in the droplet, or directly produced in droplets by In Vitro Transcription and Translation (IVTT) system [30,31]. Furthermore, the formation of open pores from some of the protein molecules can be facilitated by applying high voltage (voltage-gated channels) and manipulating the droplet content for the presence of appropriate ligand (ligand-gated channels). Fusing of one of the droplets in pair with additional third droplet delivering the material is a straightforward method to change the composition of the droplet [32]. Additionally, methods for the perfusion of the contents of droplets were developed, relying on piercing the droplet with capillaries for delivery and withdrawal of the solution from the droplet [33].

1.2.3.1.1. Lipid composition

An important addition to the DIB method is the formation of membranes using liposome solutions in droplets containing multi-component mixtures and lipid extracts from cells. It was found that heating the droplets in oil above the thermotropic transition temperature of lipids promoted the self-assembly of lipids at the water-oil interface, resulting in lipid bilayers of physiological compositions. Total lipid extract from *Escherichia coli* was used to obtain bilayers at the interface of droplets and insertion of alamethicin was measured and compared to insertion into bilayers composed of one lipid only [34]. The lipid content of the bilayer can be modified during the experiment by delivering lipid molecules into the oil around the DIB [35]. It was shown that incorporation of sterol molecules into the bilayer changed membrane tension and altered the activity of potassium channel [36]. In addition other physicochemical properties of lipid bilayer, e.g. the formation of rafts [37] or phase separation of different types of membrane forming species [38], can be dynamically changed and tracked with optical imaging. Moreover the changes of the shape of bilayer can be induced by evaporation of droplets content, resulting in buckling of a membrane and fission of lipid vesicle from the DIB – an useful model of mechanics od endo- and exocytosis in cells [39,40].

1.2.3.1.2. Droplet hydrogel bilayers

A lipid bilayer can be formed not only at the interface of two droplets, but also at the interface of droplet and planar support covered with a lipid monolayer (most conveniently a hydrogel is used as a solid support). The advantage, apart from the enhanced stability of droplet hydrogel bilayer (DHB), is the direct accessibility of optical imaging of the

surface of a bilayer e.g. with total internal reflection fluorescence (TIRF) microscopy. A hydrogel layer can accommodate an electrode for the simultaneous electrical recordings and imaging, which was proven to be useful for characterization of single protein molecules [41] and electropores [42]. Another demonstration of the capabilities of the DHB was the direct detection of proteins in the hydrogel containing fragments of membrane isolates [43] and polyacrylamide gel [44], by scanning the area of the gel with a droplet connected to a micromanipulator (Figure 6a).

1.2.3.1.3. Transport processes in DIB

Apart from the low sample consumption, the small scale of the DIB method has multiple advantages. Analytes can be detected at low concentrations in a confined volume of droplets. Therefore, droplets are an ideal tool to study transport processes across the lipid membrane. Among other applications the translocation of enzyme molecules across the barrier by Pep-1 peptide [32] and the transport of N-terminal domain of Lethal Factor by anthrax toxin (PA) [45] were directly quantified using the DIB method.

1.2.3.1.4. Manipulation with the droplets' location

Droplets are separate entities and that can be moved to form and dissociate bilayers at the interface of droplets – this feature was exploited for the development of DIB system dedicated for rapid screening of inhibitors against membrane proteins [30]. Solutions of inhibitors were deposited in microwells submerged in oil and equipped with electrodes at the bottom of each well, to form an array of droplets containing inhibitors. A droplet hanging from a moveable grounded electrode contained a solution of protein (potassium channel, Kcv). In the screening experiment the droplet containing protein molecules was transferred from the surface of one droplet to the surface of next droplet in the array, each time forming a lipid bilayer. Measured electric signal corresponded to the activity of potassium channel inhibited with patterns characteristic to specific inhibitors (Figure 6b).

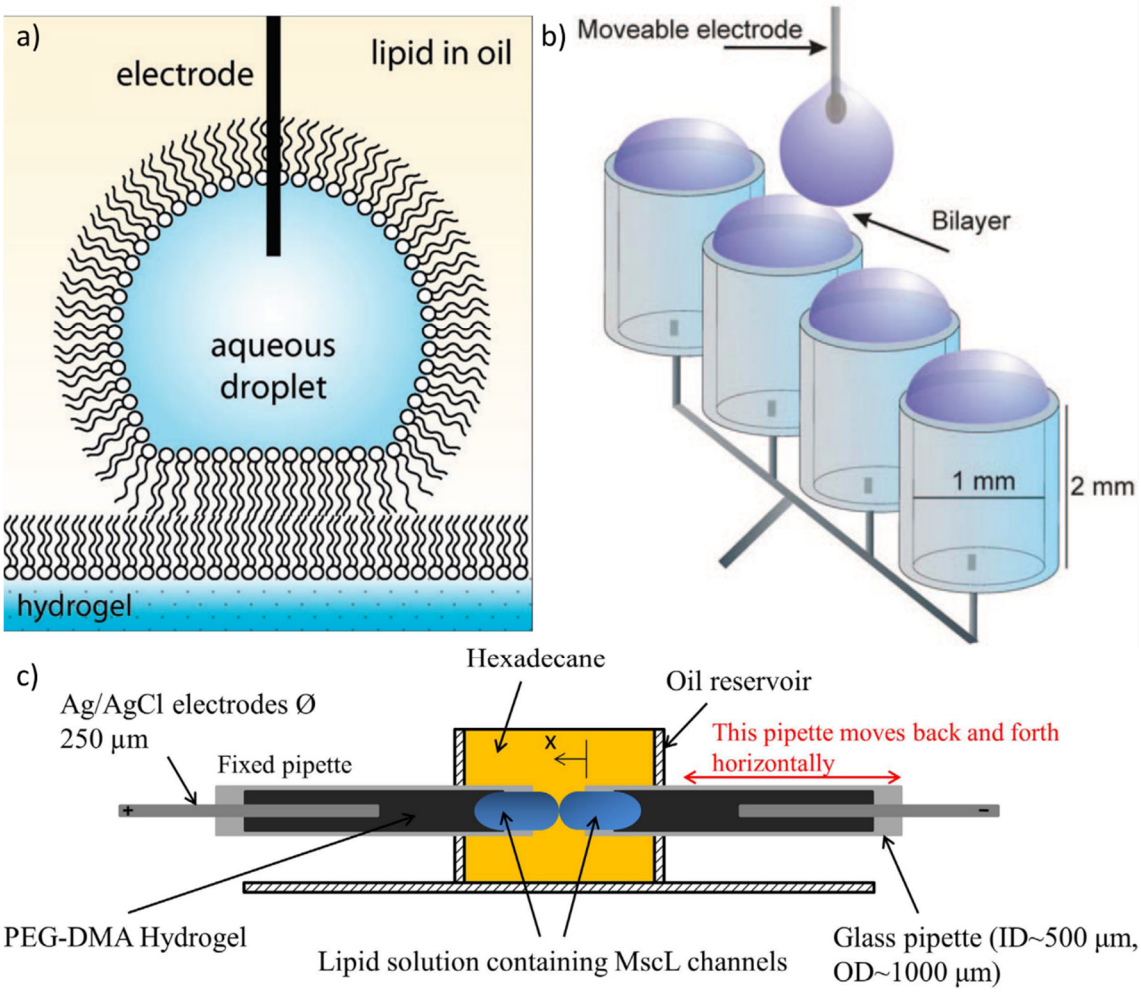

Figure 6 Applications of DIBs in membrane protein research. a) Droplet on a hydrogel support bilayers (DHBs): lipids dispersed in oil self-organize into monolayers at the interface of droplet and hydrogel support and form a bilayer when the two components are brought into contact. Droplet attached to an electrode can be moved vertically to detect molecules from the hydrogel and horizontally to control the surface area of the bilayer. Figure reproduced from [44]. b) Screening of ion-channels: a schematic shows a chip with analytes (ion-channel blockers) arranged in wells (each holding 1.5 µL of solution and containing a working electrode). A droplet containing protein solution is suspended from the moveable Ag/AgCl grounded electrode. A DIB is formed each time the droplet with protein solution is interfaced with the droplets in an array. Figure reproduced from [30]. c) Mechanical stimulation of DIB for changing the tension in the membrane: the experimental setup consists of hydrogel filled pipettes with electrodes inserted at the ends. Two lipid containing droplets are anchored to the tips of the micropipettes and placed within a cylindrical oil filled reservoir. The micropipette on the left is fixed and attached to the amplifier, while the micropipette on the right is connected to a piezoelectric actuator which allows it to move horizontally. Figure reproduced from [46].

The above-mentioned ability to control the position of droplets with respect to each other provides a straightforward method for regulation of the surface area of a bilayer. Changing the sizes of the membrane while acquiring the optical image and electric measurements from the bilayer was used to determine specific parameters related to the properties of lipid bilayer (e.g. specific capacitance) [47]. In addition, it has been

demonstrated that upon the insertion of nanopores a reduction in the size of the bilayer resulted in denser packing of the protein molecules instead of their exclusion from the membrane [48]. An interesting use of the control over the droplet location in membrane protein research is axial compression of droplets in order to increase the tension in the membrane and to obtain the gating values for the activity of mechanically stimulated channels. A bacterial mechanosensitive channel of large conductance (MscL) [27,46,49,50] as well as mechanically activated eukaryotic Piezo [51] proteins have been successfully reconstituted into DIBs (Figure 6c).

1.2.3.1.5. Networks of DIBs

Lipid-coated droplets can be arranged into structures of higher degree of organization than the pairs alone, showing a communication of compartments and cooperative behavior [52,53]. A gradual diffusion of an analyte can be tracked in a network of DIBs, e.g. the travelling waves of oscillating Belousov-Zhabotinsky reaction were imaged in the 2D sheet of droplets [54]. Simple electronic bio-devices: batteries, light sensors or electrical circuits, were constructed from droplets containing protein molecules [55]. Further, the droplets within the network can be designed to be sensitive to external stimuli. A set of aqueous droplets encased in an oil droplet shell (a so called multisome) was placed within an aqueous environment and the release of content from droplets within the network was controlled with the pH or temperature of external aqueous solution (Figure 7, [56]). The array of droplets was also selectively patterned with various proteins by containing light-activated DNA and IVTT mixture within the droplets and illuminating individual droplets for inducing the expression of proteins [31]. The networks of droplets that undergo dynamic changes in response to environmental stimuli resemble the features characteristic to tissues. Indeed, this dynamic control was shown for three dimensional structures built from tens of thousands of picolitre droplets functionalized with proteins to transfer electric signal or programmed with osmolarity gradients to fold into structures [57]. The potential of soft devices made from droplets lies in their similarity to living cells in interfacing them with tissues e.g. for the purpose of drug delivery.

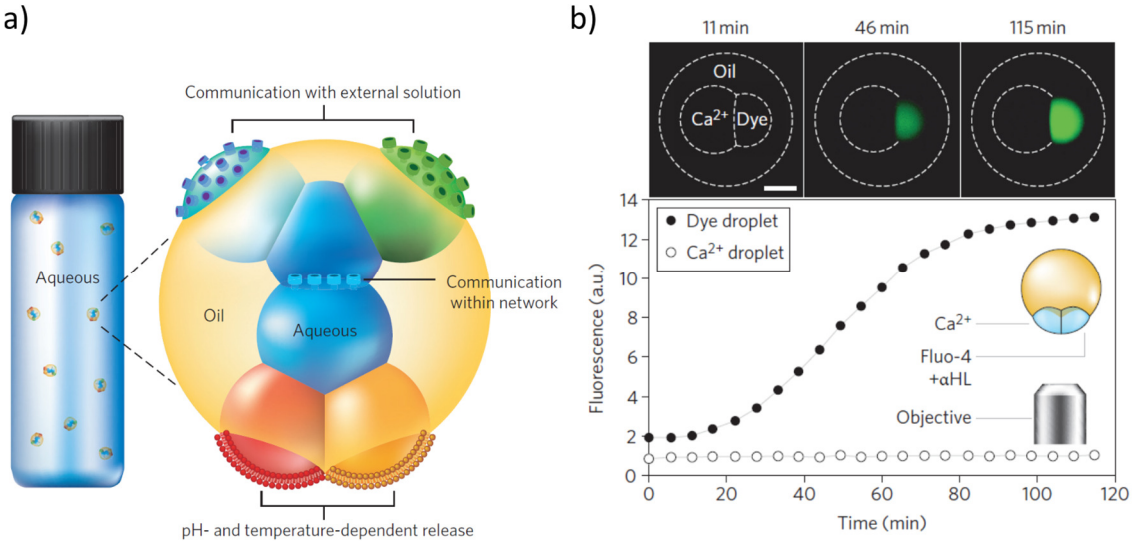

Figure 7 Multisomes. a) Illustration of a multisome: aqueous droplets encapsulated in an oil drop are connected by lipid bilayers. Protein pores in bilayers allow the droplets in the network to communicate. Pores in bilayers at the surfaces of the aqueous droplets that protrude from the oil drop enable the network to communicate with the bulk solution. Multisomes can be engineered to release the contents of encapsulated droplets by pH- or temperature-induced rupture of bilayers. b) Communication by diffusion through αHL pores: a multisome containing a two-droplet network, in which one droplet contained Ca^{2+} and the other contained Fluo-4 calcium sensitive dye and αHL pores. The droplet containing dye increased in fluoresce upon Fluo-4 being excited with calcium ions diffused across the membrane. Scale bar is 300 µm. Figure reproduced from [56].

1.3. Microfluidics for formation of lipid bilayers

1.3.1. Microfluidic techniques

Efficient preparation of artificial lipid bilayers, which are metastable structures and delicate in their nature, largely relies upon manual skills of the operator. In addition, the reagents that are required for the experiments – both the lipid solutions and protein samples – are often precious and available only in limited quantities. Therefore, the methods that would automate the formation of model lipid membranes are highly desired. Microfluidics offers a variety of technical solutions applicable for building systems dedicated for repeatable and precisely controlled preparation and measurements on lipid membranes.

Microfluidics deals with handling liquids at micro-scale, joining the knowledge from fields of physics, chemistry and engineering. Apart from studying the phenomena governing the behavior of liquids at the microscale, microfluidic technologies aim to develop microfluidic systems applicable to research in biology and nanotechnology. The prominent examples of the practical use of microfluidics in biological research and diagnostics are DNA analysis with PCR [58], single-cell analysis [59], protein

purification and crystallization [60]. Importantly, microfluidics accelerated the development of point-of-care diagnostics and wearable sensor or drug administrating devices.

When liquids are introduced into channels of sub-millimeter dimensions the physical forces dominating the behavior of liquid differ from the forces shaping liquids' flow at the macroscale. The dimensionless Reynolds number describes the relationship between inertial and viscous forces, and mainly the latter ones determine the character of flow:

$$Re = \frac{\rho \cdot u \cdot L}{\mu} \qquad \text{Eq. 1}$$

where:

- ρ - density of the fluid [kg/m^3]
- u - velocity of flow [m/s]
- L - characteristic length scales of the device [m]
- μ - dynamic viscosity of the fluid [Pa·s]

Typically, the value of *Re* number characterizing the flow of liquid in microfluidic channel is small (of the order of magnitude of 10^{-6} - 10^{1} [61]), while the threshold for transition from a laminar to turbulent flow equals to around 2000. The main consequence of the flow being purely laminar is the efficiency and dynamics of mixing. In a microfluidic channel, streams of liquids co-flow and the diffusion is the main mechanism of the transfer of mass. The dimensionless number that describes the process of mixing in a microfluidic channel is Péclet number, which expresses the relative importance of convection to diffusion:

$$Pe = \frac{U \cdot L}{D} \qquad \text{Eq. 2}$$

where:

- U - velocity of flow [m/s]
- L - characteristic length scales of the device [m]
- D - mass diffusivity [m^2/s]

As a result mixing is slow when the sample continuously flows in a microfluidic channel [61]. Additionally the local concentration can not be precisely defined due to the Taylor-Aris dispersion [62,63], along with other challenges related to the nature of a sample, e.g. unfavorable interactions with surfaces of channels [64,65].

1.3.1.1. Droplet microfluidics

An alternative to a continuous flow of liquid samples in microfluidic channels is to split it into discrete small volumes with the stream of another, immiscible liquid. Droplets generated in microchannels can range from femtolitres to microliters in volume. Four basic types of geometry of channels for droplet formation can be distinguished: a T-junction [66], a flow-focusing junction [67], a co-axial flow [68,69] and a step-emulsification [70] (Figure 8).

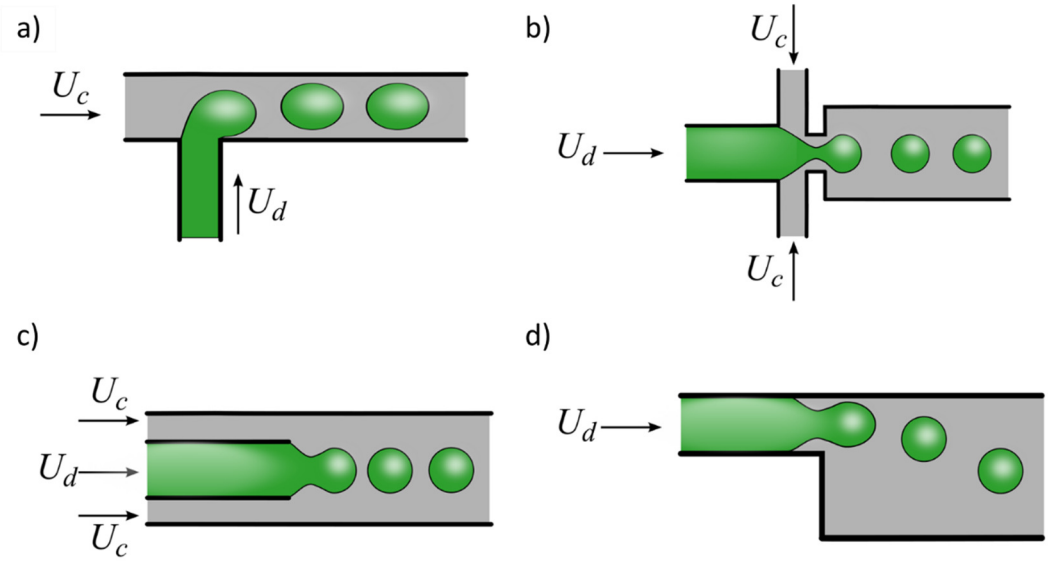

Figure 8 Different geometries used for formation of droplets. a) T-junction b) flow-focusing junction c) co-axial capillary d) step-emulsification. Flow velocities of dispersed phase (U_d) and continuous phase (U_c) along with the dimensions of microfluidic channels determine the volume of generated droplets. Figure reproduced from [71].

For generation of droplets at the microscale the governing forces are related to the surface tension which determines the dynamics of the free surface, along with the viscous shear stress associated with the resistance of the liquid to flow. The relation between these two forces is represented by the dimensionless capillary number:

$$Ca = \frac{\mu U}{\gamma} \qquad \text{Eq. 3}$$

where:

- μ – dynamic viscosity [Pa·s]
- U – characteristic velocity [m/s]
- γ – surface tension [J/m^2].

A squeezing regime of droplet formation is observed when the *Ca* number is low ($<10^{-2}$) and interfacial effects play dominant role. By manipulating with flow rates of dispersed and continuous phase the volume of obtained droplets can be precisely set. At higher values of *Ca* number, shearing forces determine the regime: through dripping mode to the jetting regime, when a jet of fluid is formed from which droplets are eventually pinching off downstream of the junction.

The highest reported performance of droplet generation using a single microfluidic device comprising droplet forming units arranged in parallel reached over 1 trillion in 1 hour and it was practically used for the high throughput production of polymer microparticles [72].

Each droplet in a microfluidic system can be regarded as an individual chemical reactor, creating an attractive opportunity for high throughput screening schemes. Multiple techniques dedicated for manipulation with droplet location and content were developed over the past 15 years.

- Incubation: Biological and chemical assays often require time at which the sample would be kept at a given temperature for the reaction to be completed. Droplets in large quantities can be stored off-chip in an enclosed container – a tubing [73] or an Eppendorf tube [74], in which they can be subjected to the specific conditions required by the reaction protocol (e.g. thermocycling). Alternatively, droplets can be collected and densely packed in wide chambers [75] or immobilized by special structures [76–79]. Locking the droplets in a designated place creates a convenient opportunity for microscope imaging.
- Detection: Droplets can be subjected to various detection techniques. Most commonly optical methods are used to follow the processes taking place in droplets. Several approaches were reported in droplet-based systems. The detection of fluorescence is very sensitive and convenient for measuring of multiple parameters as various fluorophores can be used and imaged simultaneously [80,81]. Other available optical techniques include UV-Vis [82–84], Raman scattering [85] and fluorescence correlation spectroscopy [86]. In

addition droplets were adopted for the detection using mass spectrometry [87,88] and using electrochemical methods [89].

- Sorting: Upon the optical detection of droplet content, based on the feedback from a detector or camera, droplets can be sorted into sub-populations by directing their route into separate outlet channels. Sorting of droplets can be executed actively with the use of electric field [73], laser beam [90], acoustic waves [91] or by inducing mechanical forces with valves [92]. Alternatively, droplets can be passively sorted based on their physical properties (e.g. size [93], viscosity [94]) that allow to distinguish between them.

- Merging and splitting: Despite of microscopic size of individual droplets, techniques that allow for their merging and dividing have been developed. Coalescence of droplets is an important strategy to admix reagents at a desired point of experiment e.g. when the incubation is finished. In addition, merging of droplets in a sequential fashion allows for gradual dilution of reagent and formation of gradient of concentration across the sequence of droplets. In general, in droplet microfluidic systems uncontrolled coalescence of droplets is undesired and is prevented by the presence of surfactant molecules that stabilize the interface of droplets. Therefore, to induce merging of droplets an external force has to be applied, either an alternating electric field [73,81], acoustic radiation forces [91] or thermocapillary effect created with a laser beam [90]. Interestingly, by changing the droplets shape with dedicated structures of channels, droplets can be merged in a passive manner [95,96]. For example, droplets' interface can be expanded and destabilized in order to fuse droplets by squeezing and moving them apart [97].

  Splitting of droplets is less commonly performed than merging in processing of droplets in experimental assays. The motivation behind division of droplets is to remove the excess of reaction volume or to improve the efficiency and precision of droplet formation. Droplets are split in channels when they encounter an obstruction e.g. when the main channel splits into Y-shaped branches [98].

1.3.1.2. Hydrodynamic traps

The constantly expanding use of microfluidic techniques in systems dedicated for biomedical research and diagnostics increases the requirement for devices to be user-

friendly and simple to operate. In the same time, it is desired that the device would perform a wide range of liquid handling protocols. Typical laboratory systems for the control of the flow on microfluidic chip – external valves or syringe pumps, provide good control over the flow rates and allow for programmed execution of protocols. However, these active methods of flow control are expensive and difficult to translate into a stand-alone microfluidic system that could be used by wide range of operators.

In droplet microfluidics the capillary number is low which indicates the dominance of the surface tension over shear forces. The dimensions and geometry of microfluidic channels influence the pressure gradients experienced by droplets. Therefore, at a low value of *Ca* number it is possible to execute operations on droplets based on the geometry of the device, irrespectively of other, external parameters e.g. the flow rate or time delay in the execution of the control of the flows of continuous and dispersed phases. The hard-wiring of operations on droplets into the structure of microfluidic channels has been demonstrated for several applications [99,100]. Most common application is locking of droplets in a fixed position [77,79,101]. Hydrodynamic traps were also used to meter a precise portion of liquid from a random sequence of droplets passing through a series of traps [99]. Merging of droplets in trap structures has been demonstrated for the dilution of droplet content [95,96]. The advantage of traps is that units of single functionality can be combined into modules performing more complex tasks, and that modules can be then arranged into a sequence [99]. This strategy has led to the development of a device in which droplets were metered, diluted and stored [102]. Importantly the device was operated with a pipette and researchers demonstrated the capability of determining Minimal Inhibitory Concentration (MIC) using the microfluidic chip in 5 pipetting steps.

1.3.2. Microfluidic systems for model lipid bilayers

The potential of using microfluidic techniques has been recognized for the development of new systems dedicated for the formation of model lipid bilayers. Over the past 10 years different approaches were demonstrated - both for continuous flow and droplet-based methods. It is important to note that especially in the case of droplet microfluidic devices - a care needed to be taken when adapting the existing microfluidic techniques for the formation of lipid bilayers, considering the character of reagents and low surface tension of lipid encased droplets. The organic solvents required for dispersion of lipids tend to swell the structure of polydimethylsiloxane (PDMS) – a polymer commonly used for fabrication of microfluidic devices [103].

1.3.2.1. Planar bilayers in microfluidic devices

The design of some of the proposed devices was aimed at miniaturizing the BLM setup. Two microfluidic channels were separated by a thin plate with an aperture where a planar lipid bilayer was formed by flushing the channels alternately with aqueous and lipid solutions [104–106]. An important improvement in comparison to the traditional BLM method was to include the imaging of the plane of the bilayer in combination with electrical measurements from the electrodes inserted into the channels (Figure 9a). Pore-forming properties of gramicidin were characterized in the DPhPC bilayer in the presence of various additives [105]. Immediately the potential of using microfluidic techniques for increasing the throughput of bilayer formation was recognized. One of the first microfluidic devices for the preparation of planar bilayers described 15 years ago presents the geometry of channels allowing for forming an array of 9 membranes [107]. Later systems characterized by different levels of complexity and throughput, relying on various manufacturing methods, were proposed. Le Pioufle introduced a concept of producing microapertures in parylene thin layer, sandwiched between two poly(methyl methacrylate) (PMMA) plates with machined wells (Figure 9b) [108]. The microapertures at the bottom of each well served as a support for lipid layer. Suzuki *et al*. fabricated a similar device using hybrid stereolitography technology that had an array of 96 wells, each able to accommodate a lipid bilayer [109]. In addition, an integration of electrodes for parallel ion channel recordings was demonstrated in a 9-well version of the device. Alternatively a set of 8 electrodes was moved between the 12 rows and immersed in wells in a 96-well design to acquire a signal simultaneously from nanopore incorporation [110]. Zagnoni *et al*. constructed a device from 3 plastic, reusable layers clamped together to provide for obtaining 12 bilayers in parallel. A method standard for fabrication of microfluidic chips - soft lithography - was also employed: an array of microfabricated chambers (each ca. 8 pL in volume) adjacent to a channel served for making of more than 100 lipid membranes [111]. The release of fluorescent molecules from microchambers was quantified upon the insertion of alpha-hemolysin nanopores into bilayers.

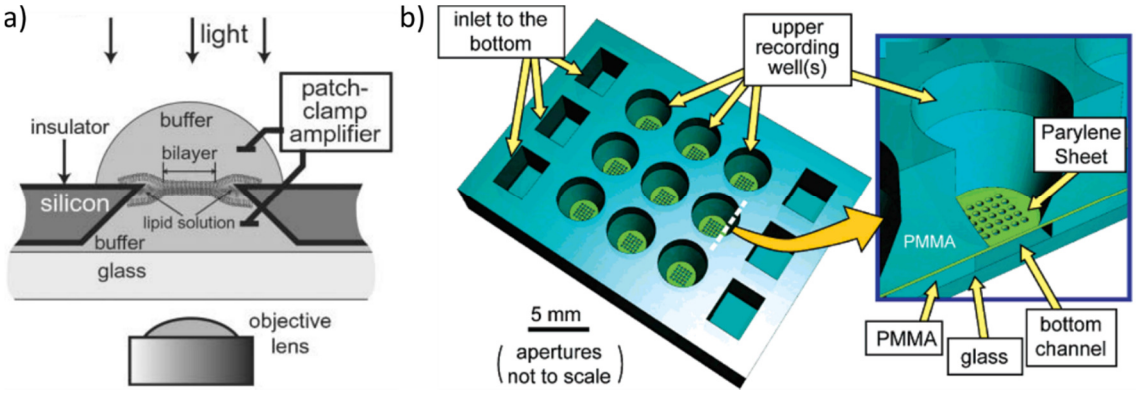

Figure 9 Microsystems for formation of planar bilayers. a) A scheme depicting an experimental setup for making a suspended lipid bilayer, accessible for both electrical measurements and optical imaging. Figure reproduced from [107]. b) Schematic of the lipid bilayer array chip. Recording wells are lined with parylene sheet with microfabricated apertures. Bilayers were formed across apertures from lipid solution introduced through the bottom channel. Figure reproduced from [108].

However, the most effective strategy to obtain a large number of lipid bilayers is to cover sub-microlitre cavities fabricated in a substrate with a lipid layer. Chips with an array of micropores can be either obtained commercially [112] or fabricated. An array of microcavities was fabricated by reactive-ion etching on silicon-on-insulator wafer [113] or by patterning through-holes in a layer hydrophobic polymer deposited on glass [114,115]. The method of phospholipid layer deposition also differed between the proposed systems. GUVs [112] and LUVs [113] with incorporated proteins were spread and ruptured to form suspended lipid bilayers on the array of micropores in silicon wafer. An additional silicon dioxide thin layer with defined pores was used in the procedure including LUVs to reduce the size of apertures accommodating lipid bilayer and to increase the chance of a single protein pore present per one microcavity (Figure 10a). Watanabe *et al.* used a different strategy to prepare an array of bilayers by alternately filling the device with aqueous phase, lipids dispersed in organic solvent and then again an aqueous solution (Figure 10b) [114,115]. The above described methods for bilayer formation allow for obtaining up to 250 000 membranes. The interior of micropores is accessible for optical imaging and quantification of transport rates of fluorophores through protein channels reconstituted in the membrane was quantified. When a limiting amount of membrane transporter proteins was present, a single-molecule analysis could be performed. High number of experimental compartments did not allow for simultaneous electrical measurements, however a version with 16 microcavities with printed electrodes on the bottom of each well was demonstrated [116,117].

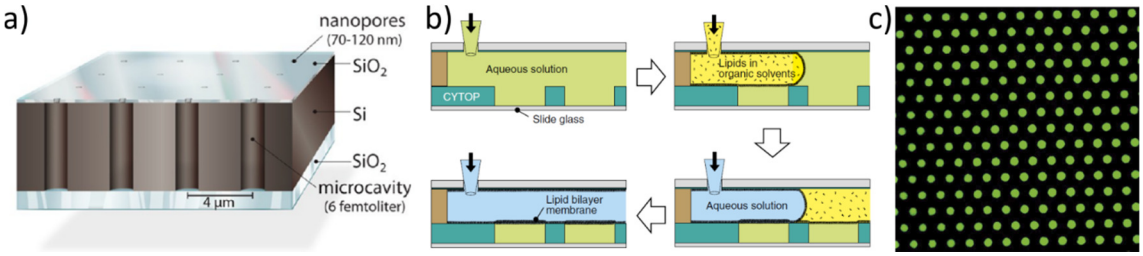

Figure 10 Microarrays for high-throughput formation of planar lipid bilayers. a) Microcavities are etched in silicon on insulator wafer and covered with not-transparent top layer with nanoapertures, that restrict the size of bilayer and block the fluorescence signal from the buffer reservoir on top. The bilayer is prepared by spreading liposomes on the surface of top layer. Figure reproduced from [113]. b) A cross-section view of schematic of microcavities fabricated from carbon-fluorine hydrophobic polymer on a glass substrate. Bilayers are formed by first filling the chip with aqueous solution, then flushing with solution of lipids in solvent followed again by aqueous solution. c) Top image of Alexa 488 encapsulated into microchambers sealed by lipid membranes Figures b) and c) reproduced from [115].

1.3.2.2. Microfluidic systems for DIBs formation

In 2006 Funakoshi *et al*. published a research which is regarded as one of the first attempts to create Droplet Interface Bilayers in a microfluidic device [118]. Apart from encasing hand-pipetted droplets in two circular wells machined in PMMA material, they also produced cross-shaped microfluidic channels. The formation of the interface at the sectional area in microfluidic channels was controlled with syringe pumps, allowing for the control over the size of the interface and for the detachment of bilayer leaflets on demand.

Hybrid devices that combined formation of droplets and their placing on a planar interface between aqueous and organic phase were proven to be promising for construction of automatable systems (Figure 11a) [119–122]. Typically, buffer stored in a custom-made container was covered with a layer of organic phase. Buffer could be exchanged during the experiment to test for various conditions [123], and producing the pendant droplet from an agarose hydrogel increased the stability of bilayer and allowed for high speed solution exchange [124]. The droplet was then carefully placed on a tip of an electrode that could by moved up and down either manually or with the aid of a servomotor to travel through organic phase and then reach the interface to form a bilayer. The principle was further expanded to an apparatus for cyclic formation of bilayers, in which an array of droplets was attached to 32 electrodes connected to a printed circuit board [125].

A variety of strategies directed at efficient bilayer formation at the interface of droplets was demonstrated. Tsuji *et al*. built a device which was first filled with an organic solvent

containing lipid molecules [126]. Then aqueous samples were dispensed into four double-wells. When an inner part of the device was rotated aqueous solutions stored in 4 wells were mechanically divided into 8 droplets. By further rotating the device, droplets were brought into contact to form 4 pairs. A similar simple and low-cost chip relied on a linear acrylic chamber array made from laser-cut PMMA stationary and movable parts in which droplets were deposited by hand in chambers and then interfaced with each other after aligning chambers (Figure 11b) [127].

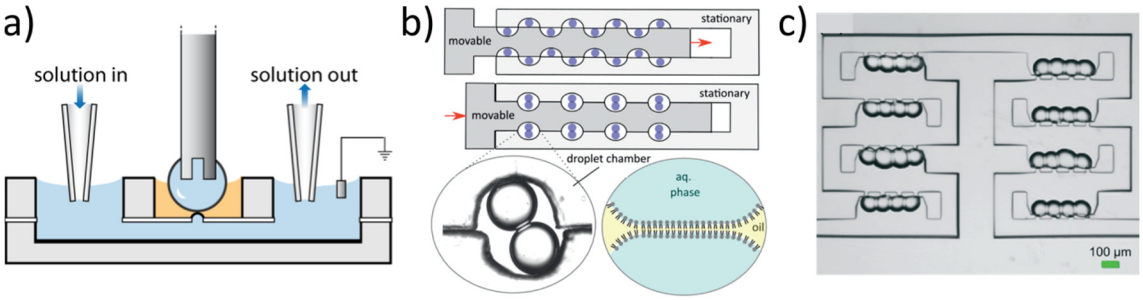

Figure 11 Droplet-based microfluidic systems for formation of bilayers. a) Two fluidic volumes separated by a small aperture serve as bilayer chip. The lower channel was filled with an aqueous solution of proteoliposomes and the central well with n-decane (yellow color in the scheme). A droplet of proteoliposomes solution was deposited on the end of Ag/AgCl pin electrode and lowered to the bottom of n-decane container to form a bilayer in the aperture. The solution in the bottom channel could be exchanged during the experiment. Figure reproduced from [122]. b) Multiplexed formation of droplet interface bilayers in a device comprising movable and stationary chambers, used for the alignment of droplets in pairs. Figure reproduced from [127]. c) Top view of droplets immobilized in special structures – an array of hydrodynamic traps. The design of microfluidic channels was based on equivalent circuit model and enables sequential filling of traps in an array without squeezing-through of the trapped droplets. Figure reproduced from [128].

An important extension of the DIB model membrane system was developed by Lein *et al*. [33]. Two versions of chips were proposed that allowed to actively change the components within droplets – one by reagent addition to one side of the bilayer and the other by perfusion of the solution. The above described systems were easy to manufacture and operate, however they were to a large extent manually operated and suffered from the large volume of droplets. Tonooka *et al*. proposed arrayed chambers for adapting semispherical picolitre volume droplets brought into contact with one large aqueous droplet [129]. The high ratio of membrane area to chamber volume allowed for a quicker detection of Ca^{2+} influx through alpha-hemolysin in comparison to assays on spherical droplets. Further, a reduction of volume of droplets (to 1 nL) and automation of droplet generation, sorting and locking in designated locations for the assembly of an array of DIBs was developed using hydrodynamic trapping (Figure 11c) [128]. A shunt channel of resistance lower than the rest of the device served to discard droplets of incorrect sizes

generated at the T-junction. The droplets that could enter the array of traps were then trapped sequentially either in pairs or in networks of 4. Pads from a thin-film electrode were placed directly under trapped droplets.

1.3.2.2.1. Droplet networks in microchannels

In comparison to conventional bulk experiments, lipid membranes can be formed three to six orders of magnitude faster in microfluidic channels [24]. The difference in time needed for droplet interface being decorated with phospholipid molecules emerges from the fact, that when the droplet flows in a microfluidic channel, the motion within the droplet and hence the advective transport are induced by intrinsic friction. Contrary, for a droplet which is static, the transport of lipids towards water/oil interface is limited to the diffusion and weak convection only. The fast formation of droplets and quick assembly of lipid bilayers in microfluidic channels are important prerequisites to use microfluidic techniques for constructing networks of droplets. Stanley *et al*. pumped water-in-oil droplets into PTFE tubing to form a densely packed 3D array of DIBs [130]. Alternately packing of two types of droplets (containing different lipid solutions) resulted in asymmetric DIBs networks of a regular and predefined pattern (Figure 12b) [131]. Multisomes – assemblies of aqueous droplets encased in an oil droplet in aqueous solution – were also produced on chip, with lipid bilayers providing communication between the droplets and with the external aqueous environment (Figure 12a) [132]. Assemblies of aqueous droplets enclosed in droplets of organic oil could also travel through PTFE tubing filled with another immiscible phase - fluorocarbon oil - for a simple to perform, syringe pump operated, high-throughput formation of DIBs [133]. Networks of droplets interconnected with lipid bilayers served to study transport processes, including diffusion through a membrane and transport through membrane proteins (Figure 12c) [134–136]. The main limitation of the systems aiming at trapping of the linear networks of droplets for monitoring of the translocation of molecules between compartments was that even though the droplets were immobilized, the contact area between them was not defined and could change during the incubation especially in PDMS-made devices due to oil extraction and droplet evaporation.

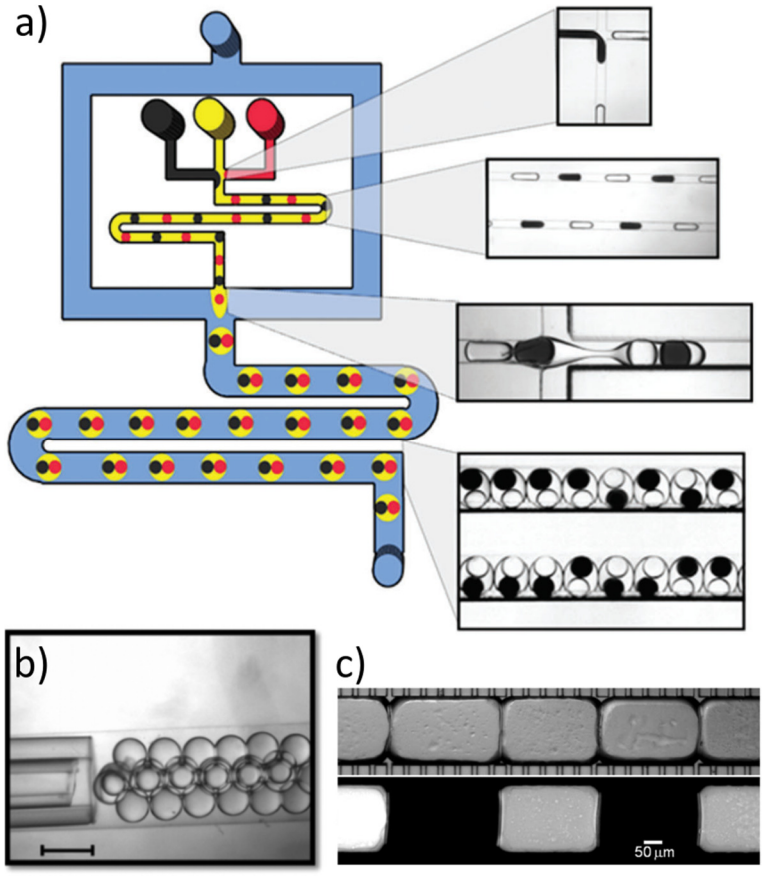

Figure 12 DIBs networks in microfluidic devices. a) Microfluidic generation of multisomes: schematic of a device and corresponding brightfield images of different regions. Alternating droplets of two different components (marked with red and black color) are generated at T-junction with a solution of organic solvent with lipid (yellow). A meander channel allows for the stabilization of a monolayer. Droplet pairs are encapsulated downstream using a flow focusing geometry with the flow of external aqueous solution (blue). The presence of bilayers was confirmed with a diffusion assay. Figure reproduced from [132]. b) Four-row DIB array network produced in a PTFE tubing. Scale bar is 400 µm. Figure reproduced from [131]. c) Droplets collected in a microfluidic channel and squeezed by oil extraction. Alternate droplets contained fluorescein for quantification of diffusion in the network of droplets. Figure reproduced from [134].

1.3.2.2.2. Storable devices for DIB formation

Based on the outstanding stability of DIBs, chips were constructed that could be shipped and deliver a bilayer ready for the user. In first demonstrations, gel encapsulation was used to improve membrane robustness and lifetime of bilayer, still requiring injection and manipulation of multiple phases to assemble functional membrane [137]. Jeon *et al*. relied on a high freezing point of hexadecane (18 ºC) used to arrest bilayer formation [138]. The device could be shipped and upon thawing the formation of membrane by thinning-out continued. Similarly flash freezing of a vial with aqueous solution on the bottom and organic lipid phase on top, with a droplet floating in the upper part, was used to make a storable device in which a droplet fell on water/oil interface upon thawing [139]. An

approach called the regulated attachment method was developed by Sarles *et al*. for reproducible formation of lipid bilayers placed within the flexible PDMS substrate [140]. Droplets enclosed in 2 wells were brought into contact and de-attached in a controlled manner by mechanical squeezing and stretching of the substrate. In an attempt to construct cell mimics, droplets of lipid-in-oil solution were injected into pieces of agarose hydrogel, followed by the injection of droplets containing protein pores into the oil droplets stored in the hydrogel [141]. The compartments were able to communicate through separating them pieces of hydrogel. Baxani *et al*. have shown that closing of bilayer networks in hydrogel shell can be automated and fully performed using microfluidic devices [142]. An attractive strategy to further increase the durability and portability of lipid bilayer is to encapsulate droplets or networks in a thermo-reversible organogel formed from hexadecane and poly[styrene-b-(ethylene-co-butylene)-b-styrene] (SEBS) triblock copolymer [143,144].

1.3.2.2.3. Alternative approaches to droplet manipulation

Typical methods to control the flow in microfluidic chips rely on the use of external devices (syringe pumps, pressurized flow systems). Alternative microfluidic driving mechanisms are dielectrophoresis (DEP) and electrowetting on dieletric (EWOD) in which samples are manipulated with electrical signal. Both DEP [145] and EWOD [146] were demonstrated to be capable of moving the droplets covered with lipid monolayers into contact to form a lipid bilayer at the interface of droplets. Optical manipulation is another strategy aimed at moving nanoliter aqueous droplets submerged in oil. By using illumination with infrared laser a thermocapillary effect and convective fluid motion within the droplets covered with phospholipids was induced in a work published by Dixit *et al*. [147]. Upon optical illumination, interactions of pairs of droplets and adhesion are induced, with a selective bilayer disruption realized using near-infrared light. Optical tweezers were also employed to construct 3 dimensional pyramidal structures from cell-sized droplets with lipid bilayers interconnecting them (optiDIBs) [148].

1.4. Research objectives

Microfluidic techniques, especially droplet microfluidics, have been proven for more than 10 years to have a great potential in construction of microsystems dedicated for formation of model lipid bilayers. The use of microfluidic methods increased the stability, accessibility and throughput of preparation of artificial membranes. In this doctoral dissertation, by exploring various aspects of droplet microfluidics, we addressed the gaps in existing experimental solutions for Droplet Interface Bilayers formation.

First, the need for an automated formation of DIBs was recognized. In droplet microfluidic systems the operations on droplets can be performed in automated fashion thanks to the precise control over the flow of reagents in microchannels. The first objective was to construct a system in which droplets would be moved on chip and bilayers formed according to a desired protocol. The system should be capable of droplet formation, positioning droplets in pairs aided by optical feedback and precise separation of them. The aim was to use the droplet microfluidic device for screening of membrane proteins activity i.e. the determination of binding kinetics of small molecules to the membrane channel. In order to be able to perform this task, the proposed system needed to be equipped with electrodes for single-channel measurements. Additionally, the device had to provide immobilization of one of the droplets from a pair (comprising solution of proteins) and exchange of the other one (droplets containing inhibitors).

The second research objective focused on implementing the automation and control over individual droplets in networks of droplets. So far, the extraction and manipulation with individual droplets from a network was limited to manual operations. A microfluidic system in which droplets are generated and exchanged on demand and the transmission of electric signal through the network can be studied should fill the existing gap.

The third objective was motivated by the fact, that often the availability of protein sample is limited. Therefore, a microfluidic system dedicated for studying of properties of membrane proteins should operate on small volumes of samples and be capable of basic preparatory steps. The third goal set in this dissertation was aimed at developing droplet microfluidic system in which on-chip dilution of a sample would be included as a part of experimental scheme.

CHAPTER 2.

Materials and Methods

In this Chapter we detail the materials used in the projects, the methods of preparation of samples, fabrication of microfluidic devices, constructing of setups and approaches to data analysis.

2.1. Reagents

1,2-Diphytanoyl-*sn*-glycero-3-phosphocholine (DPhPC, Avanti Polar Lipids, USA), 1,2-dioleoyl-*sn*-glycero-3-phosphocholine (DOPC, Avanti Polar Lipids, USA), hexadecane (Sigma-Aldrich, Germany), silicone oil AR20 (Sigma-Aldrich, USA), gamma-cyclodextrin (Cyclolab, Hungary), TRIS.HCl (Roth, Germany), KCl (Chempur, Poland), $CaCl_2$ (Chempur, Poland), Rhodamine 110 chloride (Sigma-Aldrich, USA), Fluo-8H (AAT Bioquest, USA), fluorescein isothiocyanate FITC (Sigma Aldrich, USA), HEPES (Sigma-Aldrich, USA), alpha-hemolysin (Sigma-Aldrich, USA), EDTA (Sigma-Aldrich, USA), low-melting agarose (Roth, Germany), silver wires (100 µm in diameter, Sigma-Aldrich, USA), chloroform (Chempur, Poland), sodium hypochlorite (Sigma-Aldrich, USA) were used as received.

2.1.1. Lipid solutions

The lipid in oil solutions were prepared first by dissolving phospholipid in chloroform. The chloroform was evaporated under a gentle stream of nitrogen followed by incubation in the vacuum to remove any residues of solvent. In the case of DPhPC, lipid film was re-solubilized in a mixture of:

- 75% v/v hexadecane and 25% v/v silicone oil AR20 at 1 mg/mL (in Chapters 3 and 4),
- 90% v/v hexadecane, 10% v/v AR20 at 0.01 - 1 mg/mL (in Chapter 5),
- 90% v/v hexadecane, 10% v/v AR20 at 0.5 mg/mL (in Chapter 6).

DOPC was dissolved at 2.5 mg/mL in the mix of 95% v/v hexadecane and 5% v/v AR20.

2.1.2. Protein expression and purification

In the experiments described in Chapter 3 and Chapter 5 we used purified heptamers provided by Hagan Bayley's group from the University of Oxford. Wild-type *α*HL was expressed in *Staphylococcus aureus*, converted to heptamer with deoxycholate and purified by SDS-polyacrylamide gel electrophoresis as described [149]. We kept the stock solution (50 µg/mL) on ice at all times and diluted 10-fold in buffer prior to introduction onto the microfluidic chip.

Alternatively, in the experiments in Chapter 4 and Chapter 6, we used a mixture of monomers and heptamers from Sigma-Aldrich.

2.2. Fabrication of microfluidic devices

The polycarbonate chips were fabricated from 2-, 3- or 5-mm thick plates (Macrolon, Bayer, Germany) using a CNC milling machine (MSG4025, Ergwind, Poland). The milled two plates were then thermally bonded by compressing them together for 30 min at 130°C at 0.4 MPa. Dimensions in parts of the devices were below 100 µm and fabrication of polycarbonate devices with small features is a challenging task. The desired precision of milling should be below 10 µm or even less. To improve the precision of micromilling following remarks and approaches might be taken into consideration:

- The footprint of the small structures (e.g. set of traps) should be arranged into a small space and designed into square shape.
- The tilt of the polycarbonate plate should be avoided, however sometimes is not possible to reduce the tilt below 10 µm. In that case the surface of the polycarbonate plate can be initially probed by the milling tool (e.g. by making point marks) and the depth of paths of the milling tool can be adjusted.
- Fabrication of a series of devices milled on the same large plate, differing by the depth (e.g. 5 µm), can mitigate the problems with precision of CNC machine. Then from a series of devices at least one should perform in a desired fashion.
- The pressure used for bonding of devices should be adjusted to be as small as possible to avoid the deformation of structures of channels.

2.3. Microfluidic setups for automated formation of droplet interface bilayers

2.3.1. General description of the experimental system

The experimental setup (Figure 13 and Figure 14) consisted on:

- Axon Axopatch 200B Capacitor Feedback Patch Clamp Amplifier (Molecular Devices, USA),
- Axon Digidata 1440A Digitizer (Molecular Devices, USA),
- Function generator GFG8216A (ISO-TECH, RS Components, United Kingdom),

- Oil containers, pressurized by an outer compressor using a manual pressure regulator (Bosch Rexroth PR1-RGP) and monitored the pressure using digital manometers (AZ 82100, AZ Instruments),
- Electronic valve driver, which is controlled by a NI PCIE-6321 card (National Instruments, USA) on a desktop computer,
- A set of electromagnetic valves (V165, equipped with Z070D coils, Sirai, Italy),
- Faraday cage AE1033 (Rittal, United Kingdom),
- USB2 uEye SE camera (IDS, Germany),
- Syringe pump neMESYS (Cetoni, Germany),
- Positioning system Rotaxys (Cetoni, Germany).

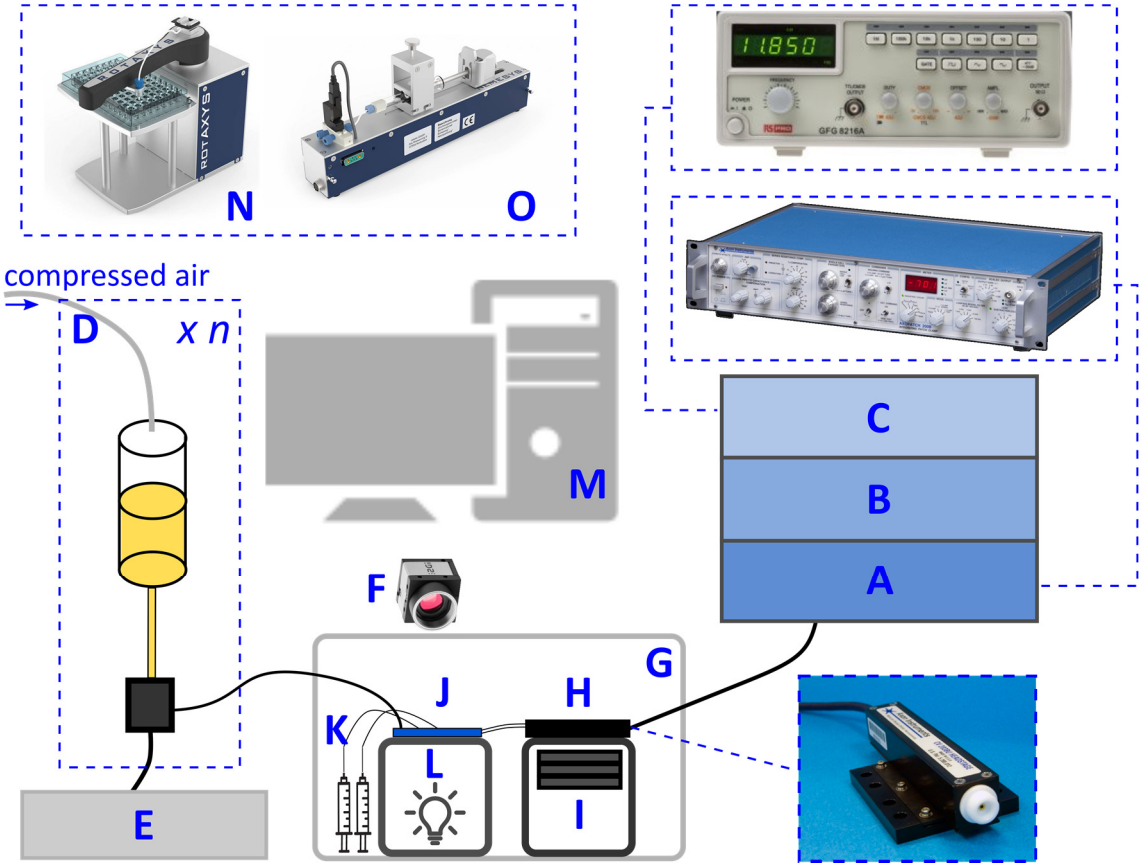

Figure 13 Scheme of the experimental setup. A – amplifier, B – digitizer, C – function generator, D – a set of pressurized oil containers connected to electromagnetic valves, E – electronic valve driver, F – camera, G – Faraday cage enclosure, H – headstage, I – radiator, J – microfluidic chip, K – syringes, L – light source, M – computer, N – positioning system, O – syringe pump. Source of images: A, H: moleculardevices.com, C: rs-online.com, F – ids-imaging.com, K, L, M: flaticon.com, N, O: cetoni.de.

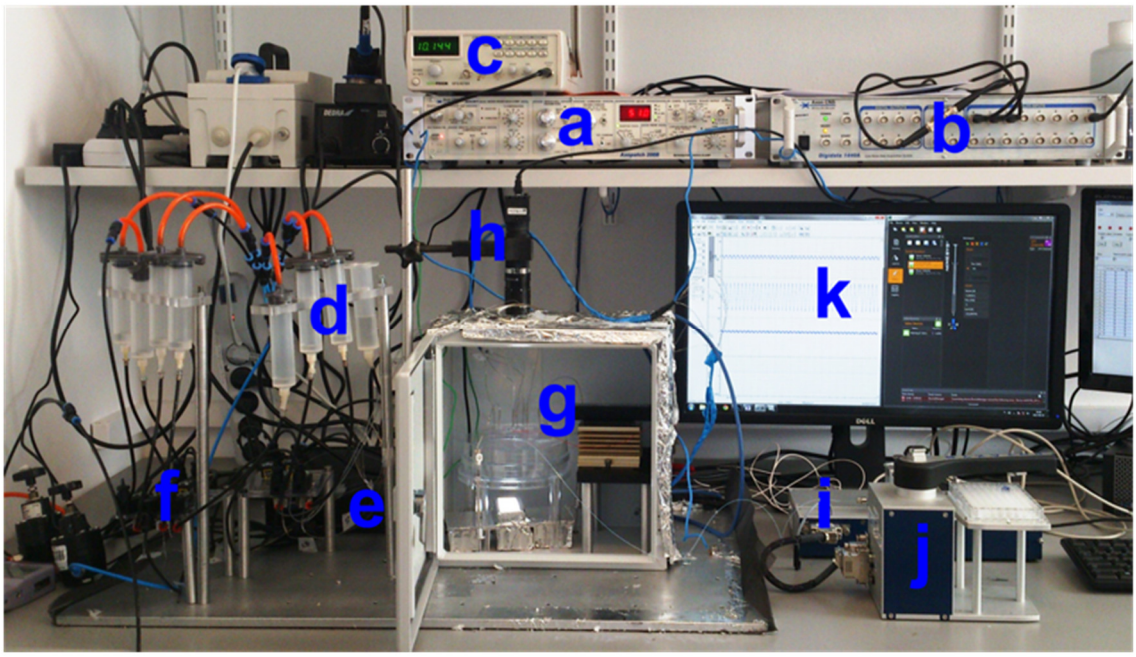

Figure 14 A photograph of the experimental setup. a – amplifier, b – digitizer, c – function generator, d - a set of pressurized oil containers, e – electronic valve driver, f – a set of electromagnetic valves, g – Faraday cage, h – camera, i – syringe pump, j – positioning system, k – computer with software to control valves, syringes, and acquire image from camera and signal from amplifier.

The interior of Faraday enclosure contains:

- A glass syringe filled with buffer,
- A glass syringe filled with protein solution,
- A source of white light OF-SMD5060NW-H (OptoFlash, distributed by TME Electronic Components, Poland),
- The chip positioned on a custom-made platform with transparent bottom,
- A headstage with electrodes (Molecular Devices, USA), placed on a radiator and connected to Axopatch 200B amplifier.

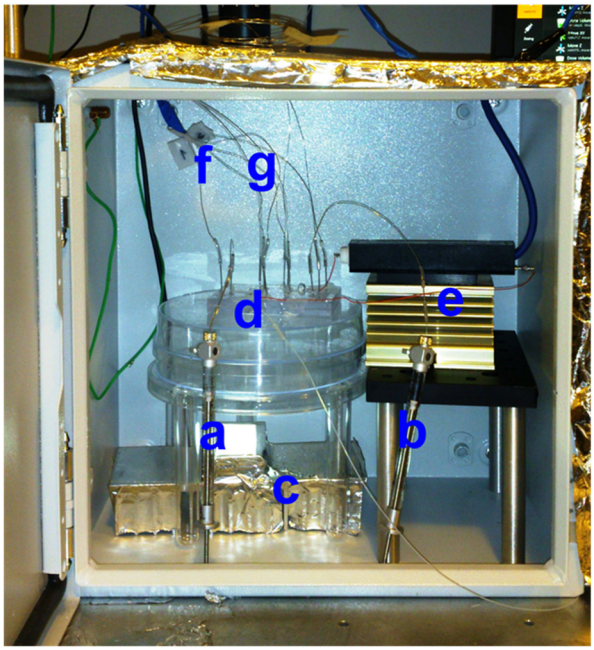

Figure 15 A photograph of the interior of Faraday cage: a – a syringe filled with buffer, b – a syringe filled with protein solution, c – a source of light, d – microfluidic chip positioned on a custom-made transparent platform, e – headstage with electrodes, placed on a radiator.

2.3.2. Control of flow with external valves

We used either 9 (for DIBs formation between a pair of droplets) or 12 (for automated dilutions of sample on chip, droplet networks) electromagnetic valves to operate microfluidic chips [150] (Figure 16). The oil was stored in pressurised containers and connected to valves via a polyurethane tubing (O.D. 8 mm, I.D. 6 mm). The pressure in the containers was controlled using manual regulators and measured with manometers. The oil was supplied from valves into the chip through steel capillaries (ca. 1 m length, O.D. 400 µm, I.D. 205 µm, Mifam, Poland). We used resistive steel capillaries to connect the device to the external electromagnetic valves. The use of steel capillaries of high fluidic resistance allows for precise control of the flow on the chip and the performance of iterative operations, including generation of droplets on demand. Alternatively, the waste chemicals were evacuated from the chip through PTFE tubing into valves, from which they were collected into a reservoir.

The opening and closing of the valves were controlled using a Lab View script through a PCIE-6321 card. The construction of valves enables to control their state by the generation of rectangular pulses of voltage, which control the bi-stable coils. The high state of pulses results in an open valve, while the low state represents a closed valve. In

addition, for the automated control of location of droplets on chip we used an edge-detection algorithm.

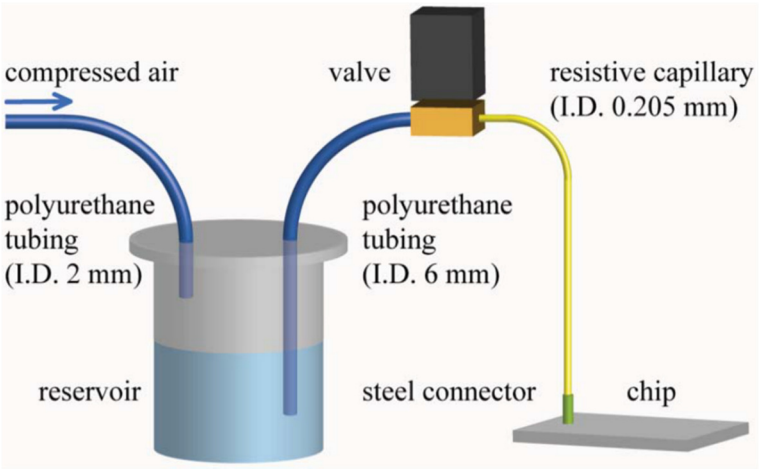

Figure 16 Experimental setup for controlling the flow with electromagnetic valves. Pressurized air is supplied to a reservoir through polyurethane tubing. From a reservoir oil flows to the valve through polyurethane tubing and from the valve to the microfluidic chip continuous phase is supplied via resistive steel capillary. Figure reproduced from [150].

2.3.3. Connection between microfluidic chip and external valves

Steel needles (1 – 4 cm long, O.D. 0.82 mm, I.D. 0.65 mm, Fishman Corporation, USA) served as inlet ports to microfluidic chips.

In the device for formation of pairs of droplets, 7 of the inlet needles were connected to valves with 100-cm long steel capillaries using segments of Tygon tubing (~2 cm, O.D. 0.91 mm, I.D. 0.25 mm, Ismatec, Switzerland). One of the capillaries was extended with a short piece of HPLC tubing (10 cm, PEEK Tubing 1/16" x 0.0025", Upchurch Scientific, USA) in order to increase the resistance to flow. 2 out of 9 needles were connected through 10-cm PTFE tubing (O.D. 1.6 mm, I.D. 0.8 mm, Bola Bohlender, Germany) with 500 µl syringes, each equipped with a built-in valve (1750SL Gastight, Hamilton, USA), which were used to store and introduce onto the chip pure buffer and the protein solution. 2 of the ports, which served as outlets, were connected with valves via 50-cm PTFE tubing. Additionally, a PTFE tubing (length 3 cm, O.D. 1.0 mm, I.D. 0.5 mm, Bola Bohlender, Germany) was connected with epoxy glue (EA 3430, Henkel Loctite, USA) to one of the channels directly.

In the device, in which we explored the possibility of automated diluting of a protein sample, 13 needles were regarded as inlet ports. 10 of them delivered oil to the chip through 100-cm long capillaries, out of which 1 was extended with a piece of PEEK

tubing (10 cm, PEEK Tubing 1/16 x 0.0025, Upchurch Scientific, USA), 3 were used for introduction of aqueous samples from syringes. 2 needles were connected to valves via PTFE tubing and were used as outlets.

In the device, that served for formation of networks of droplets, 11 needles were regarded as inlet ports. 8 of them delivered an oil to the chip through 100-cm long capillaries (out of which 3 were extended with pieces of HPLC tubing), 3 were used for introduction of aqueous samples from syringes. 4 needles were connected to valves via PTFE tubing and were used as outlets.

A sequence of droplets that contained various concentrations of inhibitors was prepared by using a precise syringe pump (Nemesys, Cetoni, Germany). Droplets were formed inside PTFE tubing (O.D. 0.6 mm, I.D. 0.3 mm, Bola Bohlender, Germany) by alternating aspiration of portions of aqueous samples (300 nL) and oil (700 nL) from a standard 96-well plate (Greiner Bio-One, Austria). The sequence of droplets containing various concentrations of inhibitors was stored inside the tubing and introduced onto the chip by applying the flow from a syringe.

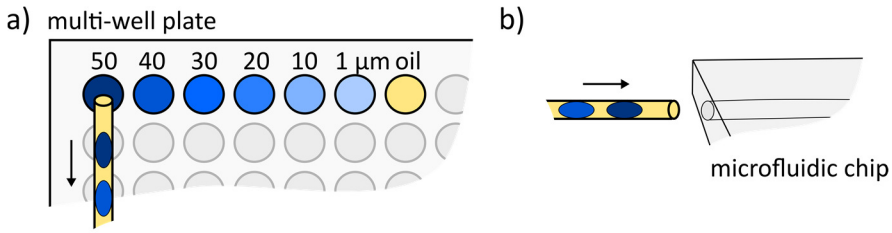

Figure 17 Using a precise syringe pump a sequence of droplets containing inhibitors was prepared by alternately aspiring portions of aqueous samples (300 nL) and oil (700 nL) from a standard 96-well plate into PTFE tubing. The sequence of droplets with various concentrations of inhibitors was stored inside the tubing before being introduced onto the microfluidic channel by applying the flow from a syringe.

2.4. Electrical recordings

We used Ag/AgCl electrodes for electrical measurements. The electrodes were prepared in the following way. In the first step pieces of silver wires of 100 µm in diameter were kept immersed in sodium hypochlorite solution overnight (12 h). Next, the tips of the electrodes were submerged in molten agarose (1% w/v), diluted in 1M KCl, 10 mM Tris.HCl, pH 7.0 buffer. Electrodes were inserted into the chambers of the trap prior to running an assay and then fixed with epoxy glue (Poxipol, Poland).

We used patch-clamp amplifier Axopatch 200B (Molecular Devices, USA) for recordings of the electrical current. The signal was acquired with a 1 kHz low-pass Bessel filter at a sampling rate of 10 kHz. We used a 400 Hz Gaussian filter to filter the electrical recordings for the analysis of single channels and capacitive current, and a 100 Hz filter for display only.

2.4.1. Size estimation from the measurements of capacitive current

We applied a potential of triangular wave shape to the bilayer (10 Hz, 50 mV peak-to-peak) and recorded the resulting square wave current at a 1 kHz sampling rate. Formation of a bilayer causes a rapid increase in the measured capacitive current, which amplitude is corresponding to the size of a bilayer:

$$I_C = \frac{C_T \times dV}{dt} \qquad \text{Eq. 4}$$

where:

- I_C – capacitive current [A]
- dV/dt – rate of change of potential [V/s]
- C_T – capacitance [F]

C_T equals to $C_M \cdot A$ (C_M – specific capacitance [F/m^2], A – area [m^2]). Using the literature value of specific capacitance for a given phospholipid in a given oil the size of a bilayer can be directly calculated.

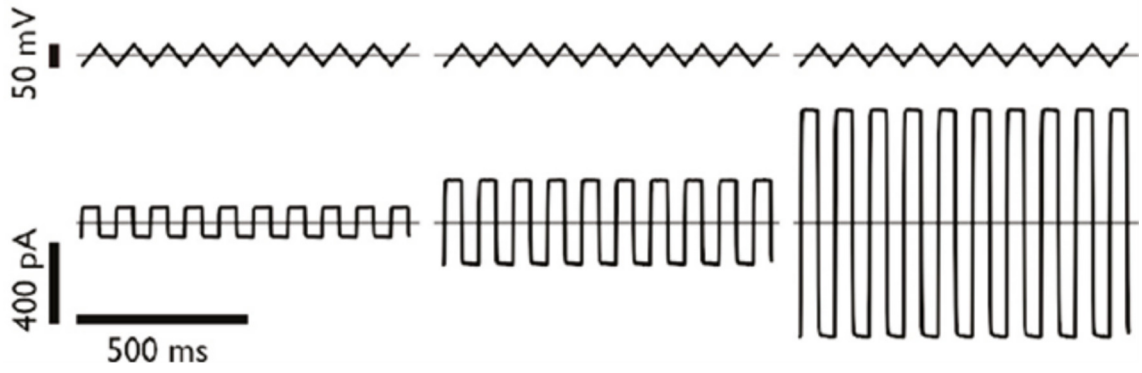

Figure 18 Schematic explaining the measurements of capacitive current. Upon the application of triangular potential (upper trace), a square wave current trace is recorded (lower trace). The amplitude of the square wave depends on bilayer area and is proportional to the bilayer capacitance. The current trace indicates increasing size of a bilayer (from left to right). Figure reproduced from [47].

2.4.2. Analysis of electrical recordings - calculations of dissociation constant K_d

Measurements of *α*HL activity in the presence of gamma-cyclodextrin were performed at +50 mV, the protein was contained in a droplet at a working electrode. We used 6 concentrations (1 – 50 μM) of *γ*CD. Only the traces that reflected the activity of single *α*HL pores were analysed. We performed the calculations of rate constants as follows:

- For data analysis, we used results from at least three different experiments from single channel recordings with an entire duration of at least 120 s.
- We derived the dissociation rate constants, k_{off}, at each concentration as the inverse of the mean residence time (τ_{off}) of *γ*CD within the pore.
- We obtained the association rate constants, k_{on}, from the slope of a plot of the inverse of the mean inter-event interval (τ_{on}) versus the concentration of *γ*CD. We calculated weighted mean K_d (k_{off}/k_{on}) values and weighted mean SDs because of the length of single-channel recordings between the experiments.

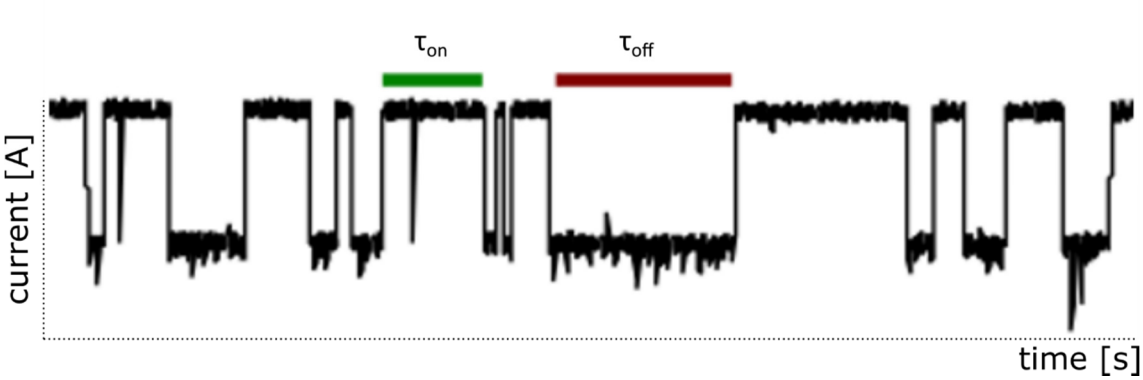

Figure 19 Analysis of current trace for calculations of dissociation constant. Schematic presents a fragment of current trace of single *α*HL pore blocked with cyclodextrin molecules. For each obtained single-channel recording, the time when the pore stays open (τ_{on}) is summed and the duration of channel blocking (the drop in current, τ_{off}) is measured.

2.5. Microfluidic setup for passive formation of droplet interface bilayers

2.5.1. General description of the experimental system

The experimental setup (Figure 20) consisted on:

- A set of 4 syringe pumps neMESYS (Cetoni, Germany),
- 4 syringes (series 1700 RN, Hamilton, USA) mounted on syringe pumps,

- Microfluidic chip,
- A1-R Eclipse Ti-E confocal microscope (Nikon, Japan),
- USB2 uEye SE camera (IDS, Germany),
- A source of white light OF-SMD5060NW-H (OptoFlash, distributed by TME Electronic Components, Poland).

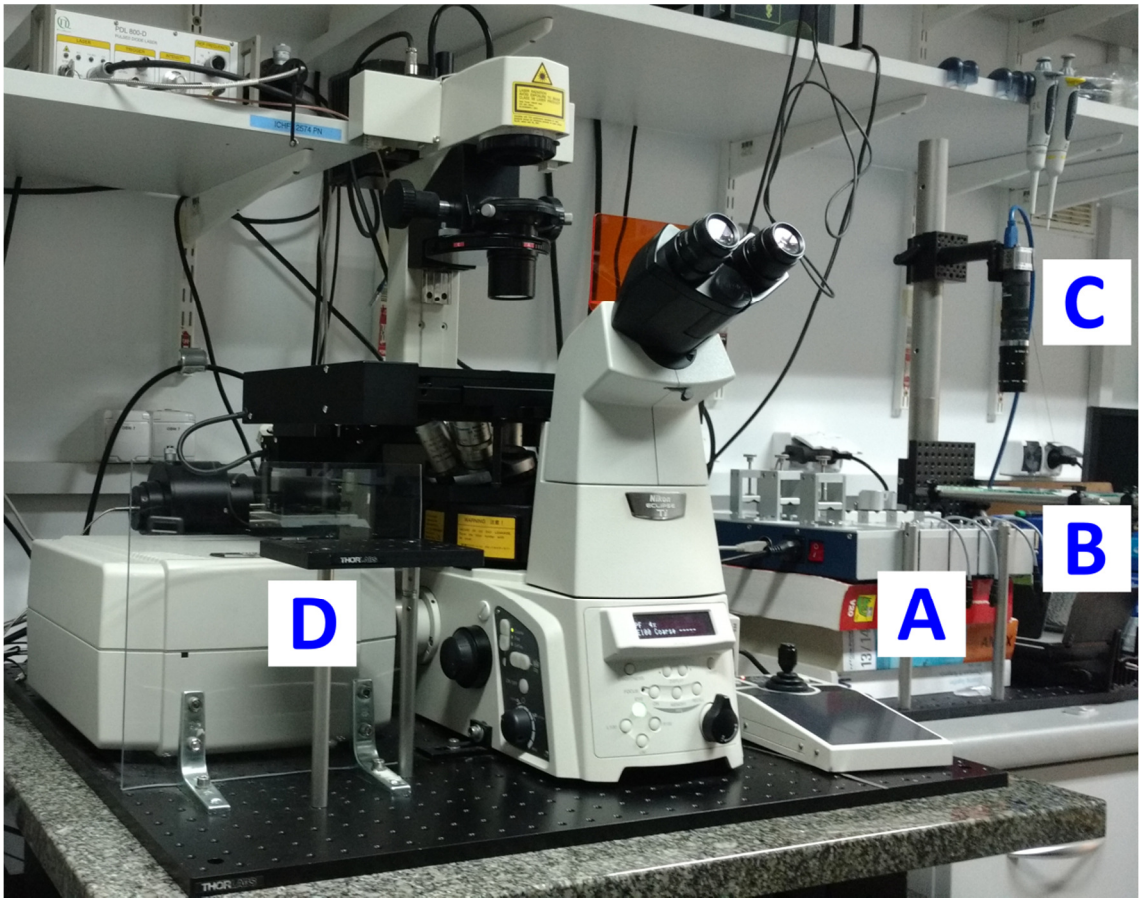

Figure 20 A photograph of the experimental setup. A: a set of 4 syringe pumps with mounted syringes, B – a stage with a light source at the bottom for imaging of microfluidic chip with a camera (C), D – confocal microscope.

2.5.2. Control of flow with syringe pumps

The flow of fluids was controlled by set of Nemesys syringe pumps (Cetoni, Germany). The continues phase, as well as aqueous samples, were supplied to the chip from gastight glass syringes (series 1700 RN, Hamilton, USA) connected to the chip through PTFE tubing (O.D. 1.6 mm, I.D. 0.8 mm, Bola Bohlender, Germany). To minimize the consumption of aqueous samples, we first filled the syringes with hexadecane, and then aspirated the small amount (10 – 20 µL) of a sample into the PTFE tubing, before connecting it to the inlet needles.

2.5.3. Fluorescent microscopy and data analysis

A1-R Eclipse Ti-E confocal microscope (Nikon, Japan) with 10x objective was used to acquire fluorescence images. We used excitation/emission wavelengths of 488/500-550 nm to record fluorescence signal from FITC, rhodamine and Fluo-8H dyes. The images from experiments were analysed in NIS-Elements AR software (Nikon, Japan). The perimeter of fluorescent donor FITC droplets was used for determination of the diameter of droplets analyzed in NIS-Elements AR (Nikon, Japan) software. The diameter of bilayers was measured in ImageJ software (National Institutes of Health, USA).

Fluorescein permeation experiment: Mean volume of droplets and area of bilayers were calculated with the assumption of spherical shape of droplets and circular area of bilayers. Droplets in pairs were located on different levels in the storage wells (53 μm difference in Z-position between donor and acceptor droplets), therefore we adjusted the level of the objective according to the middle plane of droplets. Using the software for image acquisition we extracted the mean intensity data from rectangular regions of interests (ROIs) located inside droplets. Those data were recalculated into the concentrations of FITC, assuming the linear correlation between the intensity and concentration.

Calcium permeation through *α*HL pores experiment: Mean volume of droplets and area of bilayers were calculated with the assumption of spherical shape of droplets and circular area of bilayers. We imaged the droplet containing Fluo-8 dye in the middle plane of droplets. Using the software for image acquisition we extracted the mean intensity data from rectangular regions of interests (ROIs) located inside droplets and used these values for further analysis.

CHAPTER 3.

This chapter demonstrates a microfluidic system that automates:

i) formation of a lipid bilayer at the interface between a pair of nanoliter-sized aqueous droplets in oil,

ii) exchange of one droplet of the pair to form a new bilayer,

iii) current measurements on single proteins.

A new microfluidic architecture is introduced - a hydrodynamic trap designed to localize the droplets with respect to each other and with respect to the recording electrodes. The system uses active control of the flow on chip with the use of simple external valves for automated execution of experimental protocols. We also describe here the use of the system in formation of stable artificial lipid bilayers, incorporation of alpha–hemolysin into the bilayers and electrical measurements of ionic transport through the protein pore.

3.1. Introduction

In this chapter we present an automated microfluidic system that combines the active manipulation of liquids [83,151] with passive positioning of droplets [99,101,152], and the capability to insert electrodes into the droplets for *in situ* electrical measurements on membrane proteins incorporated into a DIB. We show repetitive formation of DIBs, separation of the droplets and exchange of at least one droplet of a pair to form a new DIB, all in an automated sequence.

The technique of Droplet Interface Bilayers may evolve to a high-throughput screening platform by implementing automation. For screening applications, it is essential that the microfluidic system is capable of automated generation and manipulation of multiple droplets. Droplet on demand systems provide a high degree of control over the composition and location of each droplet [153]. Although, the generation of DIBs and networks of droplets has been demonstrated on a chip, a remaining challenge was to interface electrodes for repetitive measurements of bilayer capacitance and of conductance through single channels and pores.

3.2. Results

3.2.1. Layout of the microfluidic device

Figure 21 depicts the scheme and fabrication details of the device. In general, the width of the channels is 400 μm, except for the channels supplying the oil for separation of droplets, which have width of 200 μm. The depth of the channels equals to 400 μm, with the exception of the varying height in the trapping region, which 3D profile is depicted in Figure 21b and Figure 22b. The two cavities (dark grey in Figure 22b) lock the position of droplets by capillary forces. The shallow bypasses (marked with the light grey in Figure 22b) allow for small flow of oil around the droplets without distorting their position.

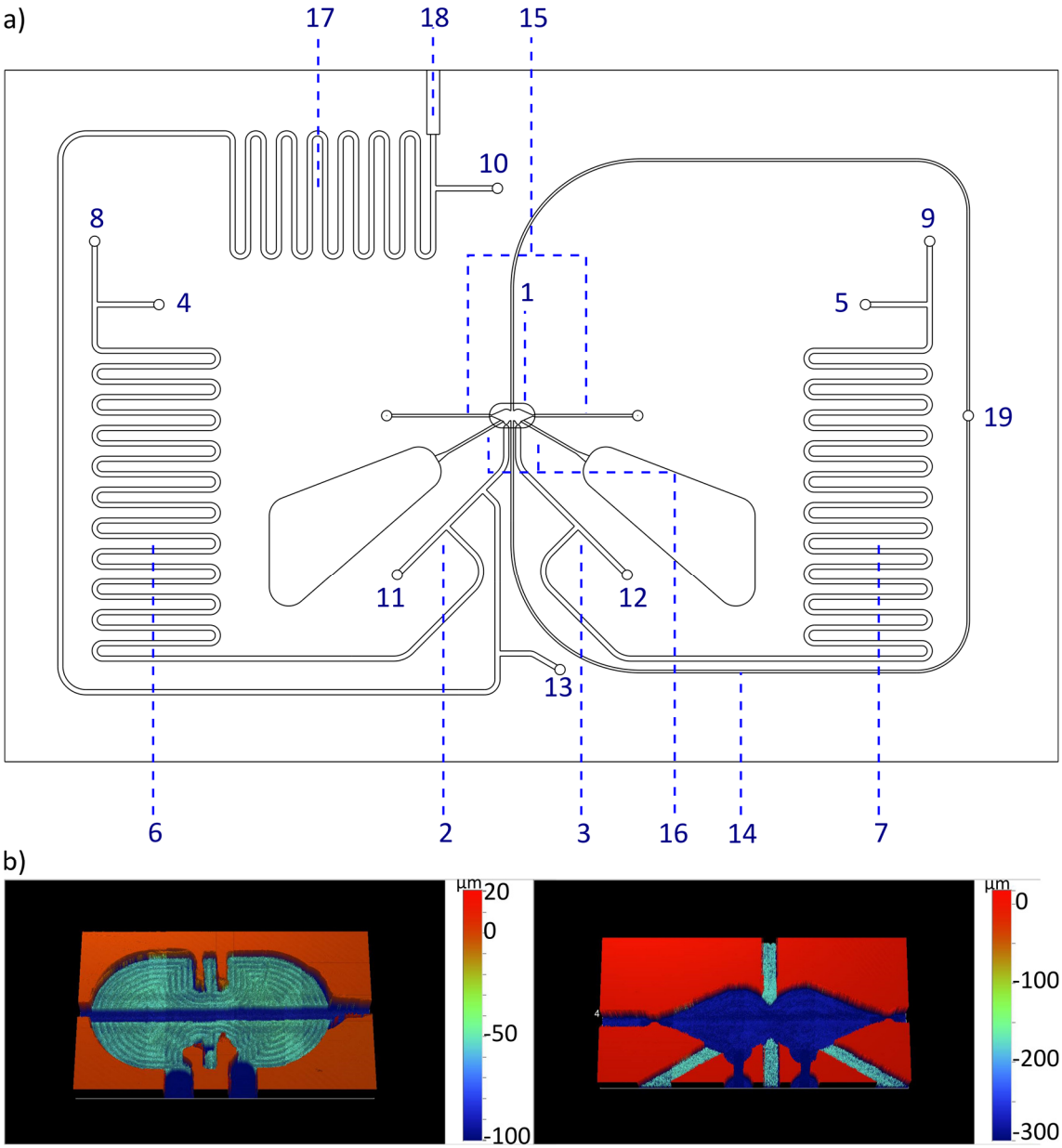

Figure 21 Geometry of the microfluidic device. a) Detailed diagram of the layout of the microfluidic chip. The numbers indicate: 1 - hydrodynamic trap, 2 - T-junction for generation of droplets with buffer, 3 - T-junction for generation of droplets with protein solution, 4 - inlet for the buffer, 5 - inlet for the protein solution, 6 - channels used as a container for buffer, 7 - channels used as a container for the protein solution, 8, 9 , 10, 11, 12, 13, 19 - inlets for oil, 14 - channel which supplies oil for the detachment of droplets, 15 - outlet channels, 16 - channels for the pair of electrodes, 17 - channels used as a container for the sequence of inhibitors, 18 – inlet for the tubing containing a sequence of droplets with various concentrations of inhibitor. The dimensions of a whole chip are 82 x 53 mm. b) The architecture of the microfluidic trap depicted with profilometric scans (Bruker ContourGT-K). Parts of the trap were milled in both polycarbonate plates. Upper plate (left panel) comprises the bypasses and parts of main channels and chamber of the trap. In the lower plate (right panel) the auxiliary channels for electrodes, perpendicular channels for separation of droplets and other part of the chamber were milled.

The chip main parts are: i) a microfluidic trap with electrodes (‘N’, Figure 22b) in which droplets are contacted to form a DIB, ii) two microfluidic T-junctions (‘D’ and ‘G’) with

additional sample-ports, and iii) an inlet port for a sequence of droplets containing various inhibitors ('F').

3.2.2. Operation of the microfluidic device

First, the microfluidic channels were filled with a continuous organic phase containing lipids (1 mg mL^{-1} DPhPC in 75% hexadecane and 25% silicone oil AR20). Then, through the inlet ('B') we transferred a small volume (tens of microliters) of buffer (1 M KCl, 10 mM Tris-HCl, pH 7.0) from a glass microsyringe. We used the port ('I') to introduce a small volume of the protein solution (alpha-hemolysin wild-type, 5 µg mL^{-1}, diluted in the same buffer). The deposition ports were closed with build-in valves and from the inlets ('A' and 'J') we opened the flow of oil in order to push the aqueous plugs to the front of T-junctions. There, a defined volume of the aqueous sample was pushed into the orthogonal channel and then broken-off with the flow of oil. A sequence of droplets containing inhibitors was deposited on the chip in a similar manner as the other aqueous samples (through the ports 'F' and 'E'), with the exception that it did not require further partitioning in the T-junction geometry. The AgCl and agarose coatings allowed for sufficient wetting of droplets to the electrodes and electrical connectivity was stable when a chip was tested intensively over a period of 3 weeks.

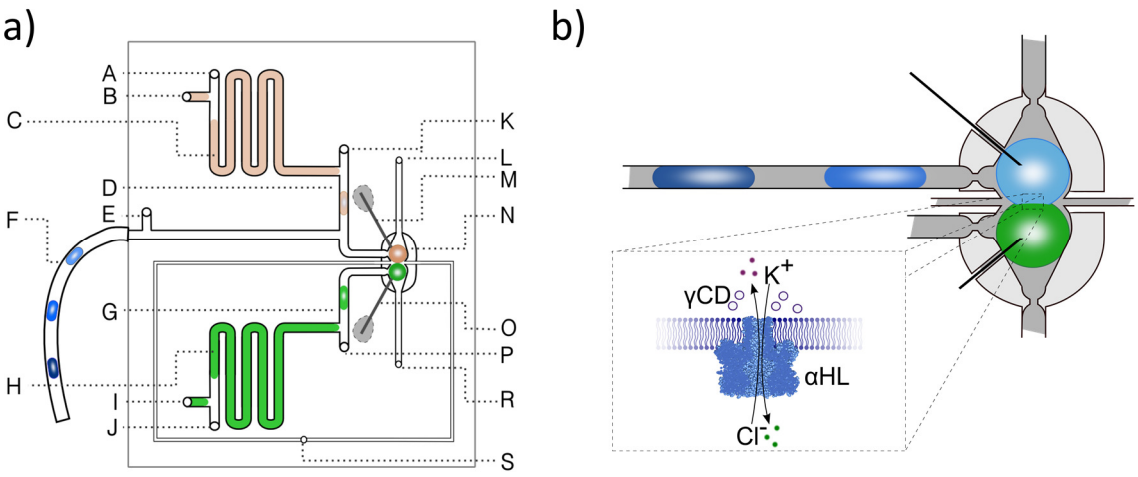

Figure 22 Operation of the microfluidic device. a) Schematic diagram of the microfluidic chip: A, E, J, K, P – inlets for oil, B, I – inlets for aqueous samples, C – aspiration module with pure buffer for washing of electrodes, D, G – T-junctions, F – tubing with a sequence of droplets containing inhibitors, H – aspiration module with a solution of proteins, M – ground electrode, N – hydrodynamic trap, O – working electrode, S – inlet for oil in a control channel, L, R - outlets b) Schematic picture of the microfluidic trap with the DIB inside. The membrane is formed at the interface of two droplets locked in the trap filled with oil. So called 'bypasses' (shallow parts of channels) are indicated with the light-grey color. The continuous liquid (oil) passes through the bypasses while the droplets are locked in the position.

3.2.3. Characterization of the bilayer at the interface of 2 droplets

The kinetics of formation of DIB in the hydrodynamic trap was monitored in two ways: visually with a video camera (Figure 23) and by capacitance measurements of the membrane (in absence of any membrane protein).

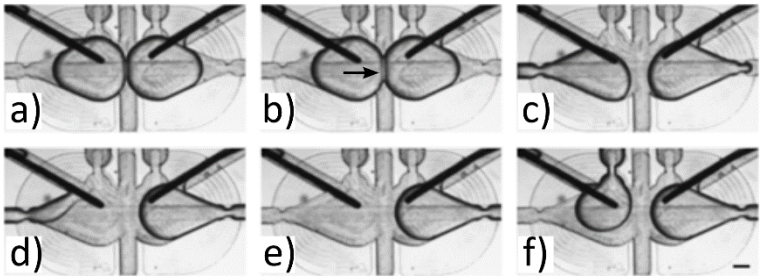

Figure 23 Micrographs illustrating the position of the electrodes in the microfluidic trap and the exchange of one of the droplets from a pair. a) Two droplets are trapped. b) Bilayer (indicated with an arrow) is formed at the interface. c-e) Removal of one of the droplets with the flow of oil. f) Introduction of the new droplet. The droplet wets the electrode immediately. Scale bar is 200 µm.

We recorded a square wave current at a 1 kHz sampling rate, which resulted from the application of triangular potential to the membrane (10 Hz, 50 mV peak-to-peak). The bilayer begins to form after about 60 sec of droplets being in close contact and this time is required for continues phase to be pushed out from between the leaflets of lipid monolayers. Then, in the case of two droplets of volume 300 nL each, we observe a rapid increase in the capacitive current I_C, that reaches typically 394 ± 13 pA.

$$I_C = \frac{C_T \times dV}{dt} \qquad \text{Eq. 4}$$

The rate of change of the potential was set to 1 V/s using a model cell with a known capacitance of 100 pF (MCB-1U, Molecular Devices). Capacitive current I_C (Eq. 4) is directly proportional to the capacitance C_T and the rate of change of potential. As a result, the value of the capacitance was 394 ± 13 pF. It was presented that from the measurement of capacitive current, the area of the bilayer can be calculated, knowing the value of the specific capacitance for given conditions. We used the value of specific capacitance for a DPhPC bilayer formed in pure hexadecane (0.64 µF cm^{-2}) [47] and estimated the contact area at the interface of trapped 300 nL droplets to be 61 500 ± 2 500 µm^2.

In the proposed system we were able to successfully trap droplets with volumes ranging between 250 and 350 nL (5 volumes tested: 250, 275, 300, 325 and 350 nL respectively). Droplets of exact volumes were generated by aspiring the buffer from a 96-well plate with the aid of a precise pump (Nemesys, Cetoni) and a positioning system (Rotaxys,

Cetoni). For each of 5 tested volumes we analysed 5 pairs of droplets, for which we collected and analysed traces of about 60 s. The average level and standard deviation of the capacitance are presented in Table 1.

Table 1 Results of measurements of capacitance and calculations of sizes of bilayers formed between droplets of various volumes.

Droplet no	Droplet volume [nl]	Mean capacitance for a single bilayer [pF]	SD of capacitance for a single bilayer [pF]	Mean capacitance for a volume [pF]	RSD of capacitance for a given volume [pF]	Bilayer area [μm^2]
1		152	9			
2		161	5			
3	250	165	8	171	10.4%	26 700 ± 2 800
4		176	8			
5		199	5			
6		302	9			
7		331	19			
8	275	295	16	308	7.0%	48 200 ± 3 400
9		292	17			
10		323	13			
11		374	8			
12		395	11			
13	300	397	19	394	4.1%	61 500 ± 2 500
14		411	7			
15		391	4			
16		521	26			
17		514	16			
18	325	546	9	525	4.1%	82 000 ± 3 400
19		534	13			
20		512	19			
21		626	21			
22		618	13			
23	350	634	14	627	3.9%	98 000 ± 3 800
24		601	6			
25		658	17			

The range of surface area of the obtained DIBs was 4-fold (Figure 24). Small fluctuations of the capacitive current proportional to bilayer size result from internal flows of oil (e.g.

convection) and they do not affect the process of pore insertion. For a single bilayer in time the area changed in the range of 1 - 6% of relative standard deviation (RSD). The overall RSD increased to 4 - 10% for a collection of droplet pairs given the slight differences in the position of subsequent pairs of droplets in the trap. We observed higher RSD (5 - 10%) for droplets of smaller volumes (250 and 275 nL) due to a reduced stabilization of position of smaller droplets by the structure of trap.

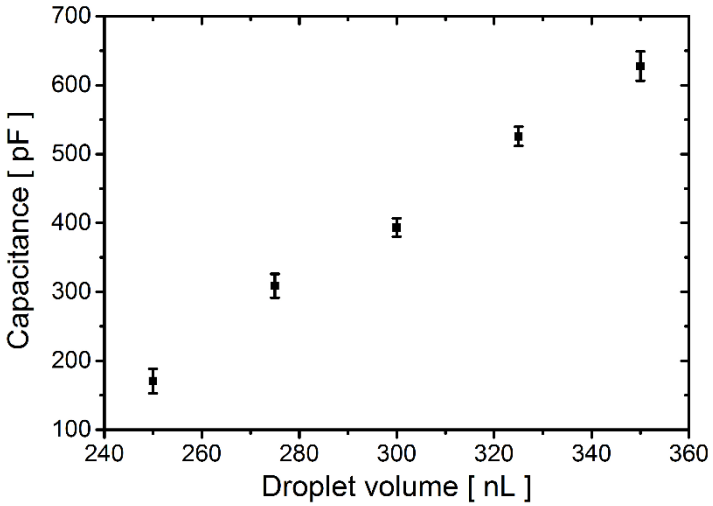

Figure 24 The volume of droplets determines the size of the bilayer. Droplet pairs of differing volume were trapped and the capacitive current was measured. Each data point represents the average capacitance values of five droplet pairs; error bars represent the standard deviation (SD). The systematic dependence of the surface area of the bilayer on the volume of the droplets is reflected by the increasing trend in the capacitance. The standard deviation of the recorded capacitance comes from initial small differences in the positioning of the droplets in the traps.

3.2.4. Alpha–hemolysin measurements

In order to test the usability of the DIB for measurements of protein activity, we trapped a pair of ~300 nL droplets, one containing a solution of WT alpha–hemolysin (5 ug/mL) and the second with the buffer only. After a successful formation of a DIB, we conducted a voltage clamp measurement at +50 mV (Figure 25). The stepwise (50 pA) increases in the current indicated the incorporation of single heptameric protein pores. Next, we replaced the buffer droplet with a droplet containing a 50 µM gamma-cyclodextrin (γCD), which is a reversible non-covalent blocker of the alpha-hemolysin pore. In the presence of inhibitor molecule inside of the channel, the current decreases to ~40% of its open-pore value.

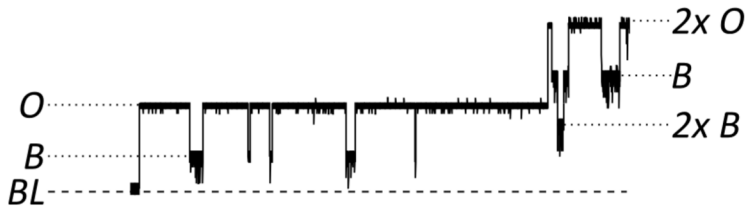

Figure 25 Fragment of the current trace (lasting ca. 20 s) showing the incorporation of alpha-hemolysin into a lipid bilayer, voltage-clamped at + 50 mV. Stepwise increase of current from 0 to 50 pA reflects the incorporation of a single pore into the membrane. The transient presence of inhibitor molecules (gamma-cyclodextrin, 5 μM) within the pore is seen as a drop in current by app. 60%. Further stepwise increase of current reflects the presence of the next *α*HL heptamer in a lipid bilayer. *BL* – baseline, *O* – open pore level, *2x* O – 2 open pores, *B* – blocked pore, *2x B* – 2 blocked pores.

Next, we checked the risk of contamination of electrode with the *γ*CD molecules (Figure 26). The efficiency of washing was tested after the droplet containing *γ*CD was replaced by a droplet with buffer alone. Rare blockades (on average 1.5 events per minute compared to ~80/min prior to washing) were recorded. Introduction of next droplet of buffer completely eliminated the blockade events. These results illustrate enough washing of the electrodes between single measurements.

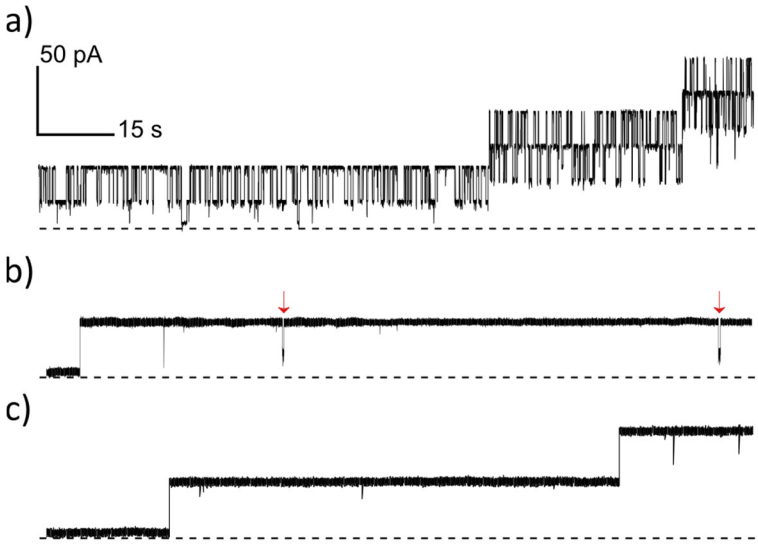

Figure 26 Efficiency of washing the protein inhibitor gamma-cyclodextrin off the electrode measured with electrodes. a) Pore blocking with high concentration of 50 μM gamma-cyclodextrin was recorded for 10 minutes. b) The droplet containing the inhibitor was removed from the trap with a stream of oil and replaced with a droplet of pure buffer (1 M KCl, 10 mM Tris-HCl, pH 7.0). Single events of blockades (indicated with red arrows) were recorded. c) After the next droplet of pure buffer was introduced into the trap, no further blockades of nanopores were observed.

3.2.5. Screening experiment procedure

The aim of the project was to execute an automated screening procedure of activity of membrane protein. Prior to running the screening procedure, we prepared a sequence of 12 droplets presenting 6 different concentrations (duplicates of 1, 10, 20, 30, 40 and 50 μM) of the inhibitor gamma-cyclodextrin (Figure 17). The droplets were collected inside PTFE tubing using a syringe pump by alternating the aspiration of portions (300 nL) of aqueous solutions of different concentrations of inhibitor and oil admixed with lipids (700 nL) from a standard 96-well plate [154].

During the screening procedure, first we introduced a solution of alpha-hemolysin (5 μg/mL) and a sequence of inhibitors onto the chip and deposited them in storage channels. Then, a droplet of ~300 nL was generated from the solution of protein and locked in a trap on an electrode. During the screening experiment the routing of droplets on chip was automated and performed according to the following protocol (the voltage of + 50 mV was constantly applied):

Step 1. **Introduction of droplet with inhibitor into the trap:** for positioning of a droplet we used an edge-detection algorithm. A view from a camera was analyzed with an image processing software, that controlled the opening and closing of valves depending on the detected image. Two points on each video image were analyzed for droplet edge detection: first point located in the area before the entrance to the trap and then inside of the trap.

Step 2. **Formation of bilayer and voltage-clamp measurement:** during 180 s period we observed formation of bilayer, incorporation of protein and measured binding events of inhibitor. At least one pore incorporated into about 50% of individual DIBs, which is consistent with the results of a previous studies [126]. We observed, that for an arbitrary chosen concentration of protein (5 μg/mL), the intervals between incorporation of the first and subsequent pores can be clearly distinguished. This allows for extraction of single-pore traces and their analysis for determination of kinetics of inhibition.

Step 3. **Removal of droplet with inhibitor and washing of the electrode:** first the droplets needed to be separated by the pulse (1 s) of the flow of oil through the auxiliary channel. The droplet containing an inhibitor was gradually removed from the trap and followed by a droplet of pure buffer of ~350 nL. The presence of wash droplet was

detected in the trap with edge-detection optical feedback and the script would not continue unless the droplet of buffer passed through the trap.

Execution of steps 1 to 3 took 210 s. It is important to note, that the exchange of the droplets disrupts the bilayer, and dislodges the protein from its structure. As a result, different protein molecules are studied in the measurements on subsequent droplet pairs. An exemplary trace of 4 subsequent exchanges is depicted in Figure 27. After the 2 screening repetitions (2 repetitions for each 6 concentrations of inhibitor, ~40 min) the system required an introduction of fresh solution of protein. We noticed that the protein incorporates into a bilayer with a decreasing rate with time. The decrease in activity can be attributed to the aggregation of protein molecules after the dilution in aqueous buffer, which causes the hydrophobic surfaces of heptamers to clump together. To overcome this obstacle, we implemented an additional module for preparation of dilutions of a sample on-chip, described in Chapter 5.

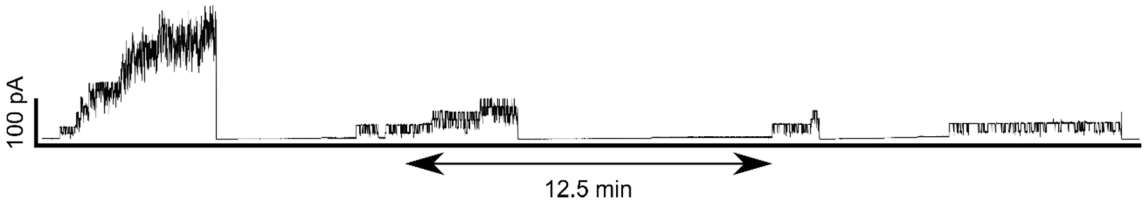

Figure 27 Rapid screening of inhibitors against single alpha–hemolysin pores. Continuous trace of current depicts subsequent formation of bilayers formed between a droplet containing a protein solution and 4 successive droplets with decreasing concentrations of gamma-cyclodextrin (50, 40, 30 and 20 μM) and incorporation of αHL pores.

In total, we collected 10 repetitions of the sequence of 6 different concentrations (1 - 50 μM γCD) (Figure 28). For calculations of K_d, we discarded the results of αHL activity inhibited by 1 μM γCD since the number of blocking events was very low. Using the current traces for single-channel measurements (lengths of traces are summarised in Table 2) we analysed the duration and frequency of blocking and calculated the dissociation constant (K_d) value for the binding of gamma–cyclodextrin to alpha–hemolysin. The obtained value of K_d (61 ± 7 μM) can be compared to the value calculated by Mantri *et al.* for αHL heptamer at -50 mV (buffer conditions 1M KCl, 25mM Tris HCl and 50 mM EDTA, pH 8), which was 47 ± 9 μM [155]. In the aforementioned work the protein was included in the compartment with a ground electrode. Contrary, in our set-up the protein is contained within droplet with working electrode. Due to the phenomenon of rectification of current, we compared our value of K_d (obtained at +50 mV) to the one obtained at -50 mV.

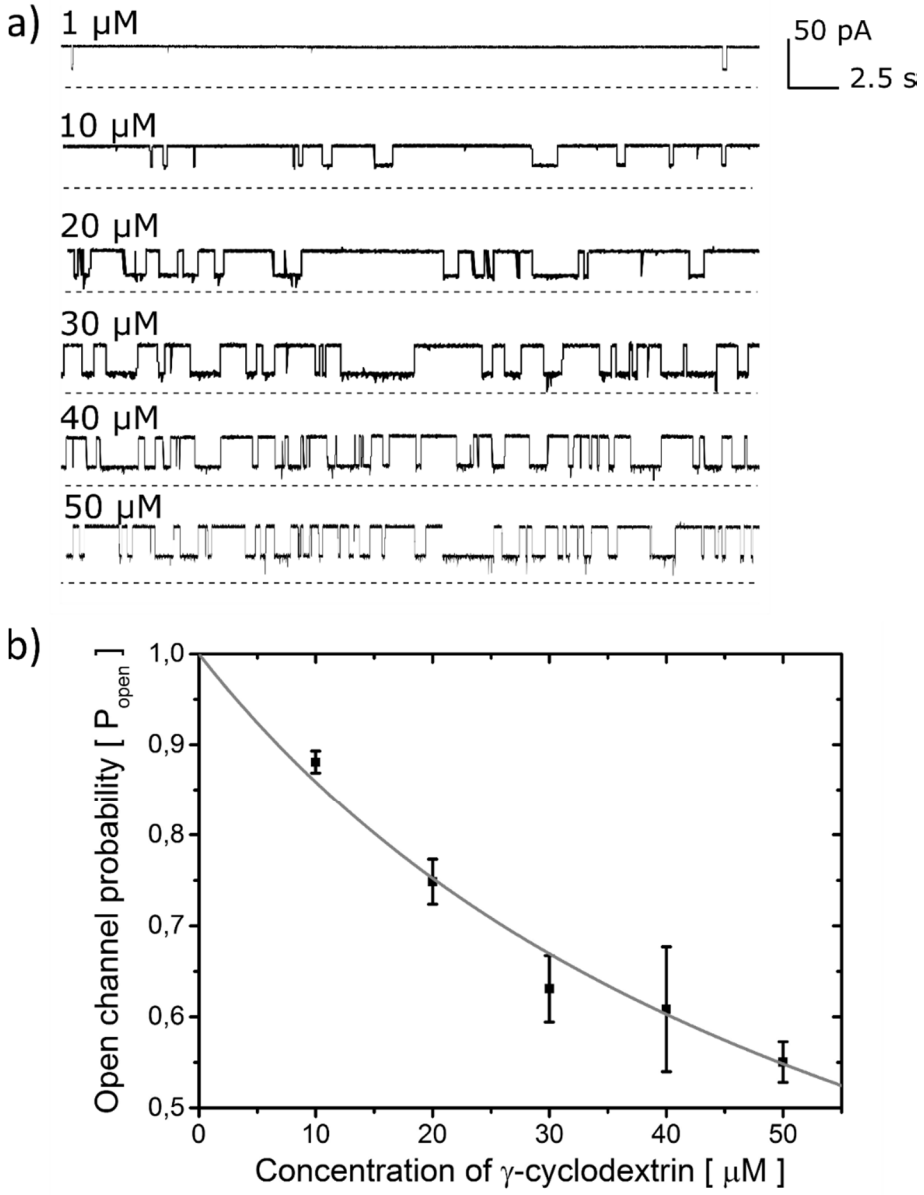

Figure 28 Screening of inhibitors against a single alpha–hemolysin channel and concentration dependence of the inhibition of a single *α*HL pore by gamma-cyclodextrin. a) Fragments of current traces of activity of *α*HL in the presence of gamma-cyclodextrin at various concentrations (1 µM - 50 µM). b) Probability of open channel (P_{open}) was plotted versus the concentration of the blocker. The error bars represent the SD from at least three trials. The sum of all the measurement intervals (recordings of current) included in the calculation of the probability of blocking of the pore at each concentration was at least 145 s. The curve was plotted using the saturation function (Equation 5) and the dissociation constant (K_d) was found to be 61 ± 7 µM.

$$P_{open} = \left(1 + \frac{c}{K_d}\right)^{-1} \qquad \text{Eq. 5}$$

Table 2 Duration of single-channel recordings collected in screening experiments. The table collects duration (in seconds) of single-channel recordings: the time between the incorporation of first channel and incorporation of second channel, or termination with exchange of droplet. "x" indicates experiments in which no channel incorporated into the bilayer.

		Concentration of gamma-cyclodextrin [μM]					
		1	**10**	**20**	**30**	**40**	**50**
Screen number	1a	x	93	x	x	24	x
	1b	x	x	57	8	x	x
	2a	x	x	106	24	44	10
	2b	x	x	x	70	x	82
	3a	22	47	x	x	27	16
	3b	x	x	82	x	92	37
	4a	25	x	x	x	66	18
	4b	x	x	20	x	x	x
	5a	62	5	13	15	x	x
	5b	92	x	x	42	34	4
	Total time [s]	**201**	**145**	**278**	**159**	**287**	**167**

3.2.6. Control of the surface area

The unique feature of the proposed system provides the opportunity to actively control the area of the obtained bilayer. By varying the rate of flow of oil injected from the perpendicularly oriented auxiliary channel we changed the surface area of the DIB formed between the two droplets. The applied flow pushed the interfaces apart with the level of the effect depending on the rate of flow (Figure 29 and Figure 30). The control over the surface area of the DIB allows us to influence the surface concentration of the inserted pores. Regardless of the contact area, the current produced by the inserted pores (~45) remained the same.

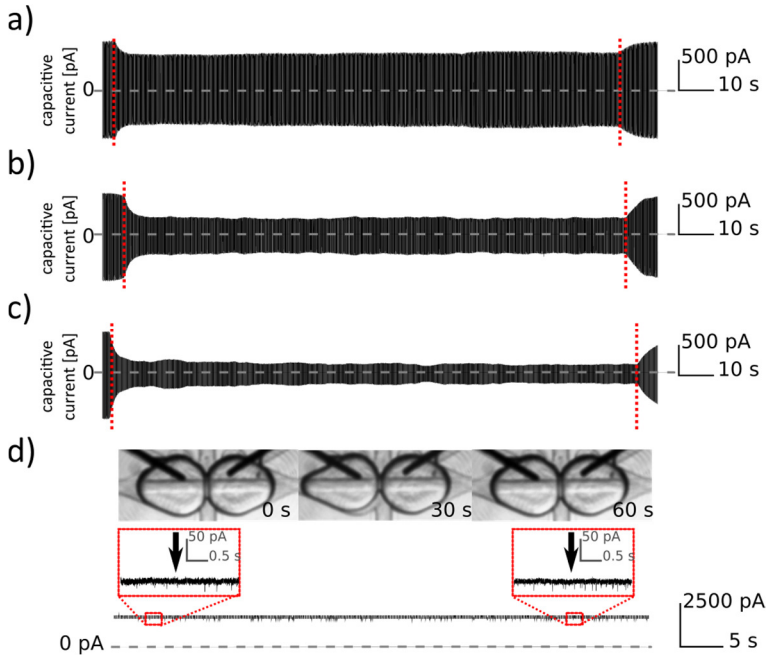

Figure 29 The size of the bilayer reflected with the measurements of capacitive current. The application of a constant flow of oil (respectively: a) 5 nL/s b) 10 nL/s and c) 15 nL/s) results in a reduction of the bilayer surface area. The vertical dotted red lines indicate the moment when the flow of oil was applied and when it was stopped. d) Increasing the concentration of nanopores in the bilayer. The surface area of the bilayer was decreased from about 85 900 μm^2 to 31 400 μm^2 upon insertion of the nanopores. In that case the areas were estimated by the analysis of images with ImageJ with the assumption that the contact area is circular. The ion current across the bilayer was constant and equal to ~2 330 pA at a potential of + 50 mV, which indicated that the number of pores in the membrane remained constant throughout the measurement. The vertical arrows in inset d) indicate the beginning and ending of a period of 45 s during which the droplets were partially separated by the flow of oil (15 nL/s).

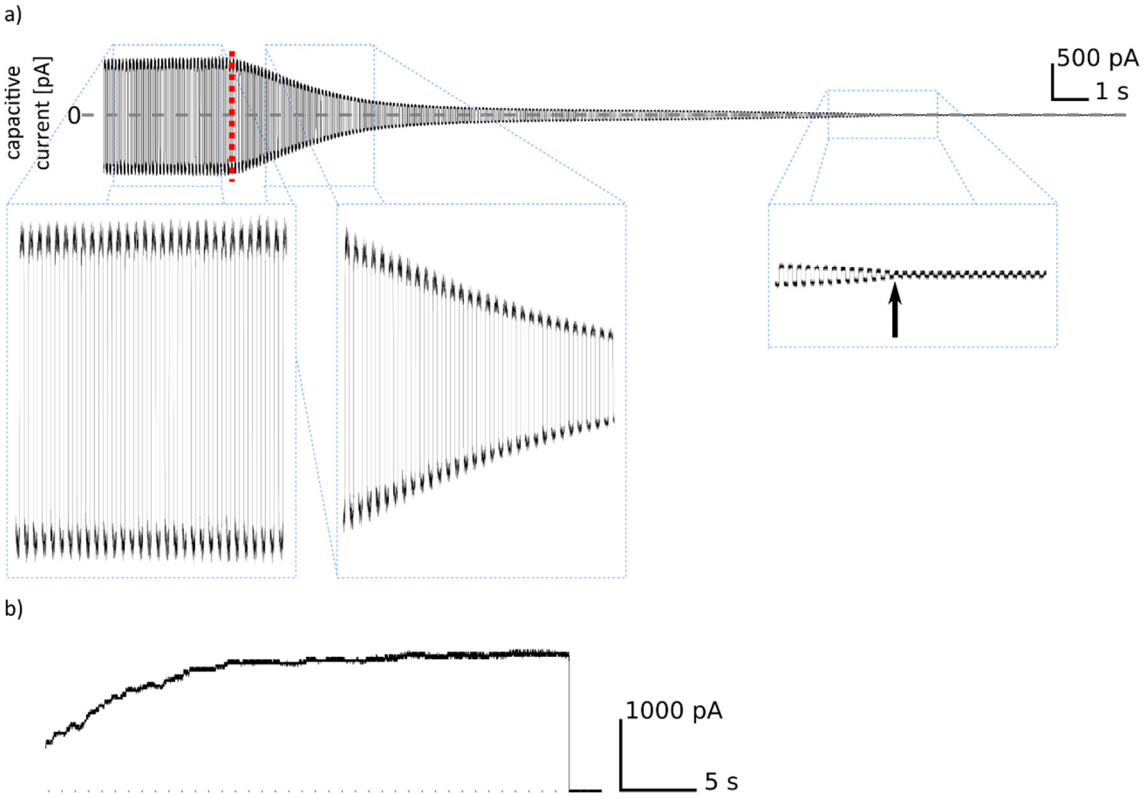

Figure 30 Measurements of capacitive current during separation of droplets. a) Before the application of oil stream the amplitude of current is steady, as shown in the first inset. The flow of oil at 30 nL/s from the channel perpendicular to the axis of the droplet pair (beginning of operation indicated with a vertical dotted red line) causes the gradual decrease in bilayer area and in capacitive current. Finally, the droplets become completely separated (this moment is indicated in the inset with an arrow). b) The separation of droplets during the voltage-clamp measurement of αHL incorporation. We used a high concentration of protein sample in one of the droplets and observed multiple insertions of pore molecules into the membrane indicated with increasing current. The flow of oil to separate droplets was applied which resulted in a separation of droplets till the moment of de-attachment. In a voltage-clamp measurement this is seen as a sudden drop of current to the base level.

3.3. Chapter summary and conclusions

In Chapter nr 3 we demonstrated for the first time an automated microdroplet system that enables fast, simple and reproducible screening of inhibitors against membrane proteins.

Droplet microfluidics have been used to generate Droplet Interface Bilayers at a high yield [130,131] but without the ability to perform electrophysiological measurements on samples encapsulated in the droplets. In comparison to high-throughput systems relying on assay of diffusion of fluorescent dye through the pore [112,113,156], the proposed system is able to carry out reproducible single-pore electrophysiological recordings with high resolution including the on-off kinetics. The technique that we report here allows for automation of these measurements and for additional operations, such as washing and exchange of both the inhibitor solution and of the protein. The exclusion of manual

handling of droplets is an important feature that increases the reproducibility of the protocol. Indeed, during the recent few years automated liquid handling commercial devices were developed for repeatable, parallel formation of artificial lipid bilayers along with electrophysiological measurements [157].

The described microfluidic system allows the use of a minimal volume of samples. This is achieved by the direct aspiration of tiny aqueous droplets (300 nL) from a micro-well plate and by modules that accept the microliter batches of liquids for further processing on chip. Our system is open for easy exchange and for automated processing of sequences of samples, an outstanding challenge that inspired a number of studies in the recent years.

The interesting feature of the system is the precise control over the area of a bilayer, achieved both statically (by tuning the volume of the droplets) and dynamically by adjusting the rate of flow of an additional stream of oil. The decrease in bilayer area did not result in a decrease in the number of inserted pores, rather with the increasing density of pores in the area restricted by the flow of oil, consistent with the results reported by Gross *et al.* [48] who studied this phenomenon in DIB formed between a droplet and supported lipid membrane.

We proved the durability of the system for the period of 3 weeks of intensive use. The electrodes did not show the loss of activity despite their intensive use – including repetitive wetting and de-wetting of electrodes with droplets. Neither the layer of agarose gel, nor the layer of AgCl on the surface of silver wire were depleted. We did not observe any changes in the performance of other parts of the chip over extended periods of operation, in particular there was no wetting of the walls of the channels with the aqueous phase.

The system presented here provided numerous opportunities for further development. The expansion of the capabilities of the system towards building of droplet networks is described in Chapter 4. The addition of a microfluidic module for the dilution of protein stock on chip is discussed in the introduction to Chapter 5. The use of in vitro transcription and translation (IVTT) for protein expression directly in the droplets may allow to avoid the steps of purification, freezing and dilution [30]. The increasing number of studies on various membrane proteins incorporated into droplet interface bilayers, suggests that DIB may constitute an alternative to the BLM method, with the cautionary note, that each type of protein must be tested for compatibility with the droplet system. The use of on-demand

droplet screening techniques may provide for fast screening of the composition of buffers and their effects on the function of protein pores [82,153]. We hope that the technique reported here is a step towards the construction of systems for high-throughput *in vitro* tests of activity of membrane proteins, in which sequential screens might be combined with parallelization. Moreover, selected droplets can be removed from the pair in an intact form and they can be directed for further experimentation. This could find an application in the more detailed studies of transport across the lipid bilayer.

CHAPTER 4.

An Automated Microfluidic System for the Generation of Droplet Interface Bilayer Networks

Chapter 4 presents a microfluidic system which allows for on-demand generation of droplets that are hydrodynamically locked in a trapping structure. The system enables formation of a network of four droplets connected via lipid bilayers. The positions of each droplet in the network can be controlled via automation of microfluidic operations. We perform electrophysiological measurements of transmissions of ionic currents between the droplets indicating interactions between nanopores and small molecules. We also demonstrate, for the first time, a microfluidic droplet interface bilayer (DIB) system in which the testing of inhibitors can be performed without direct contact between the tested sample and the electrodes recording picoampere currents.

4.1. Introduction

Networks of aqueous droplets separated by lipid bilayers have shown great potential as a model for biological transmembrane communication. In particular, networks of three or more droplets that can chemically communicate with each other by membrane proteins, may show collective behavior and exhibit properties such as light sensing or the production of energy in synthetic "biobatteries" [55,56,148,158,159]. A rapid and automated assembly of droplet networks benefits highly from advantages of droplet microfluidics technology. Dedicated structures and geometries on a chip, such as rails [160] or traps [128,135,136,152] allowed for an ordered assembly of nanoliter droplets into networks, in which a chemical signal was propagating via the transport of molecules through lipid bilayers. An interesting approach was demonstrated by Villar *et al.* [57] who 3D-printed out a network composed of tens of thousands of picolitre droplets—a structure that resembles a tissue-like material, an idea currently being explored by OxSyBio company [161].

To this extend, microfluidic techniques for the preparation of droplet networks suffered from few limitations, in comparison to the manual handling of nano- and microliter droplets [162]. For example, individual droplets could not be addressed (e.g., removed from the network). In addition, most microfluidic studies relied on the fluorescent monitoring of the diffusion of small molecules between the compartments [130,160,163], rather than electrophysiological measurements of ionic currents [126,128,164]. Importantly, the electrophysiological measurements require direct contact of an electrode with the measured sample containing tested proteins or inhibitors. So far, this problem has been solved by cyclic washing of electrodes with pure buffer or by fabrication of arrays comprising multiple electrodes [30,117,165].

We address the aforementioned limitations by designing and fabricating a microfluidic system, that enabled for generation of networks of aqueous droplets in a controlled way. Aqueous droplets are first generated on demand, and then assembled into a linear network locked in the hydrodynamic trap, similarly to the 2-droplet system described in Chapter 3. Distinguishingly, in the trap, four droplets are arranged in a line to form a network comprising three bilayers at the interfaces.

Again, we were able to control the contact surface between the droplets and on demand remove one or both of the inner droplets from the network on demand.

We are also able to study the electrical properties of the DIBs network via electrodes integrated on the chip. The outer compartments of the networks — droplets containing a high concentration of alpha-hemolysin nanopores – were penetrated with silver-chloride electrodes. A large number of protein nanopores spontaneously inserted into bilayers separating the outer and inner droplets, resulting in a high perforation and reduced electric resistances of the outer lipid membrane. Consequently it was possible to take insight into the electrical processes that take part at the middle bilayer of the network [166]. The physical separation of the outer droplets that host the electrodes from the inner (test) droplets allowed us to perform screening of the interactions of small molecules with the single protein molecule, without needing to wash the electrodes between exchanges of the samples.

4.2. Results

4.2.1. Layout and operation of the device

The general design of the microfluidic chip (Figure 31 and Figure 32) and its operation are similar to the 2-droplet system described in the Chapter 3. In contrast, the structure of the trap comprises four, instead of two, cavities locking the droplets of approximately 500 nL in volume. There are three sample ports with T-junctions for storage of samples (aqueous solutions of buffer and samples with dissolved protein or inhibitor) on a chip. In order to change the size of bilayers and address individual droplets, thin channels perpendicular to the axis of the network were included in the design.

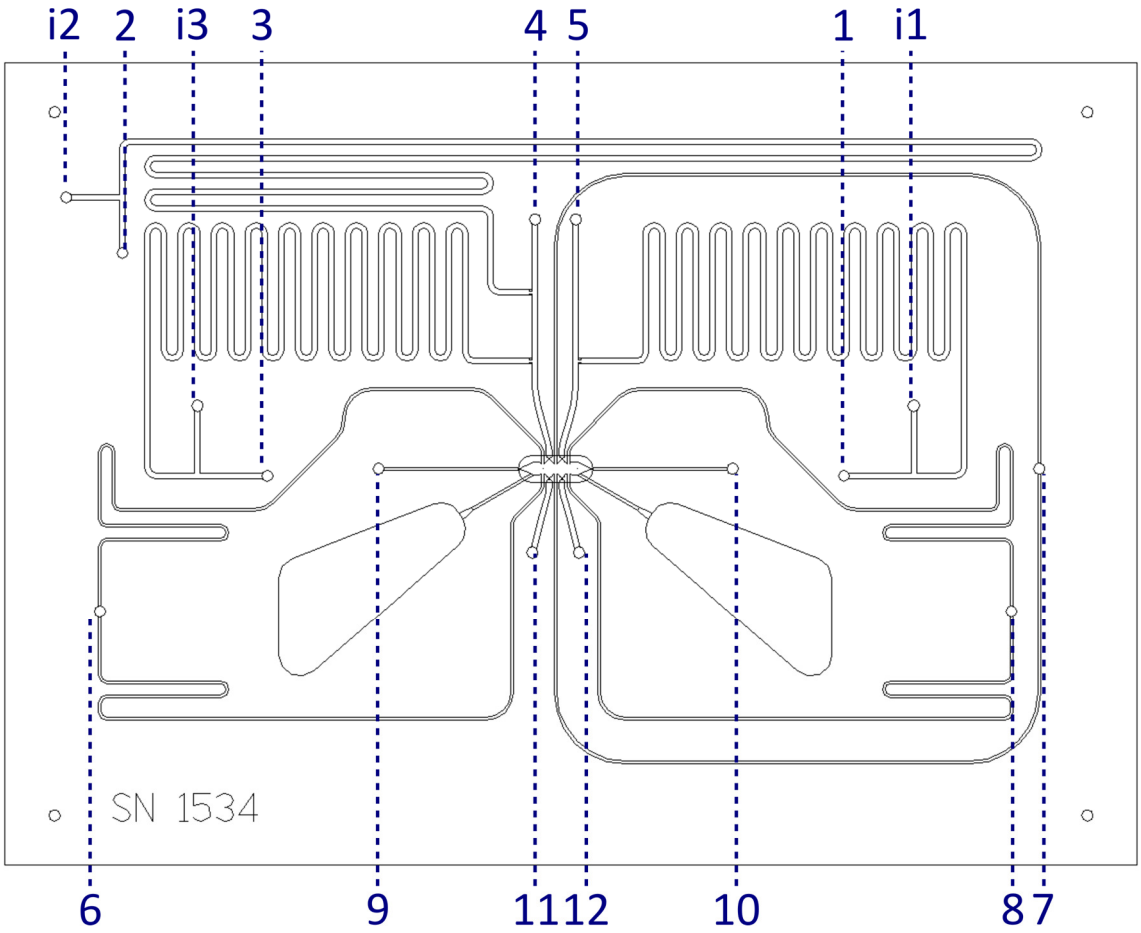

Figure 31 Detailed diagram of the layout of the microfluidic chip. The numbers indicate: 1–8 - inlets for oil, 9–12 - outlets, i - inlets for aqueous samples: i1 - buffer/solution of inhibitor, i2 - solution with high concentration of alpha-hemolysin (300 nM), i3 - solution with low concentration of alpha-hemolysin (3 nM). The dimensions of a whole chip are 82 mm × 53 mm.

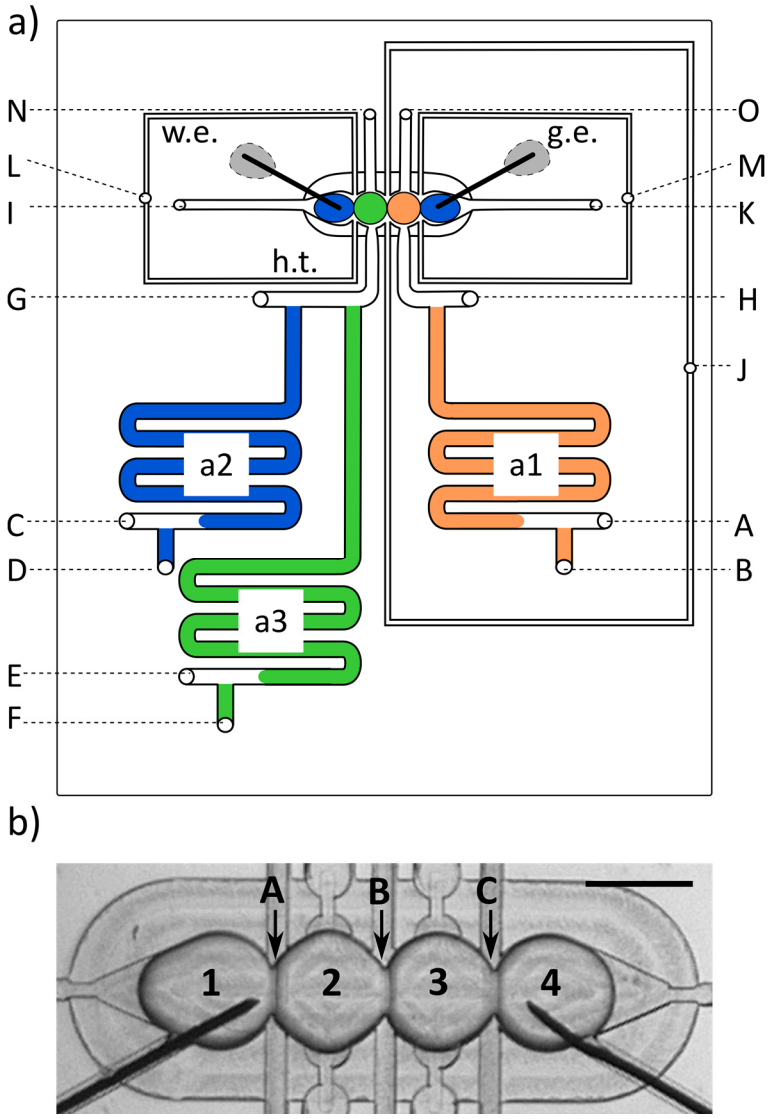

Figure 32 Operation of the microfluidic device. a) Scheme of the microfluidic chip: A, C, E, G, H, J, L, M - inlets for oil; B, D, F -inlets for aqueous samples; I, K, N, O - outlets; a1, a2, a3 - aspiration modules for aqueous samples: 1- buffer/solution of inhibitor; 2 - solution of alpha-hemolysin (300 nM); 3 - solution of alpha-hemolysin (3 nM); w.e. - working electrode; g.e. - ground electrode; h.t. - hydrodynamic trap. b) A micrograph of the hydrodynamic trap comprising a network of four aqueous droplets (1 M KCl, 10 mM HEPES, pH 7) interconnected with DPhPC bilayers: outer bilayer A between the first and second droplet, middle bilayer B between the second and third droplet, outer bilayer C between the third and fourth droplet. The scale bar is 1 mm.

4.2.2. Formation of a network of droplets in a trap

The operations such as generation of droplets their transportation to the trap and the on demand removal of one of the droplets took less than 20 s all together. Once the droplets were locked in the trap, the formation of the bilayer from DPhPC phospholipid (1 mg/mL) at the interface of droplets was the limiting step which took approximately 60 s (Figure 32b and Figure 33). In order to confirm the successful formation of bilayers, we applied

a triangular potential (10 Hz, 50 mV peak to peak) and recorded the resulting square wave capacitive current (Figure 34).

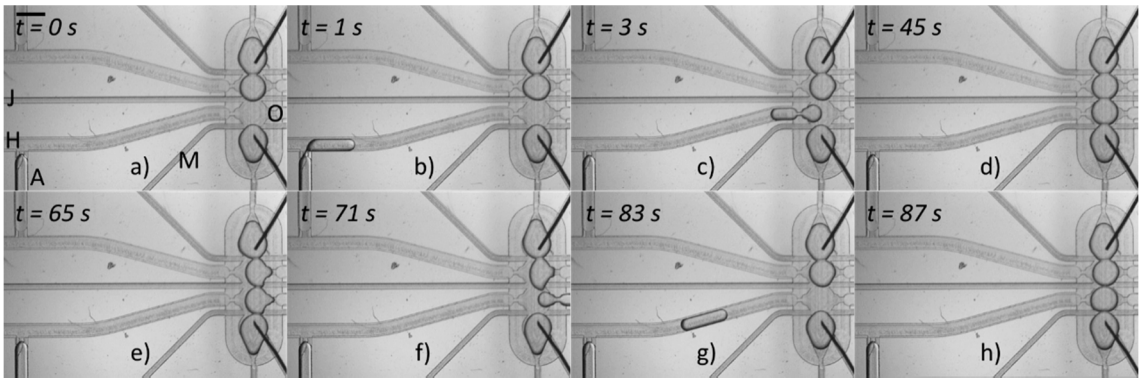

Figure 33 Formation of the network of droplets and exchange of one of the components. a) Initial state in which three droplets are already positioned within the hydrodynamic trap. The letters correspond to respective valves (as denoted in Figure 32) which are used in the consecutive steps of the protocol. Outlet 'O' remains open during operations; b) A droplet is generated at the T-junction. The aqueous plug is pushed by applying the flow from valve 'A'; c) Oil applied from valve 'H' pushes the droplet into the trap; d) After about 60 s of incubation, droplet interface bilayers are formed within the network between the new droplet and the surrounding droplet. e, f) The flow of oil from the thin perpendicular channels (applied from 'M' and 'J' inlets at the same time) pushes the droplet from the trap into outlet 'O'; g, h) A new droplet is generated and transferred into the trap. It takes approximately 4 s to generate and transfer a new droplet into the trap, and about 7 s to remove one of the droplets from the network. The scale bar is 1 mm.

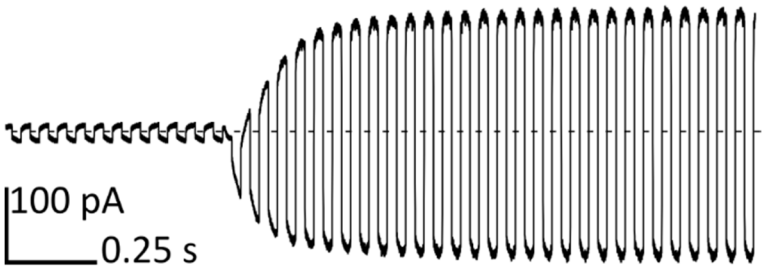

Figure 34 Measurement of the capacitive current during the formation process of the bilayer between droplet No. 3 and the neighboring droplets.

The main goal of the project was to measure the signal from the bilayer located in the center of the network - at the interface of droplets Nos. 2 and 3. High electrical conductivity of the outer bilayers is required to achieve this goal and this feature was ensured by inclusion of high concentration of αHL nanopores in the droplets positioned at the ends of the network. We determined the highest concentration of alpha-hemolysin nanopores, which gives stable bilayer i.e. does not lead to the disruption of the membrane and coalescence of droplets due to excessive perforation (Figure 35). For this purpose, we performed measurements using the 2-droplet system, described in Chapter 3. The aim of this measurement was to verify whether:

- the lipid bilayer withstands the insertion of high number of channels,
- the droplets can be separated without the coalescence,
- after the reformation of bilayer there is enough number of pores available for insertion into the membrane after the reformation of bilayer.

The experimental procedure consisted of trapping of a pair of droplets, from which one contained nanopores. Then, after the formation of a bilayer and measurement of electrical signal, droplets were separated with a short pulse of flow of oil. After the droplets were de-attached, they remained in the trap and bilayer was reformed at the interface of droplets. We found that 9.9 µg/mL (300 nM) of nanopores is the suitable concentration for the formation of stable bilayers of a low electrical resistance (lower than 5 MΩ after several seconds, see Paragraph 4.2.4.). Measurements were performed after 1.5 h incubation of a sample on the chip, indicating that solution with high concentration of *α*HL monomers has long-term capability for efficient insertion of pores to the membrane. It is however important to mention that in some experiments, after several exchanges of droplets, the problem of aggregation of protein (described in Chapter 3) affected the pool of active channels available for incorporation into the bilayer and the resistance of edge bilayers increased into around 20 MΩ.

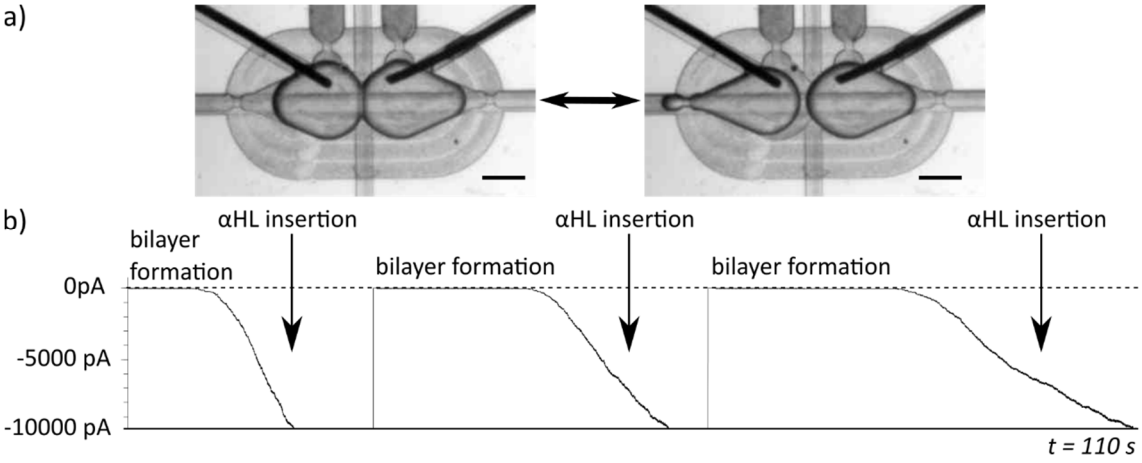

Figure 35 Measurements of the dynamics of incorporation of high concentration of alpha-hemolysin into bilayers. a) Micrographs of experimental setup. The bilayer was cyclically formed at the interface of two droplets, each composed of 1 M KCl, 10 mM HEPES. One of the droplets contained 300 nM *α*HL. Scale bar is 500 µm. b) Recording of current from the bilayers clamped at -50 mV. After the formation of a bilayer, the current decreased gradually due to the insertion of subsequent nanopores. The maximum current that can be recorder by Axopatch instrument is 10 nA, which indicates that more than 200 pores were present in the bilayer (1 pore gives the change of current equal -50 pA). After the signal reaches the maximum capacity of the amplifier, we separated the droplets and allowed for the reformation of the bilayer.

4.2.3. Validation of the integrity of the bilayers in the network

We confirmed the mechanical stability of the network by selective detachment of droplets from the network (Figure 37). In the network, droplets nos. 1 and 4 contained a high concentration of αHL in buffer (300 nM αHL, 1 M KCl, 10 mM HEPES, pH 7), whereas droplets 2 and 3 are composed of buffer without protein.

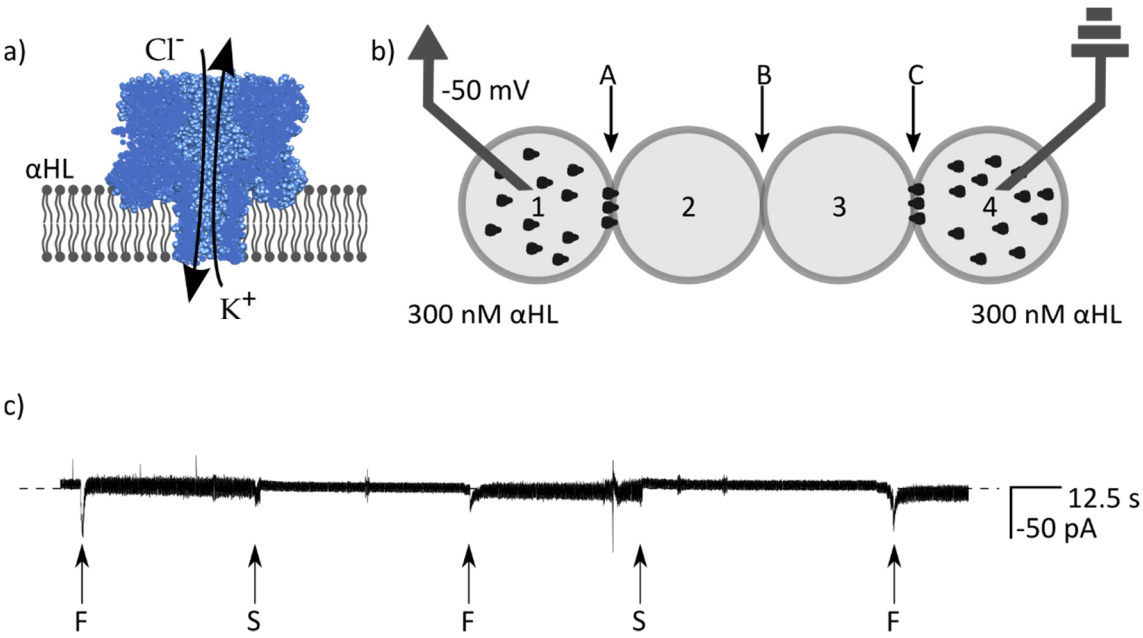

Figure 36 The stability of the network. a) Schematic drawing of alpha-hemolysin nanopores inserted in the lipid bilayer. b) Scheme of the experimental setup for testing the stability of the network. Droplets no. 1 and 4 contain 300 nM αHL, droplets no. 2 and 3 are composed of pure buffer. Bilayers are marked as A, B, C; c) Recording of current from the voltage clamp experiment (at -50 mV). The dashed line indicates a base level of current (0 pA). During the formation of bilayers (indicated with 'F') a short decrease of current was observed, followed by a slightly higher current level, which results from higher electrical noise. In the experiment, we first separate droplet no. 1 from droplet no. 2 (the rest of the network remains intact). The moment of disruption of bilayer A is marked with S (first from the left). After the flow of oil is stopped the network is reformed to its initial structure (middle 'F'). Next, the second separation was performed with separation of droplet no. 4 from no. 3 and disruption bilayer C (second 'S' from the left). Next, the whole network is reformed and the signal remains stable at the level of 0, indicating that there is no ionic conductance through the bilayer B. Selective de-attachment of the outer droplets and subsequent reformation of the network proves that alpha-hemolysin nanopores do not escape from the original droplet.

By applying the flow of oil from thin perpendicular channels we pushed away and separated droplets Nos. 1 and 4 from the network. After we stopped the flow of oil, the droplets returned to their initial position and we observed the reformation of the bilayers. The electrical stability of the network was tested under the voltage clamped at the constant level of -50 mV. The formation of the bilayer was visible as an increase of the level of noise in the recording of the electric current between the electrodes. The integrity of the bilayer B was confirmed by the lack of events indicating the leakage of potassium ions,

which could be caused by unwanted transfer of alpha-hemolysin nanopores from the outer droplets nos. 1 and 4 to the inner droplets nos. 2 and 3. It is worth noting that the transfer of *α*HL across the DIB is rather improbable due to the asymmetric structure of alpha-hemolysin nanopores comprising cap and barrel domains [7].

In addition, the control over the sizes of individual bilayers was tested (Figure 37). By generating short pulses of flow of oil, we pushed the droplets apart and temporally reduced the sizes of lipid membranes in the network. With the longer application of the flow of oil, droplets were completely separated and the electrical connection between the droplets lost.

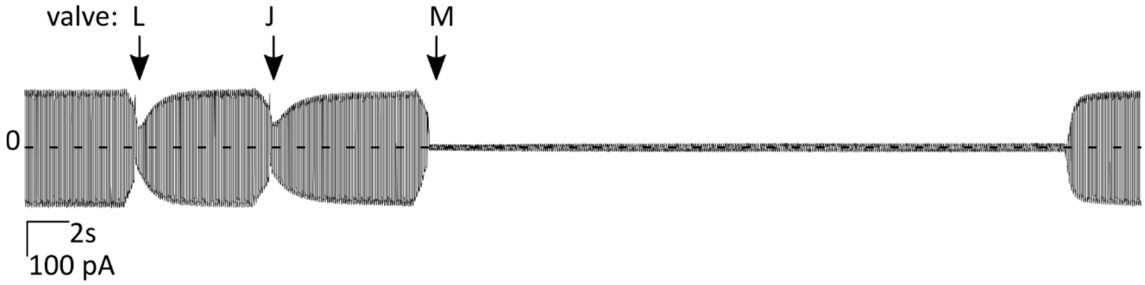

Figure 37 Regulation of the size of bilayers and on demand separation of droplets. The recorded trace shows an example of the capacitive current proportional to the size of a bilayer. The flow of oil was applied from valves (operating respective channels: 'L', 'J', 'M'). Oil flew for a short period of time through the thin channels, perpendicular to the long axis of the droplet network, and gently pushed droplets apart ('L' and 'J'). If the flow of oil is applied for enough long period of time, it detaches the droplets completely ('M').

4.2.4. Transmission of the electrical signal through the network

The main point of the project was to prove the electrical communication within the network. Again, we lock the droplets containing high concentration of *α*HL at the edge positions in the trap (1 and 4), and a droplet with pure buffer in position no. 3. In the next step, a droplet containing a low concentration (0.01 μg/mL, 3 nM) of alpha-hemolysin is placed in position no. 2 (Figure 38). The flow of potassium ions is almost unrestricted through bilayers A and C due to their low electrical resistance, resulting from a high number of pores. The applied voltage (-50 mV) is not constant in the system composed of more than 1 bilayer – instead, it is gradually redistributed among the bilayers [166]. Therefore, unlike the step-wise increase of current upon incorporation of single pores into the bilayer at the interface of 2 droplets, we recorded exponential increases of the ionic current that do not immediately achieved a steady-state value.

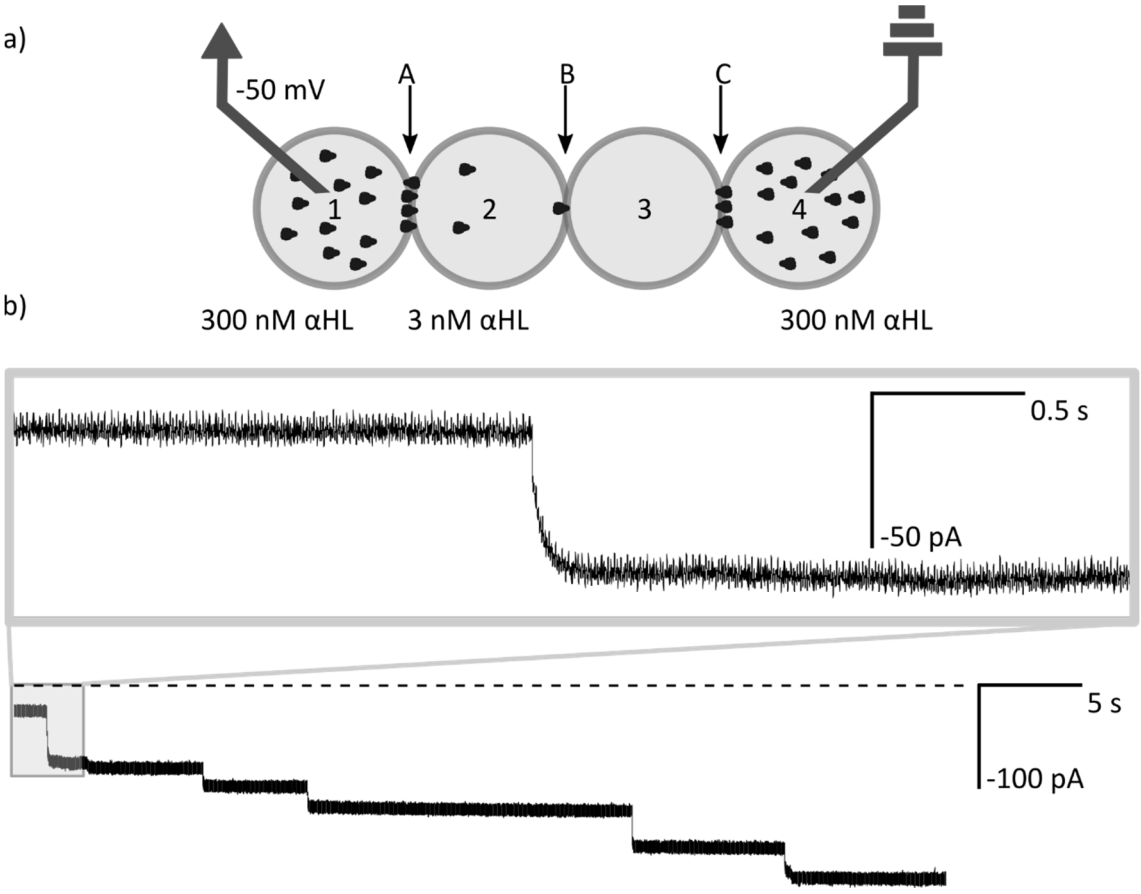

Figure 38 Transmission of the signal through the network. a) Schematic drawing of the experimental setup: droplets no. 1 and 4 contain 300 nM αHL, droplet no. 2 contains 3 nM αHL and No. 3 is composed of pure buffer. Bilayers are marked as A, B, C; b) Recording of ionic current from the voltage clamp experiment (-50 mV). The dashed line is a base level of current (0 pA). Electric traces show step-changes of current, which indicate the insertion of αHL nanopores into the bilayer B. The incorporation of channels does not always contribute to 50 pA changes in the current, which can be attributed to the variation in the structure individual pores formed from a solution of monomers. The inset depicts a single-channel insertion of the exponential shape.

We performed an analysis of the transient states of the system: we derived the formula describing the time-dependent change of an ionic current upon insertion of a next channel in the bilayer in the middle of the network (Figure 39). As the formula requires that the current at the time zero is not equal to zero, we assumed that there is already at least one nanopore present in the bilayer B i.e., $I(t = 0) \approx$ -50 pA. The time decay is described by factor β, which is the function of capacitance of bilayer B C_B, resistances of bilayers A, B and C: R_A, R_C, R_{Ch} and number of pores n. The resistance of two edge bilayers (A and C) determines the duration of the exponential decay phase - the time needed for a change of current after the creation of a new pore is longer with the increasing resistances R_A and R_C. When the resistances are drifting to zero values, the current response becomes instantaneous, which was presented previously in demonstrations of a simple double droplets network.

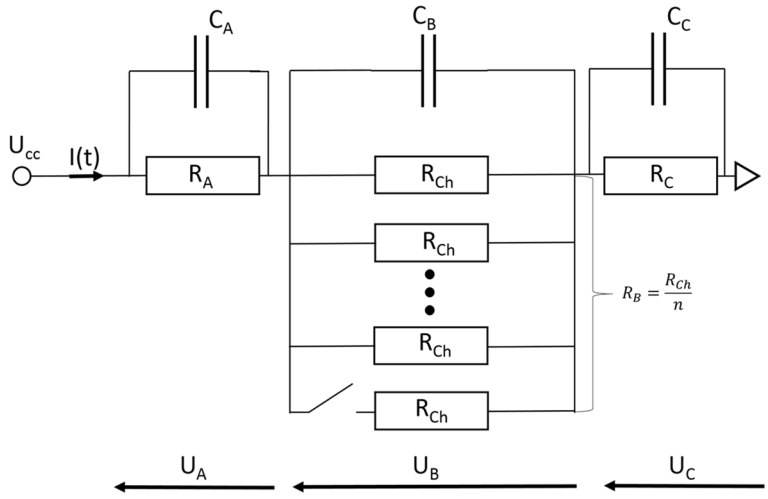

Figure 39 Model of electric circuit built from 4 droplets. R_A, R_B, R_C - total electrical resistances of the bilayers A, B and C, respectively; R_{Ch} - resistance of the single αHL nanopore; U_A, U_B, U_C - voltage drops across the subsequent bilayers: A, B and C, respectively; n - number of nanopores inserted in the bilayer B; U_{CC} - electrical potential applied to the droplet interface bilayer (DIB) network.

We assumed that the resistance of bilayers A and C is smaller than the resistance of bilayer B: $R_A \approx R_C \ll R_B$, but the capacitances are similar for each of the bilayer: $C_A \approx C_B \approx C_C$. The insertion of additional pores in the bilayer B causes drop of voltages (UA and UC), changes of voltages may be described by $U_A(t) = R_A I(t)$ and $U_C(t) = R_C I(t)$. The electric circuit can be simplified by omitting capacitors C_A and C_C. To calculate *I(t)* we write the following formulas:

$$U_{CC} = U_A(t) + U_B(t) + U_C(t) = R_A I(t) + R_C I(t) + U_B(t) \quad \text{Eq. 6}$$

Hence:

$$I(t) = \frac{U_{CC} - U_B(t)}{R_A + R_C} \quad \text{Eq. 7}$$

Furthermore, we also write:

$$I(t) = C_B \frac{dU_B(t)}{dt} + \frac{U_B(n+1)}{R_{Ch}} \quad \text{Eq. 8}$$

From the differential equation of combined equations 7 and 8 we obtain following formula:

$$U_B(t) = \frac{\alpha - \sigma}{\beta} e^{-\beta t} \quad \text{Eq. 9}$$

Where:

$\alpha = \frac{U_{CC}}{(R_A + R_C) C_B}$,

$\beta = \frac{1}{C_B}(\frac{1}{R_A+R_C} + \frac{n+1}{R_{Ch}})$.

and

$$\sigma = \frac{U_{CC}}{(R_A+R_C)C_B} - \frac{1}{C_B}(\frac{1}{R_A+R_C} + \frac{n+1}{R_{Ch}}) \frac{U_{CC}}{R_A+R_B+\frac{R_{Ch}}{n}} \frac{R_{Ch}}{n}$$

From the fact that $U_C \approx U_A$we write that

$$I(t) = \frac{0.5(U_{CC}-U_B(t))}{R_A} = \frac{1}{2R_A}(U_{CC} - \frac{\alpha}{\beta} + \frac{\sigma}{\beta}e^{-\beta t}) \qquad \text{Eq. 10}$$

The measurements of electric current shown to be consistent with the model (Figure 40).

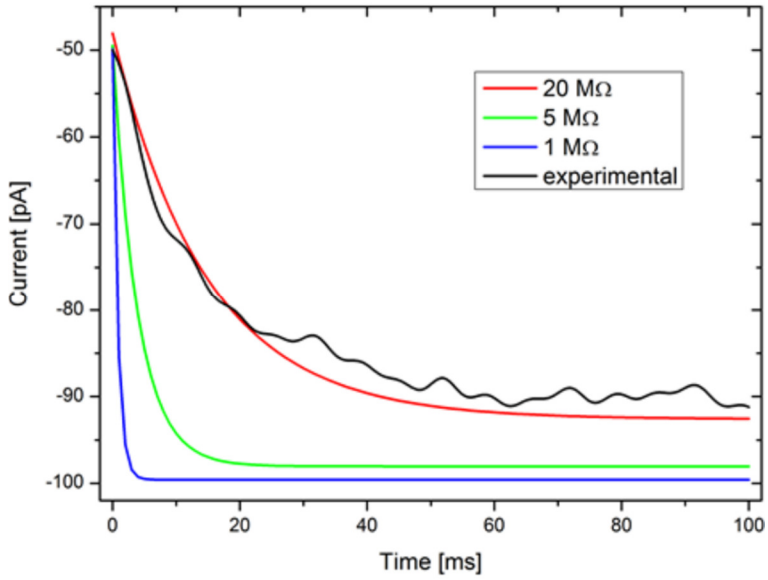

Figure 40 The theoretical changes of ionic current upon insertion of second *α*HL nanopore to the middle bilayer (the presence of first nanopore is assumed in the middle bilayer) for various resistances of each of edge bilayers. The resistances of 20, 5 and 1 MΩ correspond to respectively ca. 50, 200 and 1000 *α*HL inserted to each of two edge bilayers (A and C). The black line represents exemplary current recordings of the insertion of protein nanopore - the experimental trace is similar to the theoretical curve for the resistance of outer bilayer that equals 20 MΩ. This indicates that there were around 50 nanopores already inserted in each of the outer bilayers.

In addition, the general performance of the constructed system is similar to the one presented by Hwang *et al.* [166]. In comparison to the system constructed by Hwang *et al.*, the edge bilayers (A, C) had lower resistance and consequently decay times were shorter. We proved the robustness of the system by changing the droplet containing the low concentration of alpha-hemolysin with a fresh one over the period of at least 1 h. Interestingly, we did not observe a drop of current, which would indicate the loss of activity of *α*HL trapped in outer droplets.

4.2.5. Interactions of small molecules with nanopore in the network

We tested the capability of detecting interactions of small molecules with nanopores present in the middle membrane. We formed a droplet containing 10 µM *γ*CD and locked this droplet in the network in position no. 3 (Figure 41). We measured a signal from single *α*HL channel being transiently blocked with *γ*CD molecules – the current trace is being depicted in Figure 41b.

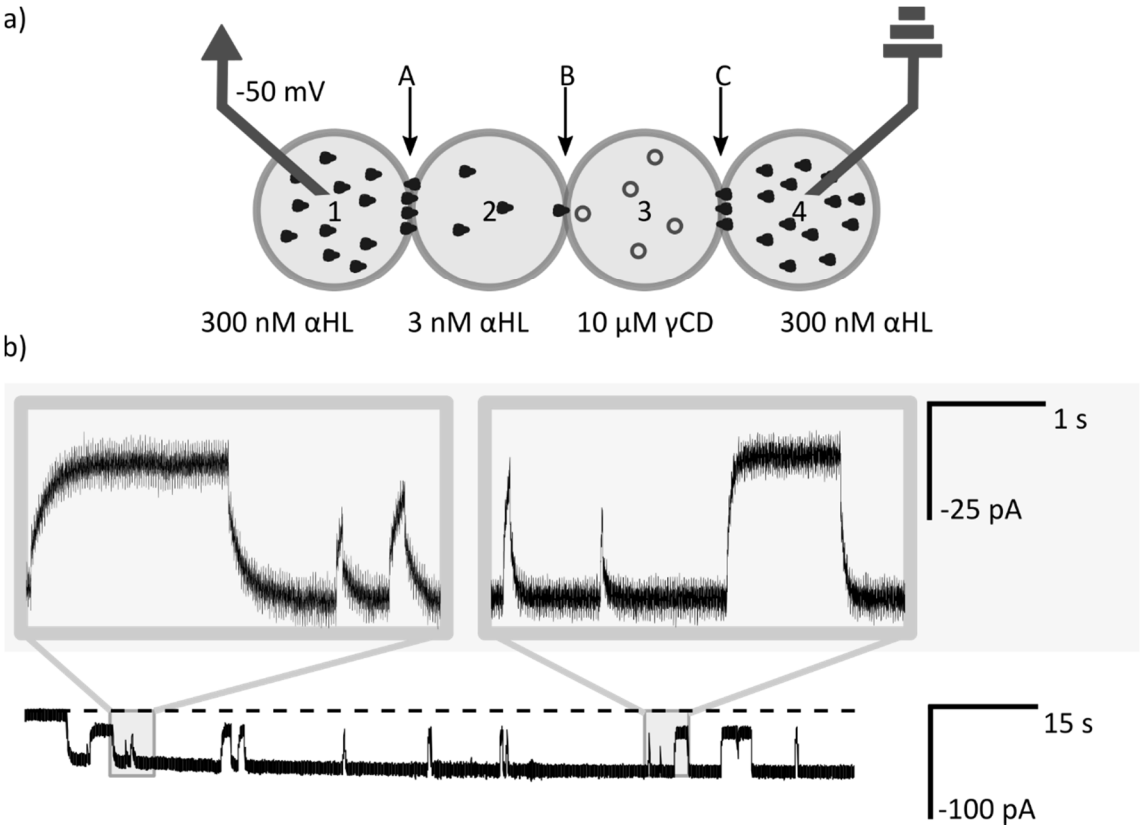

Figure 41 Measurements of the interaction of a nanopore with small molecules in the network of droplets. a) Schematic drawing of the experimental setup for. Droplets No. 1 and 4 contain 300 nM *α*HL, droplet No. 2 contains 3 nM *α*HL and No. 3 contains 10 µM *γ*CD. Bilayers are marked as A, B, C; b) Recording of ionic current from voltage clamp experiment (-50 mV). The dashed line is a base level of current (0 pA). The selected fragment shows interactions between a single *α*HL channel with *γ*CD molecules. Transient changes to the level of -20 pA come from the steric inhibition of the flow of ions by *γ*CD molecules while the level of app. -50 pA is attributed to the open-channel conformation. Insets show the exponential nature of changes of electric current.

4.3. Chapter summary and conclusions

In the Chapter 4 the development of a novel microfluidic chip dedicated to the formation of networks built from droplets interconnected by lipid bilayers is described. Similarly to the system described in Chapter 3, the droplets within the network can by individually addressed — generated on a chip, transported to the hydrodynamic trap for the formation

of the bilayer, incubated and removed from the network without disrupting the rest of the structure.

In contrast to the previous work, the electrodes are excluded from the direct contact with the inner compartments of the network. No cyclical washing of electrodes is required, that was a necessary step in the screening procedure performed using the previously described, 2-droplet system. The separation of electrodes from the investigated reagents reduces the risk of adsorption of the tested chemicals on the electrodes and unwanted carryover of compounds between the tested droplets, as well as creates the potential for performing long-term screening experiments. We relied on alpha-hemolysin nanopores as a means to provide high permeability of bilayers. We did not observe a significant depletion of monomers even after long-term operation of the device (Figure 35), however the insertion rate slightly decreased in subsequent bilayers formed between the sample droplets and the same droplet with a high concentration of nanopores. Other types of molecules, such as artificial nanopores, might also be used to ensure the communication within the network [167,168].

We demonstrated that alpha-hemolysin nanopores may be used to functionalize bilayers in the network, so that the electrical communication within the network is achieved. Interestingly, the inhibition with gamma-cyclodextrin of single channels can be measured within the network formed of four droplets containing various concentrations of nanopores. However, the obtained current traces show that very short events of pore inhibition did not always reach a value of 60% of the current. A system requires time to establish a new steady-state, and detection of short changes is limited by decay phases that depend on the resistance of edge bilayers. Still, from the analysis of traces we can safely assume that the decay time is shorter that 0.1 s and it is much shorter than in previous analyses of membrane protein inhibition in the networks e.g., the system presented by Hwang *et al*. It is worth to mention, that nanopores in the bilayer C are also transiently inhibited, however the high number of channels in the edge bilayer act as resistors connected in parallel. Each of the channels present in the edge bilayer contributes to less than 0.25% of the transmission of the total current. The inhibition of one of the channels in bilayer C results in the drop of measured current by only 0.15 pA. Considering the level of electric noise, such small changes are not noticeable in the measured signal.

CHAPTER 5.

Automated Dilutions of Sample On-chip

Chapter 5 briefly describes an attempt of construction of system capable of automated dilutions of sample in-situ, on the microfluidic chip. Motivated by the observation, that undiluted stock solution of alpha-hemolysin retains pore-forming protein activity over long periods of time, we aimed at preparing dilutions of protein sample directly from the stock solution stored on microfluidic chip. We present measurements of successful pore insertion from the sample stored for up to 3 days. However, the technical obstacles encountered during the development of the system limited further implementation of the diluting module in a full screening scheme.

5.1. Introduction

As a next step of expanding the capabilities of microfluidic systems for formation of artificial lipid bilayers, we aimed at including the possibility of diluting the sample directly on a microfluidic chip. Precise preparation of dilutions of test samples is one of the critical steps in determination of kinetics of inhibitors. Generation of serial dilution in microsystems is challenging mainly because of the small volumes of the samples (e.g. potential inhibitor) - a feature that requires ultra-high precision in liquid handling protocols. Moreover, the nature of a protein sample may require that the preparation of dilutions of the stock solution is performed on-demand. Transmembrane proteins possess hydrophobic residues which allow to anchor the protein to the membrane. Various additives, mostly detergents, stabilize transmembrane proteins and prevent from the aggregation. When diluted in an aqueous buffer lacking additives, protein molecules may be prone to aggregation due to their partially hydrophobic nature. We observed however that αHL can be stored in room temperature in undiluted form up to few hours, and still retains its activity upon dilution. The residues of SDS that are present after the gel electrophoresis are possibly having a stabilizing effect on αHL heptamers in a concentrated form. However, the detergent additives can not be added in higher concentrations to prevent heptamers from aggregation, as they act disruptive on the structure of lipid bilayer.

Although droplet microfluidics offers several strategies for generation of gradations of concentration (a sequence of dilutions) in microdroplets, none of them is directly applicable to long-term automated screening of the activity of membrane proteins. The effective strategies, such as joining a few miscible streams immediately upstream of the droplet generator or using the Taylor-Aris dispersion [169–171] create long sequences of hundreds or thousands of droplets with continuously modulated concentration of the analyte. Contrary to preparation of a continuous gradient of dilutions, various concentrations in microdroplets may be prepared in discrete manner. Droplet on demand technologies allow to form predetermined combination of concentrations in individually addressable droplets [172–174], yet as the concentrations are adjusted by varying the relative volumes of merged droplets, it is difficult to prepare samples presenting large ranges of concentration. A pioneering study by de Mello and coworkers demonstrated generation of dilutions over many orders of magnitude by literally diluting the content of a stock droplet with smaller droplets containing the solvent [95]. Recently, Postek *et al.*

described a system capable of precise 2-fold dilution, that relied on the metering of a sample and buffer in a single hydrodynamic trap, and serial dilution obtained by coalescing droplets with the aid of electric field [175]. These systems have neither, however, been optimized for automation nor have they been interfaced with modules for generation of Droplet Interface Bilayers.

Here we tested the implementation of on-chip dilution for long-term screens of the function of membrane protein – alpha-hemolysin.

5.2. Results

5.2.1. Geometry of the microfluidic chip

The structure of microfluidic device was similar to the one described in Chapter 3, except of the additional trap-structures added for the dilution of a sample (Figure 42). The device consists of: i) a hydrodynamic trap for formation of DIB, ii) aspiration modules for protein, buffer and inhibitor/buffer, iii) dilutor modules for a protein sample. The dilutor module consists of two traps – one of which meters a precise volume of liquid, and second which serves for slowing down droplets and subsequently trapping two of them in close contact, inducing their coalescence. The trap that meters a droplet comprises a barrier that perpendicularly obstructs the channel to 30% of its height and widenings of the channel milled to 70% of its normal depth. Droplets longer than the trap block the entrance for the continuous phase to the bypasses when they encounter the trap. The droplet is being pushed until the moment that the rear of the droplet aligns with the entrance to the bypasses and the oil starts to flow around the droplet. As a result, the droplet is split in two at the barrier – one part of a well-defined volume stays locked in the trap and the remaining part goes into the waste channel. The second type of trap – merging trap – is similar in structure to the metering trap, with side intrusions instead of a barrier. The intrusions act as obstacles that increase the Laplace back pressure, inducing coalescence between two droplets immobilized in the trap. The total length of a pair of droplets is longer than the trap, and upon the merging of two droplets the aqueous plug is being pushed towards a mixing channel. Two silver wires coated with AgCl and a thin layer of agarose gel serve as the electrodes for the electrophysiological measurements on the proteins. One electrode is inserted into each of the two chambers of trap A. Similarly to the work described in Chapter 3 and 4, we used valves to control the flow of oil from pressurized containers.

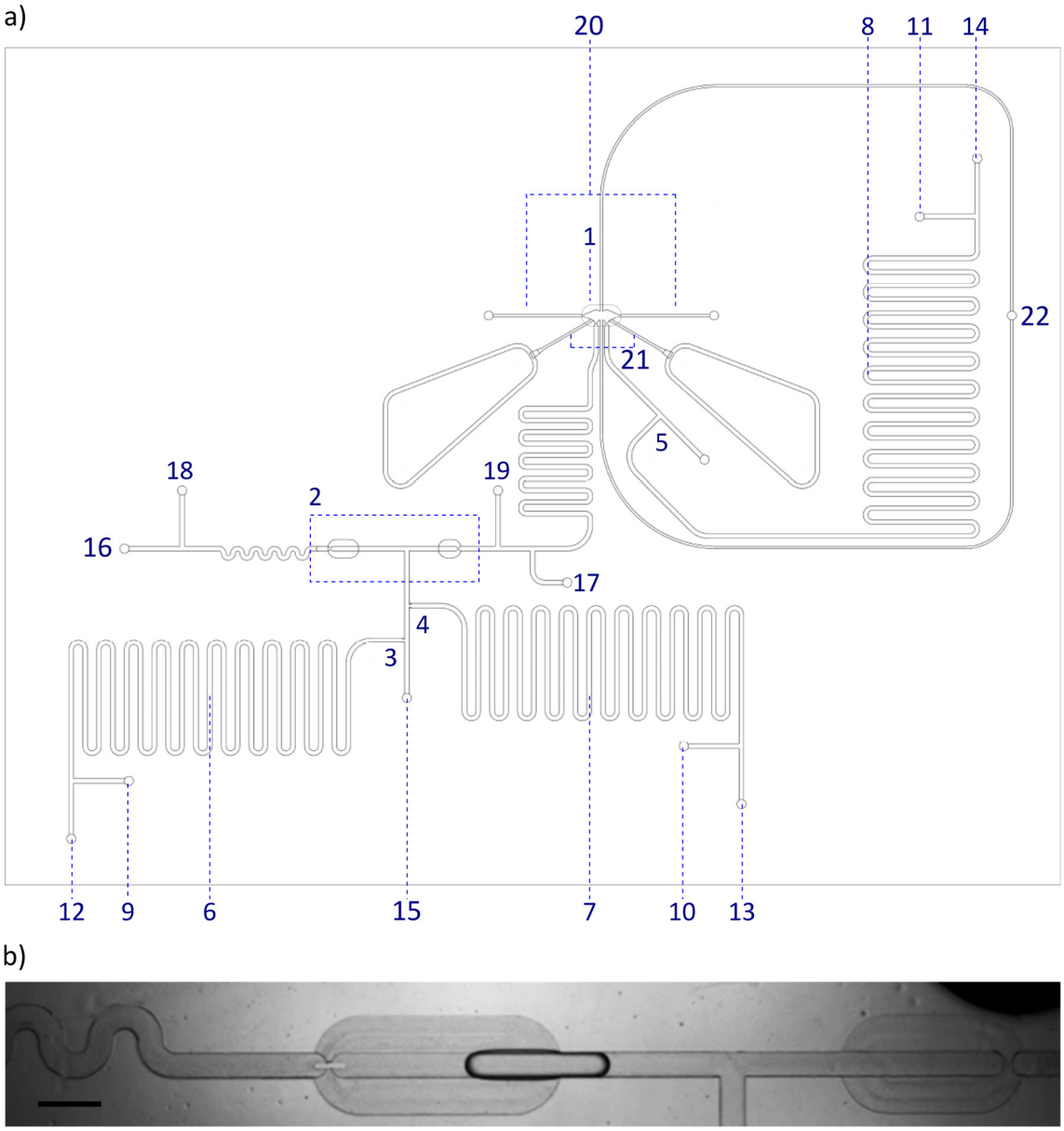

Figure 42 Geometry of microfluidic device for dilution of a sample on-chip. a) Detailed diagram of the layout of the microfluidic chip. The numbers indicate: 1 - hydrodynamic trap for a pair of droplets, 2 – set of traps for metering and merging, 3, 4, 5 - T-junctions for generation of droplets, 6 - channels used as a container for protein, 7, 8 - channels used as a container for the buffer, 9 - inlet for the protein solution, 10, 11 - inlets for the buffer, 12, 13, 14, 15, 16, 17, 22 - inlets for oil, 18, 19, 20 - outlet channels, 21 - channels for the pair of electrodes. b) A micrograph of a dilutor module comprising a metering trap (right) and merging trap (left). The width of the slit in the barrier in the merging trap is 100 µm. Scale bar is 1 mm.

5.2.2. Operation of the chip

We first filled the whole system with a continuous organic phase (90% v/v hexadecane, 10% v/v AR20) containing various concentrations of the lipid (DPhPC, 0.01-1 mg/mL). The concentration of lipid and silicone oil varied between the inlets. The inlets that supplied the oil for the operation of dilutor modules had no DPhPC lipid in the oil. No (or residual) presence of lipids, which act as surfactant molecules, facilitated coalescence

of two droplets in the merging trap. We decided for this approach instead of using electric field for coalescence induction, due to the fact that very strong electric field would disturb the measurement of picoampere currents on the same chip. The inlets close to the DIB-trap supplied a DPhPC rich (1 mg/mL) mixture of oils, which allowed for the formation of stable bilayer at the interface of droplets in the DIB-trap. Once we filled the chip with oil, we opened the ports and transferred small volumes (tens of microliters) of buffer (1 M KCl, 10 mM Tris-HCl, pH 7.0) and protein stock solution from a glass microsyringe connected to the chip via PTFE tubing. After closing the deposition ports we opened the flow of oil from inlets into the channel containing the sample to push the front of the aqueous aliquot to the T-junction.

The detailed operation of the dilutor module is shown in Figure 43. First, the droplet of undiluted sample is precisely metered (the excessive volume is directed to the waste channel) and the droplet is routed back to the merging trap. Then, a new droplet of a buffer is metered (the excess is directed to the waste channel) and the flow is reversed. The buffer droplet is transported to the merging trap where it coalesces with sample droplet. The content of a merged droplet is mixed in a winding channel. Finally, the droplet is routed back to the metering trap. The excess of volume is directed for further measurements in DIB trap and the remaining sub-volume is moved back for the repetition of dilution steps.

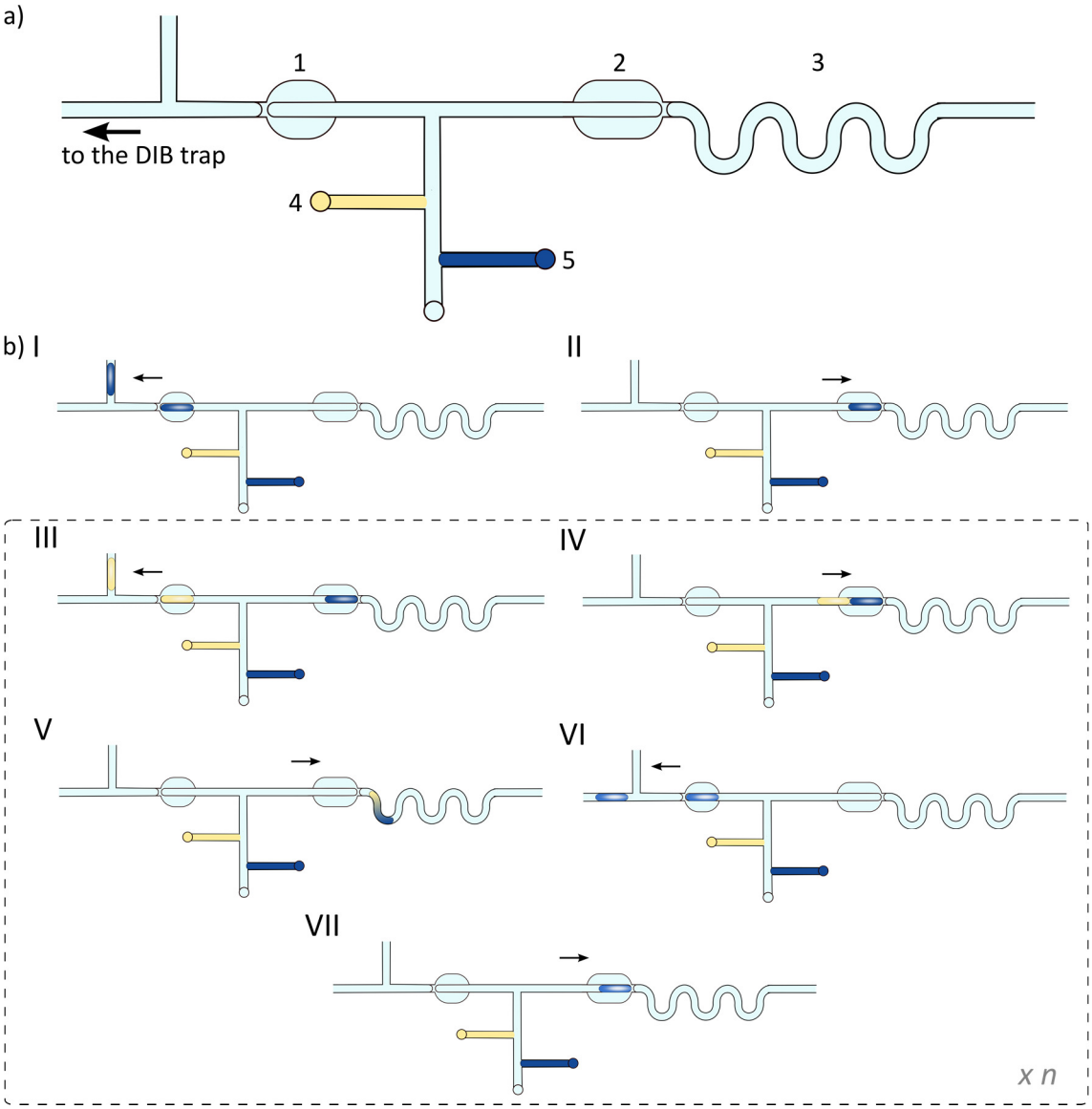

Figure 43 Schematic of droplet dilutor module and its operation. a) Droplet serial dilutor consists of: 1 – metering trap, 2 – merging trap, 3 – mixing module, 4 – buffer stored on a chip, 5 – stock solution of protein stored on a chip. b) Operation of the dilutor: a portion of buffer is metered (I, excess is discarded through a waste channel) and directed to the merging module (II). Next a droplet of defined volume is prepared from analyte sample (III) and reversed towards merging trap where it encounters a droplet of buffer (IV). Two droplets merge and the content is mixed in a winding channel (V). In the next step the big droplet is directed to the metering trap, where it is split into 2 smaller droplets. One stays in the trap and the other is directed to the trap to form a DIB (VI). The droplet of mixed solutions is reversed to the merging trap (VII) where it can be subjected to further dilutions by repeating steps III – VII.

5.2.3. Dilution of protein

The initial results concerning the storage of αHL on chip and preparation of dilutions were promising. We managed to use the above described system for preparing dilutions of protein from the stock solution (50 µg/mL) stored for long periods of time on chip. We compared between the activity of protein diluted 10-times off-chip to the 8-fold dilution

obtained on-chip and observed the same number of channels incorporated into the bilayer in both of the approaches. However, if the stock was pre-diluted (e.g. 2 times) to lower concentration and stored in channel (to reduce the number of operations required to obtain a desired concentration) a gradual loss of activity was observed (similar to observed in Chapter 3).

In addition, we performed an experiment to verify that storage of an undiluted sample on the chip does not cause aggregation or degradation of the protein. The undiluted sample was stored on chip at the beginning of the procedure and was not supplemented during the experiment. Figure 44 presents the time needed for insertion of app. 200 channels (equals to the detection limit of 10 000 pA in the given salt conditions and voltage clamped at 50 mV) in relation to the time passed from the deposition of the stock on chip. There is no systematic trend in the measured values suggesting that there is no decay in the activity of the protein. After the 48 and 72 hours of the protein storage in microfluidic chip in RT, the maximal level of current was reached within 160 s and 100 s, respectively.

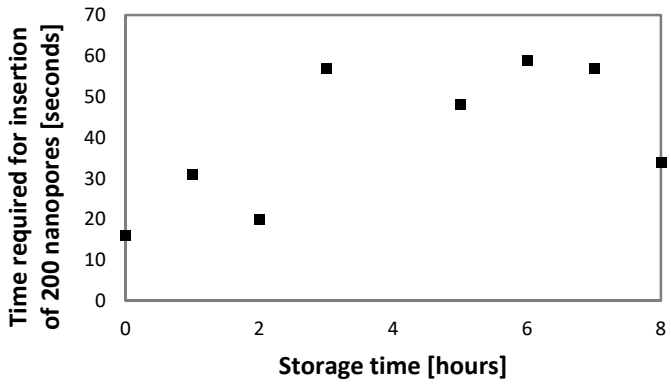

Figure 44 A time required for achieving the level of current of 10 000 pA (ca. 200 nanopores present in bilayer) from an undiluted sample stored in the microfluidic device.

The initial results of serial dilutions are collected in Table 3. Regardless of the time of the storage of *α*HL stock solution on chip, similar level of current was generated by protein samples upon dilution.

Table 3 Serial dilutions of *α*HL stored in microfluidic device.

Time [hours] after the deposition of a sample on chip	Dilution fold			
	2^1	2^3	2^5	2^7
	Current [pA]			
0	Max	1600	200	150
1	Max	1060	240	80
2	1260	0	0	0
3	Max	650	66	0
4	Max	560	70	0
5	6000	530	160	-
6	2380	550	60	75
48	Max	660	0	-
72	Max	180	0	475

5.3. Chapter summary and conclusions

However, in the course of experiments we encountered major technical difficulties. The concentrated protein sample tend to wet the surface, which resulted in a lack of repeatable metering of sample and uneven dilution ratios. In addition, the fully functional system would need up to 18 valves, that required a programming of the new driver. At this point, we decided to explore an alternative to automated microfluidic systems – a passive system, in which the sample is processed by a set of hydrodynamic traps within the chip, rather than actively routed with the aid of valves.

CHAPTER 6.

Passive and Parallel Microfluidic Formation of Droplet Interface Bilayers (DIBs) for Measurement of Leakage of Small Molecules Through Artificial Phospholipid Membranes

Chapter 6 describes passive microfluidic system for easy and rapid generation of Droplet Interface Bilayer pairs, each formed between two aqueous nanoliter droplets comprising arbitrarily defined chemical composition. The system allows for rapid quantification of leakage of small molecules through artificial phospholipid bilayers. The droplets are generated, diluted and stored in-situ on the microfluidic chip in microfluidic Meter&Store (M&S) modules. Meter&Store modules are sets of hydrodynamic traps, which enable hard-wired operations on small, ca. 9 nL in volume, aqueous droplets. These operations comprise splitting, merging and derailing the droplets to side storage wells. As a consequence, the droplets are locked and positioned next to each other and form bilayers at the point of contact between the aqueous compartments. The basic capacity of the trap-based system is formation of an array of 12 lipid bilayers in less than 5 minutes. Thanks to the small volumes of the droplets, the system is capable for monitoring the transport across the artificial membrane within relatively short intervals of time. The readout is based on the use of dyes and alleviates the difficulty of parallel electrophysiological measurements. Additionally, a set of trap modules provides the possibility for in situ preparation of dilutions of a sample. We use this functionality to prepare on-chip dilutions of alpha-hemolysin nanopores and quantify the calcium ions flux through the pores.

6.1. Introduction

In this chapter, we report a microfluidic system for the rapid, parallel and facile formation of arrays of model lipid bilayers. Here, the control over the content and position of an individual droplet and the ability to generate multiple such droplets are the main motivation for the use of droplets for formation of artificial membranes. In contrary to the systems described in Chapters 3 and 4, we relied on fluorescence read-out instead of electric measurements.

One of the simplest and the most efficient methods to characterize the transport processes in the lipid membrane is the measurement of the changes in concentration of a given compound in compartments separated by the bilayer. Determination of the rate of passive permeation through the artificial bilayer is one of the methods in the assessment of transcellular transport of a given chemical compound which is very often of a drug candidate. Microfluidics provides the possibility to repeatedly form nanometer-thick stable bilayers, and to monitor the interior of the aqueous microcompartments. However, there are just a few examples of microfluidic systems based on fluorescence read-out designed for measurements of passive permeation of small molecules through the lipid bilayer [130,134,135,163].

Ota *et al.* presented a PDMS device with an array of microchambers – recesses of walls in parallel channels – for measurements of flux of calcein dye through alpha-hemolysin nanopores [111]. By alternately flushing the channels with aqueous sample and with an immiscible organic solvent containing a phospholipid, bilayers were formed between the microchambers and the main channels. Monitoring of diffusion of calcium ions through alpha-hemolysin nanopores was demonstrated as a proof-of-concept experiment by Castell *et al.* who presented a method of deposition of an aqueous droplet on the surface of planar hydrogel for formation of an array of bilayers [156]. Fluo-8 dye was used to detect the transport of Ca^{2+} cations. Additionally, authors measured the inhibition of ionic flux through αHL by gamma-cyclodextrin. Tonooka *et al.* constructed a device, in which an array of hemispherical picolitre droplets is brought into contact with one larger droplet [129]. Silicon wafers containing thousands of cavities were used to generate membranes either from spread lipid vesicles [112,113] or from lipid solutions in organic phase [114,115]. Recently, Schlicht *et al.* proposed a non-complicated passive system for generation of droplet networks [136]. The device was an improved design of the

microdroplet-based shift register [152] and the trapping structure were fabricated using standard soft lithography. However, the contact area between the droplets was not uniform and varied during the experiment, possibly due to evaporation of droplets or swelling of PDMS structure, which prevented a quantitative analysis between the compartments.

So far, the proposed systems were limited by the high degree of complexity in terms of the fabrication and equipment needed for the operation of the device e.g. piezo actuated nano-injection systems for dispensing of nanoliter droplets. The challenge lies in the construction of simple-to-operate system that could be operated in a conventional biochemistry laboratory, without specialized infrastructure. Here we describe such a method - a microfluidic device that allows for generation of up to 12 lipid bilayers with all the liquid samples simply delivered from syringe pumps. The processing of a sample on a chip – diluting, partitioning into droplets and formation of pairs of droplets - is hard-wired in the hydrodynamic traps for passive handling of fluids. We demonstrate the efficient formation of lipid bilayers at the interface of droplets and monitor the passive permeation of fluorescent dye from the donor to the acceptor droplet. We also show the quantification of the transport rate of calcium ions through alpha-hemolysin nanopores as a function of concentration of the protein.

6.2. Results

6.2.1. Geometry of the microfluidic chip

The whole valve-free device, dedicated for parallel formation of DIBs, consists of microfluidic T-junctions for dosing of aqueous samples and a set of 9 or 12 Meter&Store modules (Figure 45 and Figure 47b). A simplified design of the device consisting of 9 traps was used for the experiments that did not require dilutions of sample. For operating in the dilution mode, we added an additional metering trap and storage well for precise dosing of a sample. The width and depth of the channels is 160 μm, except for dimensions of selected details (e.g. barrier and bypasses) in trap modules (Figure 46). Small dimensions of channels significantly reduced the capacity of the whole device to approximately 10 μl, and the total volume of oil required for the execution of the whole protocol on the chip equals to ca. 30 μl. The flow rate of oil applied in the sequence of operations of trapping, merging, diluting was between 0.1 and 0.3 ml/h.

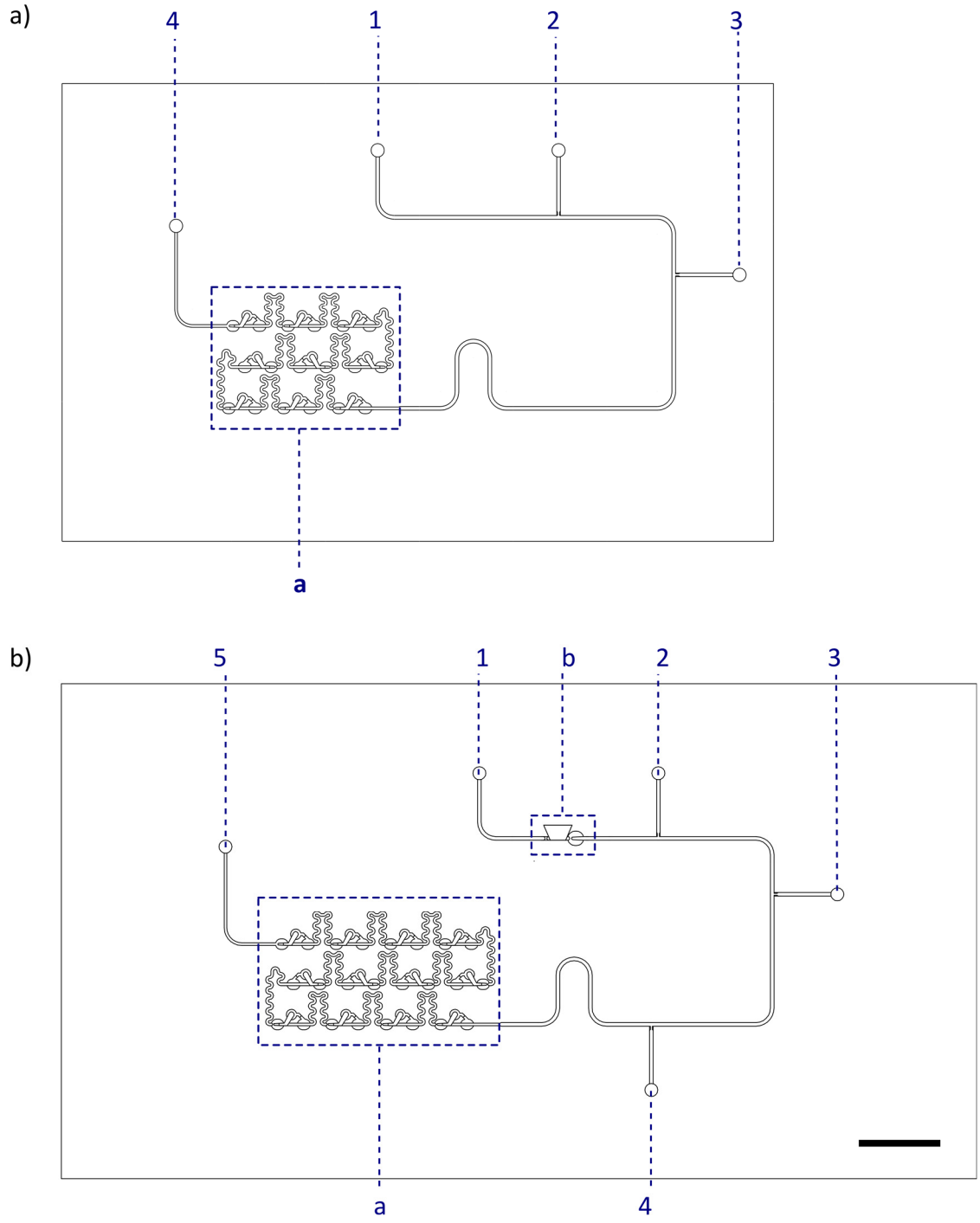

Figure 45 The layout of the microfluidic devices. a) 9-trap device: 1 – inlet for the continues phase, 2 – inlet for a sample, 3 – inlet for a buffer, 4 – outlet, a – a set of 9 Meter&Store modules. b) 12-trap device with dilutor: 1 – inlet for the continues phase, 2 – inlet for a concentrated sample '1' (protein/inhibitor), 3 – inlet for a dilution buffer, 4 – inlet for a sample '2', 5 – outlet, a – a set of 12 Meter&Store modules, b – a module for metering of a precise portion of sample 1. The scale bar is 5 mm.

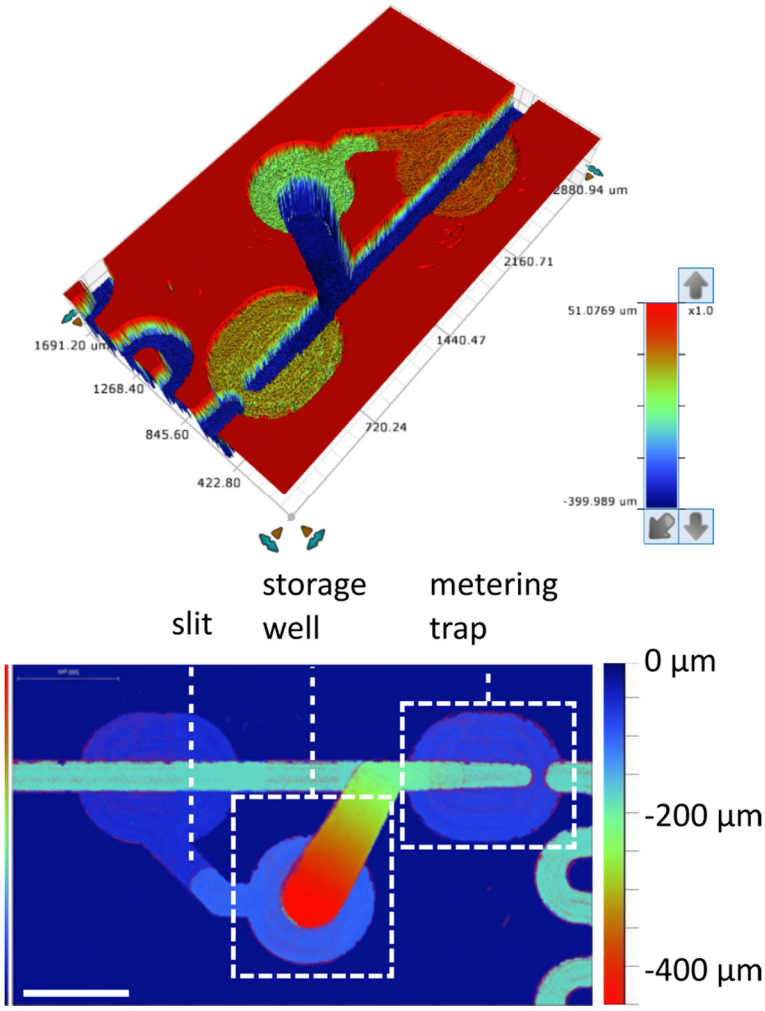

Figure 46 Profilometry scans (recorded by Bruker ContourGT-K) depicting the architecture of the microfluidic trap. The trap consists of a part for metering of droplets, a widening and deepening storage well and a slit for equalizing of the flow of oil.

6.2.2. Formation of bilayers in traps

The basic functional module of the system is the Meter&Store (M&S) unit. Here, we scaled down the dimensions of the M&S module to operate on droplets with volume of less than 10 nanoliters – ca. 100 times smaller than in the system presented earlier by Derzsi *et al.* [102].

A single Meter&Store module consists of a metering trap and an adjacent storage well (Figure 46b). The metering part comprises a barrier that perpendicularly obstructs the channel to 33% of its height and a pair of bypasses – a widening of the channel milled to 33% of its normal depth. In case when an aqueous plug is longer than the trap, it encounters the barrier and the rear of the droplet blocks the entrance for the continuous phase to the bypasses. As a result, the flow of continues phase pushes the droplet until the

moment that the rear of the droplet aligns with the entrance to the bypasses and the oil starts to flow around the droplet. Eventually the droplet is split in two at the barrier – one part of a well-defined volume stays locked in the trap and the remaining part being pushed further into the main channel. When we stop the flow of continuous phase, the droplets locked in the metering traps begin to spontaneously flow back to the adjacent storage wells. The flow of droplets towards the bottom of wells is achieved passively with capillary forces that pull the droplet out of the converging metering trap (Figure 47a).

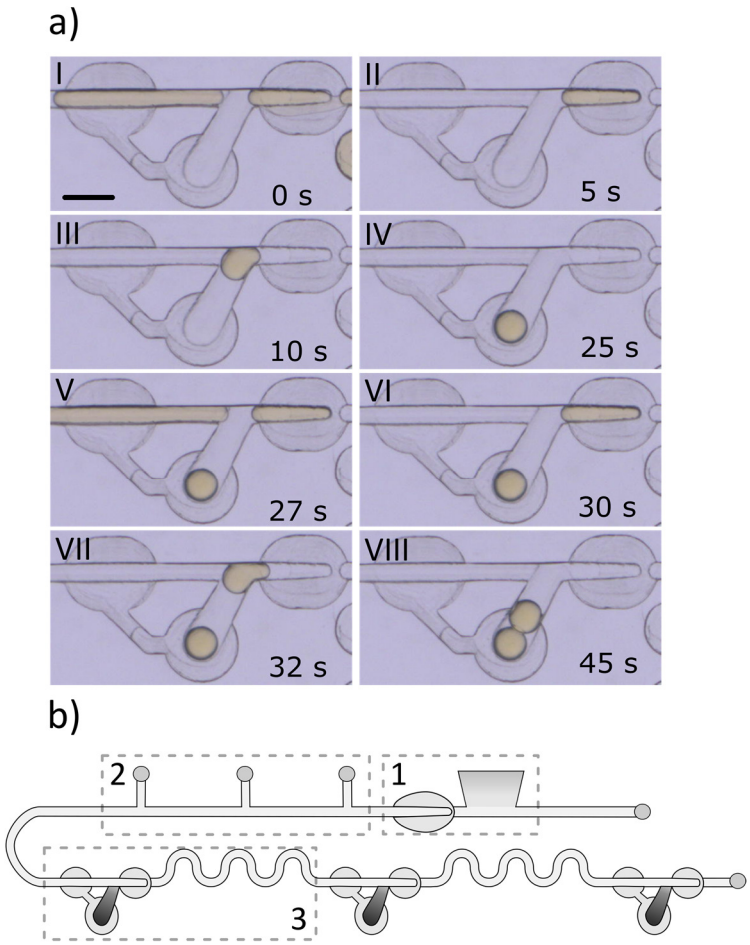

Figure 47 Operation of the trapping module. a) Formation of DIBs in a single Meter&Store module: a random sequence of droplets of aqueous sample is metered into defined portions in metering traps (I) and after the flow of oil is halted (II) the droplet is passively dragged to the bottom of the well (III - IV). Next, metering of a second type of aqueous sample is performed (V – VI) and the droplet is directed to the storage well (VII) to contact the already stored droplet and form a lipid bilayer at their interface (VIII). Scale bars is 500 µm. b) General scheme of series of traps in the microfluidic device for DIBs formation and sample dilution on-chip: "1" – metering module dedicated for operations in dilution mode, "2" – inlets for aqueous samples, "3" – Meter&Store module with serpentine channel for mixing of droplets content.

The storage wells served as containers for pairs of droplets, at which interface the lipid bilayers were formed. In the first step, we filled the chip with continuous phase. In the next step we deposited first type of aqueous sample and push it through the chip and aliquot into droplets of volumes equal to ca. 9 nL that were predefined by the geometry of the microfluidic modules. After we halt the flow of oil, the droplets formed in the metering traps are derailed to the adjacent storage wells by the action of capillary forces. Then, the other type of aqueous sample was introduced onto chip and flown through the set of metering traps, and aliquoted in the same way as the first type of a sample. These droplets, again, after stopping the flow of oil, spontaneously moved into the storage wells. In the storage wells the two droplets met and touch each other. As both of the droplets are covered with a monolayer of 1,2-diphytanoyl-sn-glycero-3-phosphocholine (DPhPC) or 1,2-dioleoyl-sn-glycero-3-phosphocholine (DOPC) lipids, they do not coalesce, but rather form a lipid bilayer at their interface. The removal of droplets from storage wells was executed by applying the flow of oil at rate higher than 5 ml/h.

6.2.3. Permeation of fluorescein through lipid bilayers

We studied the permeation of FITC molecules across DOPC bilayers. By analysis of changes of concentration over time we determined the permeation coefficients. For this purpose, we generated a collection of 9 pairs of droplets comprising ‘acceptor’ (150 mM KCl, 10 mM HEPES) and ‘donor’ (100 µM FITC, 150 mM KCl, 10 mM HEPES) compartments (Figure 48a). We measured the intensity of fluorescence of each droplet every 5 minutes over a period of 2 hours and plotted the changes in the concentration of fluorescein versus time (Figure 48b). Mean volume of droplets (8.7 nL ± 0.5 nL) and area of bilayers (10 250 μm^2 ± 1 400 μm^2) were calculated with the assumption of spherical shape of droplets and circular area of bilayers. For the data analysis, we assume that the concentration of fluorescein within each of the droplet is homogeneous and the diffusion coefficient of fluorescein in water is $D = 0.49 * 10^{-9}\,m^2/s$ [176]. Therefore, any inhomogeneities are relaxed over a characteristic time $t = (r^2)/D$ which is 33 s for the droplet of radius r = 128 µm.

To describe passive transport from one compartment to the other we assume that current of FITC molecules is proportional to the concentration difference in the donor and the acceptor:

$$j = k(c_d - c_a) \qquad \text{Eq. 11}$$

This equation also defines the permeability coefficient k. The above current multiplied by the surface of the membrane, jS, gives flux of FITC molecules (numbers of molecules passing through the membrane in unit of time). Number of molecules which pass through the membrane in a unit time can be also expressed by rate of change of number of FITC molecules in donor or acceptor, therefore we have,

$$jS = -V\frac{dc_d(t)}{dt} = V\frac{dc_a(t)}{dt}, \quad \text{Eq. 12}$$

where V is the volume of each droplet. We introduce concentration difference

$$c(t) \equiv c_d(t) - c_a(t) \quad \text{Eq. 13}$$

and assume that the sum of the concentrations is constant (no leakage of FITC outside droplets),

$$c_a(t) + c_d(t) = const = c_0. \quad \text{Eq. 14}$$

Combination of the last four equations leads to the following evolution of concentration difference,

$$V\frac{dc(t)}{dt} = -2Skc(t) \quad \text{Eq. 15}$$

Its solution with initial conditions corresponding to our experiment (no FITC in acceptor, concentration c_0 in donor), $c(t=0) = c_0$, has the following form

$$\frac{c(t)}{c_0} = e^{-t\frac{2Sk}{V}}. \quad \text{Eq. 16}$$

The above time dependence of the difference of concentration $c(t)$ should describe our experiments for each of 9 different pairs of droplets. We introduce concentration difference averaged over different pairs of droplets, $\langle c(t)/c(0)\rangle$, i.e. averaged over 9 experiments. According to equation 16 its logarithm should satisfy the following relation:

$$-log\langle\frac{c(t)}{c_0}\rangle = t\frac{2Sk}{V} \quad \text{Eq. 17}$$

The logarithm of average normalized concentration difference, $f(t)$, is shown in Figure 48c. We obtained the permeability coefficient equal 5.39 x 10^{-8} m/s.

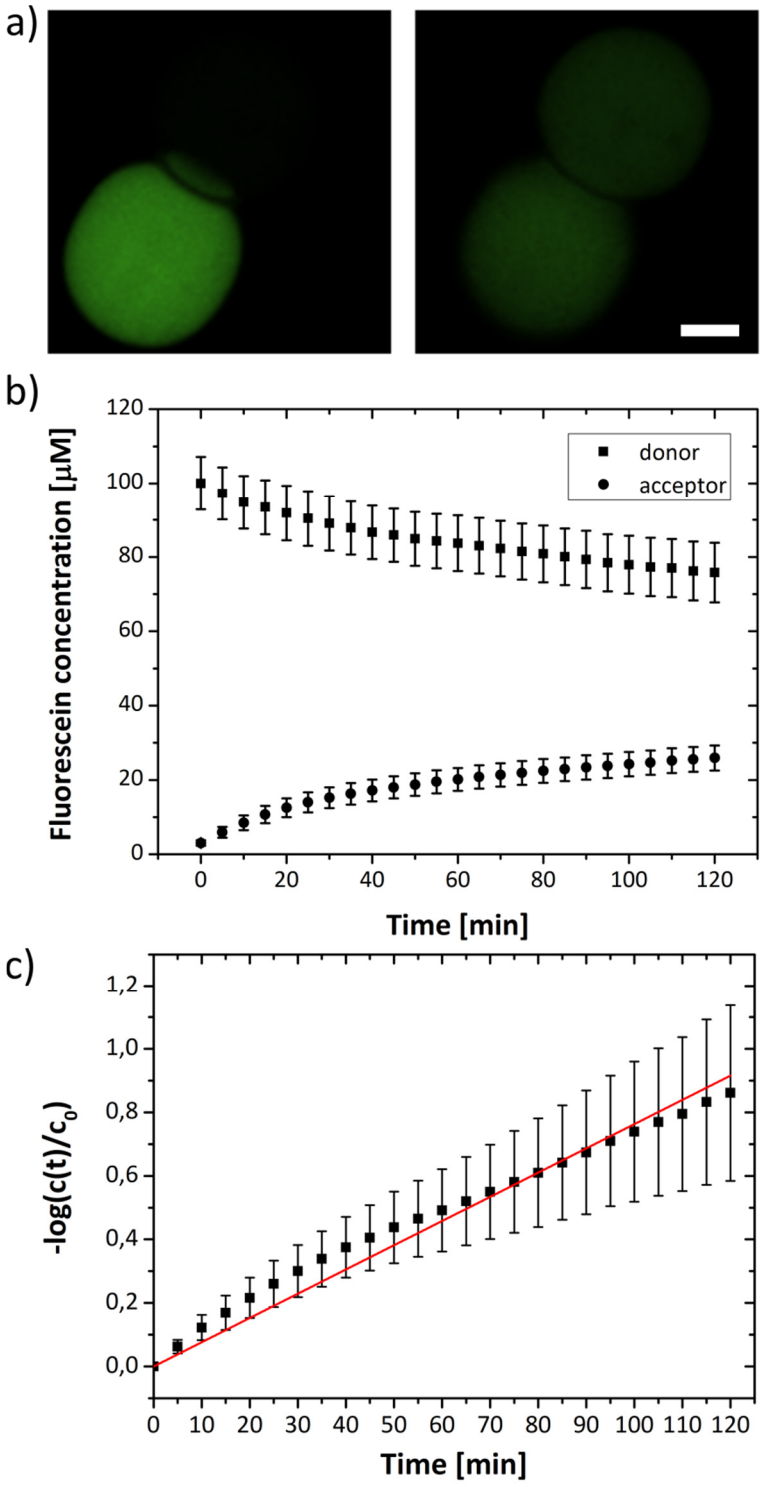

Figure 48 Permeation of fluorescein dye through lipid bilayers. a) Snapshots of the trapped pair of droplets before the measurement (left panel) and after 120 minutes of incubation (right panel). The donor droplet was 100 µM FITC, 150 mM KCl, 10 mM HEPES and the acceptor droplet was 150 mM KCl, 10 mM HEPES. Scale bar is 100 µm. b) Changes in fluorescein concentrations measured within droplets in time (n = 9). c) The logarithm of the concentration difference between two droplets in a pair is linear in time (data averaged over 9 pairs of droplets).

6.2.4. On-chip dilutions

We also used the very same Meter&Store system to demonstrate that it can be used for generation of dilutions of the sample. In Figure 49, Figure 50 and Figure 51 snapshots from a procedure of generation of dilutions are presented. The inlets are signed as: 'in-1' – inlet for oil, 'in-2' – inlet for a concentrated sample (buffer 150 mM KCl, 10 mM HEPES, pH 7 spiked with a red dye), 'in-3' – inlet for a dilution buffer (150 mM KCl, 10 mM HEPES, pH 7), 'in-4' – inlet for a buffer (150 mM KCl, 10 mM HEPES, pH 7). Continuous phase comprised DPhPC at a concentration of 1 mg/mL in the mix of 90% v/v hexadecane and 10% v/v silicone oil AR20. In the snapshots, we use a bold font to mark the inlets, from which the flow was applied at the moment the photo was taken. Scale bar in the left bottom corner of inset 'a' is 5 mm. The device can be operated in two modes – by the initial dilution of the sample prior to metering of the buffer (experiments with dilution of protein) or inversely - by metering the buffer in the first step (snapshots presented in Figure 49, Figure 50 and Figure 51). In the Figure 53 a close up of preparation of dilution is depicted.

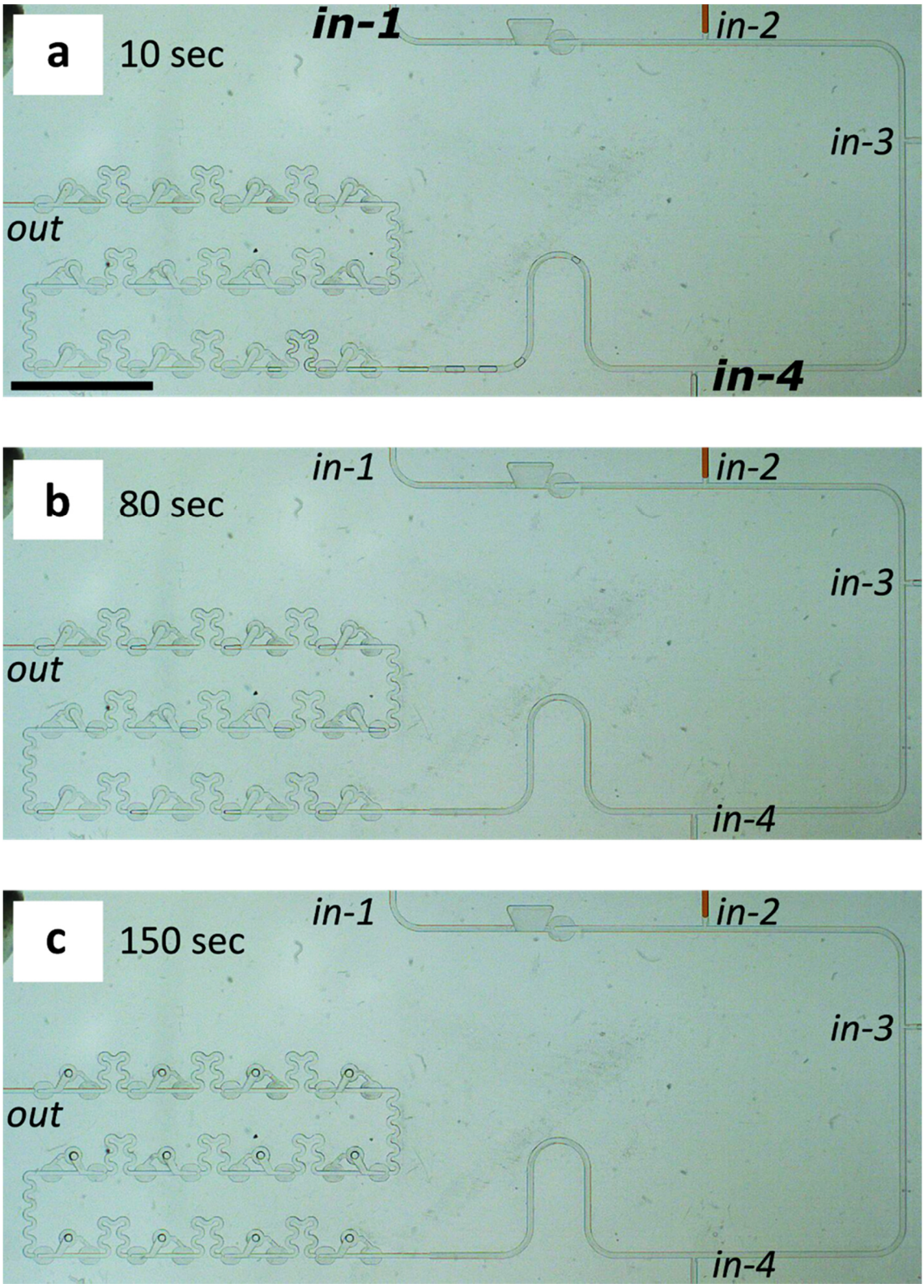

Figure 49 Snapshots depicting the metering and storage of buffer droplets. a) First, we generate a sequence of droplets of a buffer and b) split them into 12 droplets in a series of traps. c) In the next step we switch the flow of oil off and allow droplets to flow to the bottom of adjacent wells.

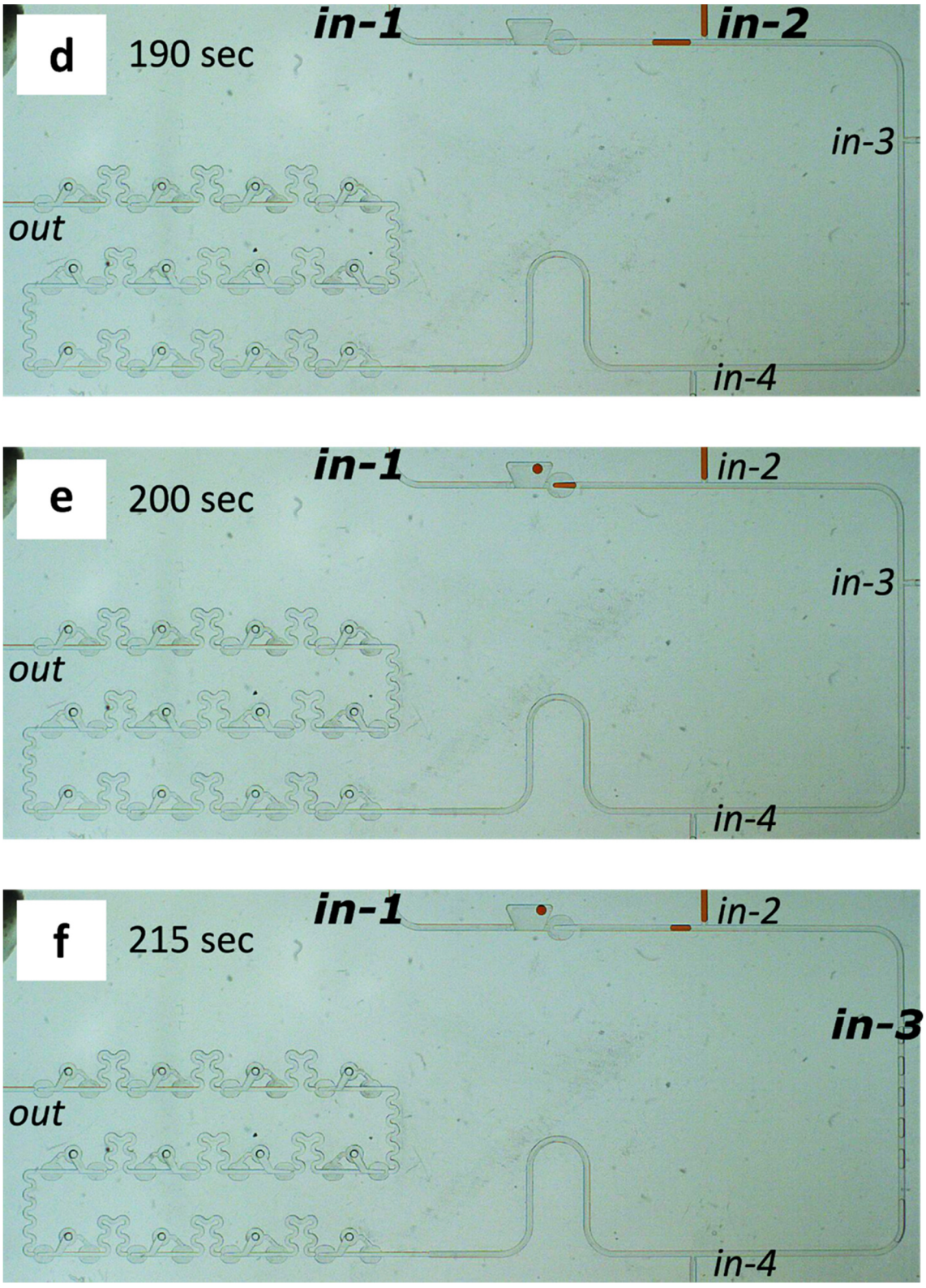

Figure 50 Snapshots depicting the metering of a droplet of a sample and generation of a train of buffer droplets. d) From the inlet 'in-2' we aspire a small volume of concentrated sample with reversed flow of oil and e) meter it into a predefined portion. f) The flow of oil from the inlet 'in-1' is applied and droplets of buffer from the inlet 'in-3' are generated.

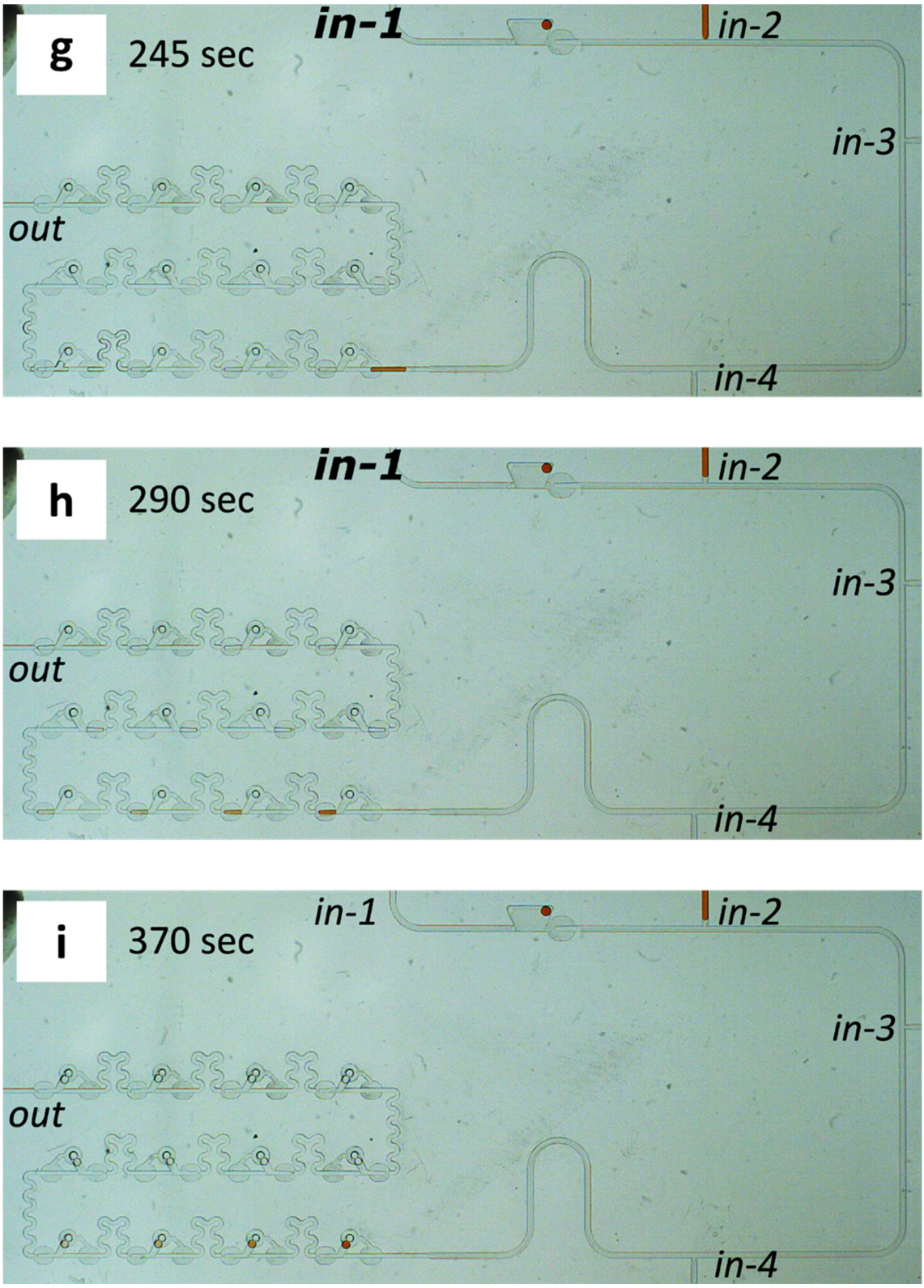

Figure 51 Snapshots depicting the dilution of a sample and formation of pairs of droplets. g) We push the droplets of a dilution buffer, which is immediately followed by a droplet of a concentrated sample. h) The sample is diluted in the subsequent traps and, i) after switching off the flow of oil, the droplets are directed to the storage wells, where they form bilayers at the interface with already stored droplets.

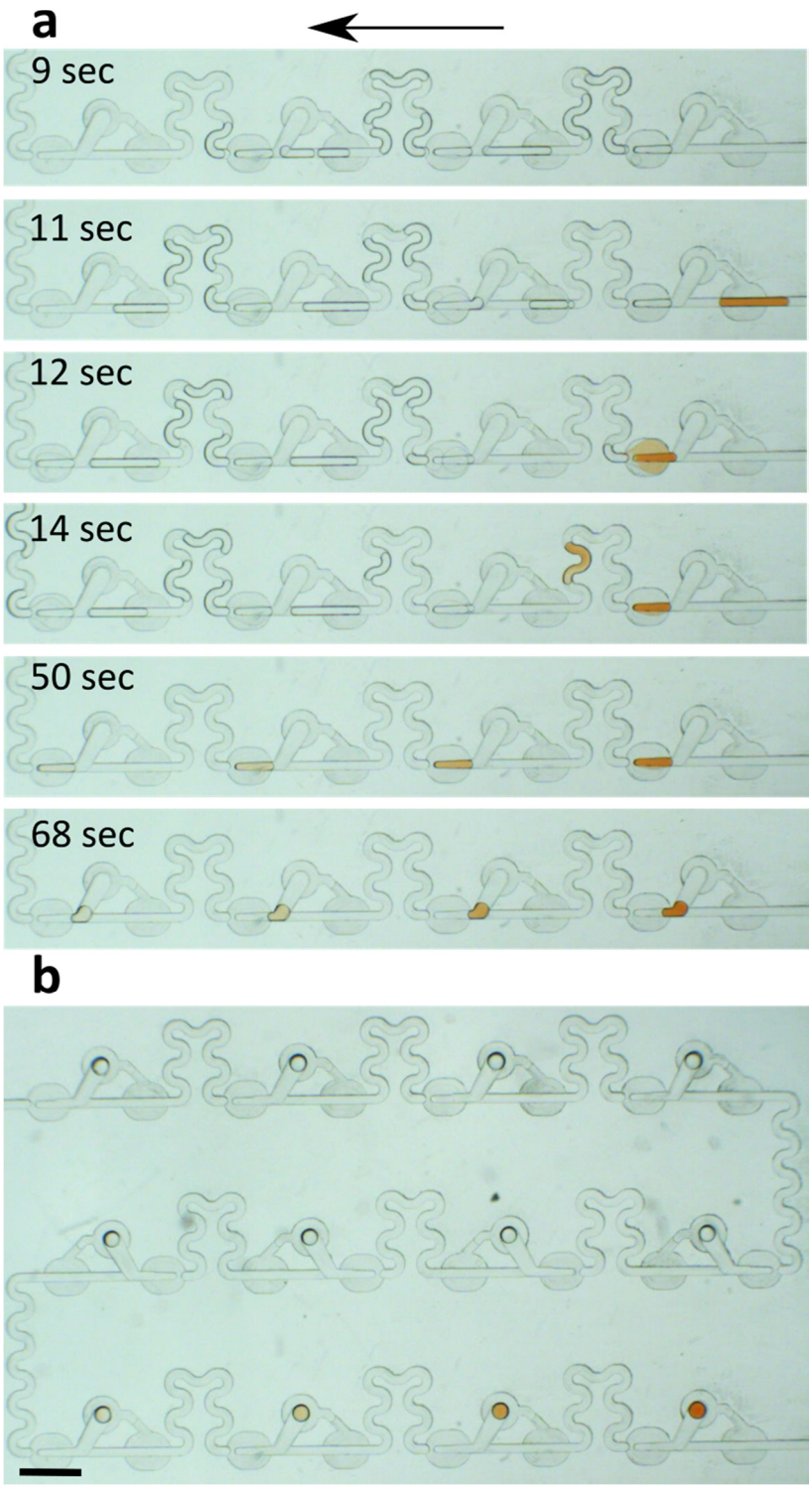

Figure 52 Dilution on a chip. a) The preparation of dilution of a dye is shown for first 4 traps in line. The arrow shows the direction of flow of oil and droplets. b) A view of droplets stored in wells, composed of gradually diluted dye. Scale bar is 1 mm.

We have evaluated the performance of the dilutor using Rhodamine 110 dye. Figure 53a shows the pairs of droplets in which one droplet contains consecutively diluted dye. The assembly of droplets was prepared as follows:

- first the plug of 20 μM rhodamine is aspirated with a reverse flow of oil from one of the inlets to a trap for a precise metering,
- then the flow of oil is switched to the dosing mode and in the same time droplets of pure buffer are generated at one of the T-junctions,
- next we generate the flow of oil which moves the train of droplets of a buffer immediately followed by a single droplet of undiluted rhodamine to the set of Meter&Store traps,
- the sample is diluted in the subsequent traps and, after switching off the flow of oil, the droplets comprising dilution series are directed to the storage wells,
- in the next step we generate a sequence of droplets of a buffer and split them into 12 droplets that flow back to the wells where they form bilayers at the interface with already stored droplets.

The experiment was repeated 7 times. We have determined the dilution ratio equal to 1.6 ± 0.2 between following traps based on the comparison of the fluorescence intensity inside the droplets (Figure 53b). Further, we used the dilution ratios between successive droplets to calculate into the expected concentrations of rhodamine and plotted these values on the log scale (Figure 53c).

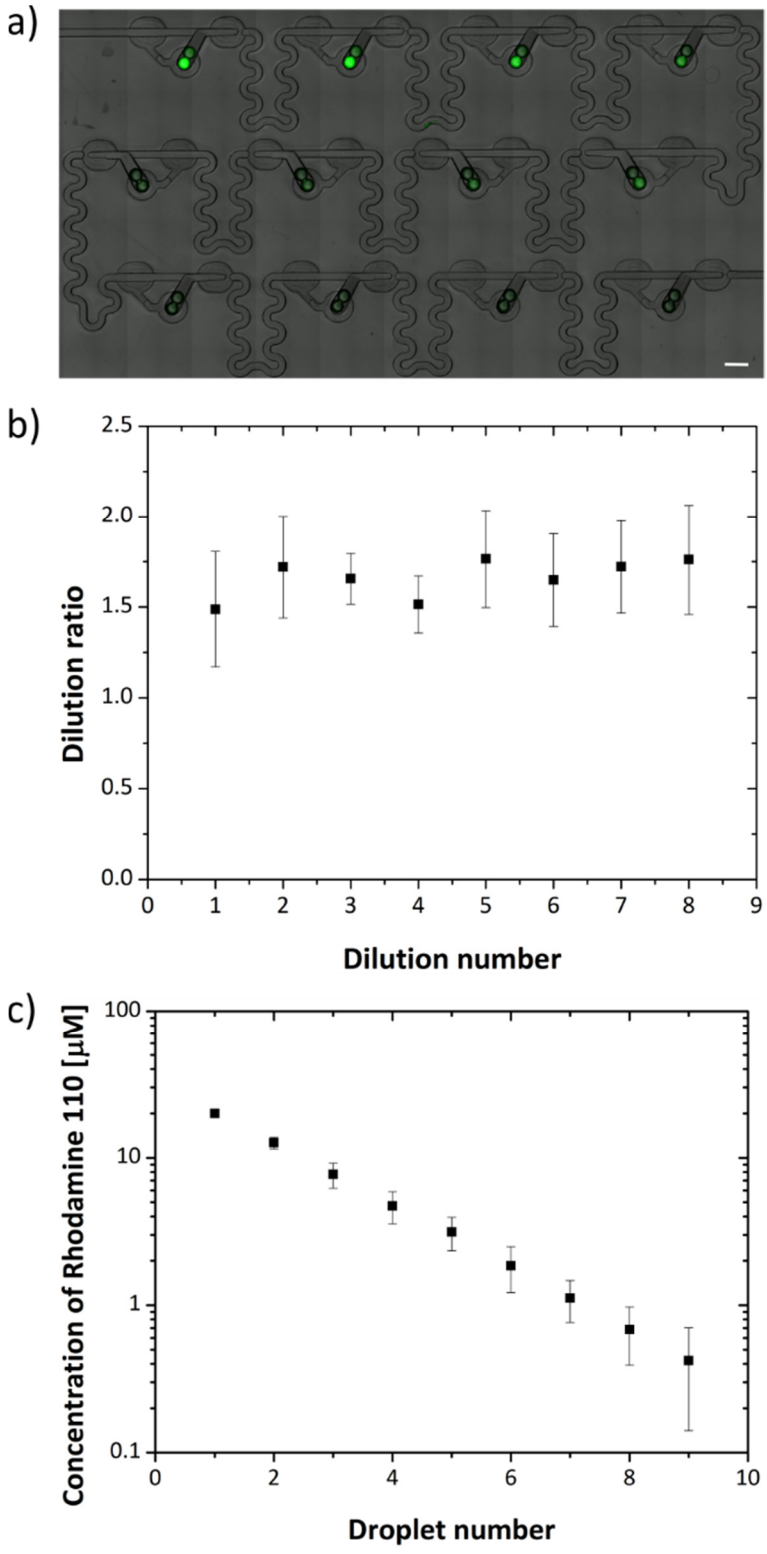

Figure 53 Dilutions on a chip. a) A snapshot presenting the result of dilution of Rhodamine 110 (20 µM) dye in 12 subsequent traps. The droplets were stored in wells and exposed to droplets of buffer. The fluorescence intensity was measured for the Rhodamine containing droplets. b) The dilution ratio between the following trap modules calculated from the intensity of fluorescence, n = 7. c) From the intensity of droplets, the concentration of rhodamine was calculated (n = 7). The level of fluorescent signal in the last three droplets (no. 10 - 12) was below the sensitivity of the detector and could not be included in this plot.

6.2.5. Dilutions of protein sample on-chip

Further, the activity of varying concentration of *α*HL protein in bilayers formed by DPhPC lipids (dissolved at 0.5 mg/mL in oil) was studied. As *α*HL pores penetrate lipid bilayers by forming water-filled channels in its structure, the channels non-selectively and passively allow the flow of small molecules, including calcium ions. We monitored the increase of fluorescence in droplets containing the calcium sensitive Fluo-8 dye. The increase of fluorescence is attributed to the transport of calcium ions through the *α*HL channels in bilayers. In the control experiment, we did not observe any leakage of calcium ions when no *α*HL pores were present (Figure 54).

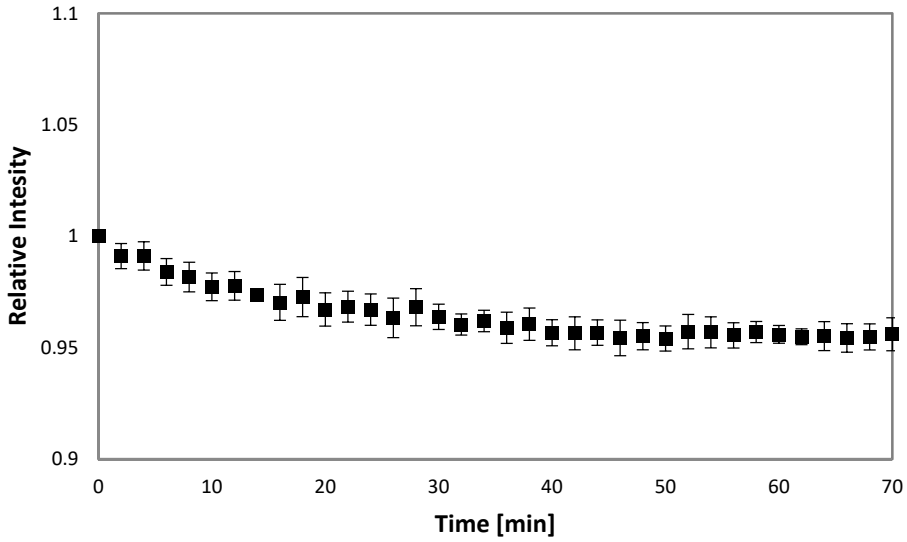

Figure 54 Control experiment for the leakage of calcium ions in the absence of nanopores. Fluorescence intensity of droplets containing 10 µM Fluo-8H, 10 mM HEPES, 0.34 mM EDTA, interfaced with droplets containing 100 mM $CaCl_2$, 10 mM HEPES.

In the first step of preparing dilutions of protein on-chip, we meter a portion of concentrated stock solution of protein (600 nM *α*HL, 150 mM KCl, 10 mM HEPES, 250 µM Fluo-8H, 0.34 mM EDTA) in a metering trap and then immediately prepare a sequence of aqueous plugs with buffer (150 mM KCl, 10 mM HEPES, 250 µM Fluo-8H, 0.34 mM EDTA) at one of the T-junctions. A trap for metering of a solution of protein consisted of a metering trap and storage well, that had 2 times larger volumes than the single Meter&Store unit. The metering of the undiluted protein sample priori to a dilution on-chip allowed for accurate and repeatable execution of dilutions. We flew the buffer (followed by the protein plug) through the Meter&Store units.

The dilution itself proceeded in the following way. Buffer was metered into predefined volumes and, as we do not stop the flow of oil, the droplets did not flow back into the storage well. Instead, they were immediately merged with a droplet containing αHL, that followed them. The plug, which was generated and pushed out as a result of merging of buffer with the concentrated protein, had a volume equal to the initial volume of protein sample. In the winding channel mixing of the content of droplet took part by convection, before the droplet entered the next Meter&Store unit for further dilution. This way, we were able to prepare droplets with gradually decreasing concentration of protein molecules. After the flow of oil was switched off, the droplets were passively (i.e. by capillary forces) directed to the bottom of the side storage chambers. In the next step of the experiment, we generated a sequence of plugs containing calcium ions (100 mM $CaCl_2$, 10 mM HEPES) at one of the T-junctions. The plugs were metered in the 12 Meter&Store units and stored in the wells after switching the flow of oil off.

We measured the values of fluorescence intensity corresponding to transport rate of calcium ions depending on the number of protein pores present in the bilayer and plot them versus time (an exemplary trace is shown in Figure 55). The more nanopores are present in the membrane, the faster is the increase of fluorescent signal coming from the excitation of dye with the calcium molecules. At some point the curve reaches a plateau meaning that the number of calcium ions exceeds the number of available Fluo-8 molecules. The model used previously in the Paragraph 6.2.3. to describe the diffusion of fluorescein molecules is modified to calculate a permeability coefficient. Based on the obtained curves and literature data on nanopore dimensions and diffusion of calcium ions in a protein channel, we derived the permeability coefficients of membranes and the equation for the number of protein pores at any time. As an example, we estimate that for the concentration of 600 nM of αHL, after 40 minutes of measurement, 1.2×10^4 pores were present in the bilayer (see the next chapter for the full description of the model and calculations).

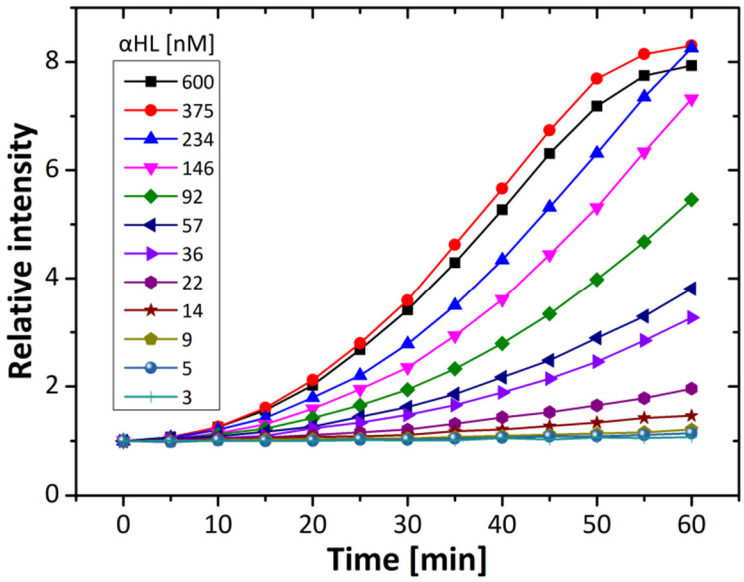

Figure 55 Dilutions of protein sample on-chip and transport of calcium ions through *α*HL nanopores. *α*HL nanopores were diluted on chip and the transport of calcium ions was measured depending on different concentrations of nanopores. An exemplary plot shows the mean intensity of the droplet area observed from excitation of Fluo-8 over time. The concentration of *α*HL nanopores was calculated using the value of dilution ratio equal to 1.6.

6.2.6. Model of permeation of calcium ions through αHL nanopores

6.2.6.1. The description of the system

In the experiment of dilutions of protein, we have 12 pairs of donor and acceptor droplets. The volume of droplets containing 600 nM alpha-hemolysin, 10 µM Fluo-8H, 10 mM HEPES, 0.34 mM EDTA was 8.6 nL ± 0.5 nL, and area of bilayer 9 050 µm^2 ± 900 µm^2. Concentration of calcium ions in the acceptor droplet is denoted by $c_a(t)$ and concentration in the donor droplet is denoted by $c_d(t)$. Initially in the acceptor droplet there are no calcium ions. From the beginning, there is a lipid membrane between the donor and the acceptor droplets. The membrane without any nanopores is impermeable to calcium ions. Initially, in the acceptor droplets there is a protein alpha-hemolysin (initial concentration $c_{ah}(0)$) which in the course of time builds in into the membrane, making the nanopores for calcium ions. It causes diffusion of calcium ions from the donor to the acceptor droplet. Additionally, in the acceptor compartments there is Fluo-8 dye at a concentration c_{Fluo-8} = 250 µM. The Fluo-8 molecule emits light in the presence of Ca^{2+}. In the experiment we monitor 12 pairs of droplets by recording the relative intensity of light emitted by Fluo-8 in each acceptor of the twelve pairs.

6.2.6.2. The relative intensity of light and concentration of the calcium ions

To calculate the concentration of calcium ions in the acceptor droplet we are using the following procedure. For each pair of droplets there is the same initial concentration of calcium ions in a donor, c_0. We assume that the increase of the relative intensity is proportional to concentration of calcium in the acceptor droplet:

$$i_a(t) = \frac{I_a(t)}{I_0} = 1 + \beta_r c_a(t), \qquad \text{Eq. 18}$$

which defines β_r parameter. We estimate β_r from the experimental data from Fig. 4 using the curve corresponding to the droplet with concentration of c_{ah} = 600 nM. The increase of concentration of calcium ions in the acceptor results in the fluorescence of Fluo-8 molecules. The emission of light is increased as long as concentration of calcium ions is lower than concentration of Fluo-8. Only one calcium ion is needed for one molecule of Fluo-8 to trigger the emission and after saturation of all Fluo-8 molecules with calcium ions additional amount of Ca^{2+} cannot further increase the level of fluorescence. In the curve for c_{ah} = 600 nM there is a plateau, which means that number of Ca^{2+} is approximately the same as the number of Fluo-8 molecules, i.e. $c_a\,(t = 60min) = c_{Fluo-8}$ = 250 µM. Using this value in Eq. 17 we obtain:

$$\beta_r = \frac{\frac{I_a(t=60min)}{I_0} - 1}{C_{Fluo-8}} = 2.77/mM. \qquad \text{Eq. 19}$$

We assume that β_r is the same for all pairs of droplets.

6.2.6.3. Model describing the evolution of concentration of calcium ions

We adopt the same model of diffusion through a membrane as described in the previous section which is summarized by equations 11 - 15. Additionally, the permeability coefficient $k(t)$ depends on time because of the presence of αHL, therefore the equation 15 has the following form:

$$V\frac{dc(t)}{dt} = -2Sk_p(t)c(t). \qquad \text{Eq. 20}$$

Thus, the permeability coefficient can be calculated for each time according to the following equation:

$$k_p(t) = \frac{-V}{2Sc(t)}\frac{dc(t)}{dt}. \qquad \text{Eq. 21}$$

6.2.6.4. Calculation of $k_p(t)$ from experimental data

From equations 18 - 20 and 12 - 13 included in expression 21 we obtain

$$k_p(t) = \frac{V/S}{\beta_r c_0 - 2i_a(t) + 2} \frac{di_a(t)}{dt}. \quad \text{Eq. 22}$$

We calculate permeability $k_p(t)$ using the above formula from the experimental data, using V =8.7 nL and $S = 9050\mu m^2$. The results presented in Figure 56 show a linear increase of permeability in the first 40 minutes of the experiment. After this time, there is not enough of free dye molecules and we are not able to detect all of the transported calcium ions (which results in the decrease of the calculated permeability). We fit a straight line to each of the experiment from Figure 56 for the data obtained within first 40 minutes of the experiment. Slope of each of the curve gives the rate of change of permeability (presented in Figure 57) which shows that the rate of change of permeability coefficient is proportional to the concentration of alpha-hemolysin:

$$\frac{dk_p}{dt} = R_p c_{\alpha h} \quad \text{Eq. 23}$$

We exclude the experiment with the highest concentration of alpha-hemolysin and fit the curve to the data from Figure 56, which results in obtaining a coefficient:

$$R_p = 1.0x \frac{10^{-6} m^4}{s^2 mol} = 0.001\, m/(s^2 M) \quad \text{Eq. 24}$$

The rate of change of the permeability is constant for the first 40 minutes (linear increase of all curves for the first 40 minutes in Figure 56), therefore the evolution of the permeability coefficient is described as follows:

$$k_p(t) = R_p c_{\alpha h} t \quad \text{Eq. 25}$$

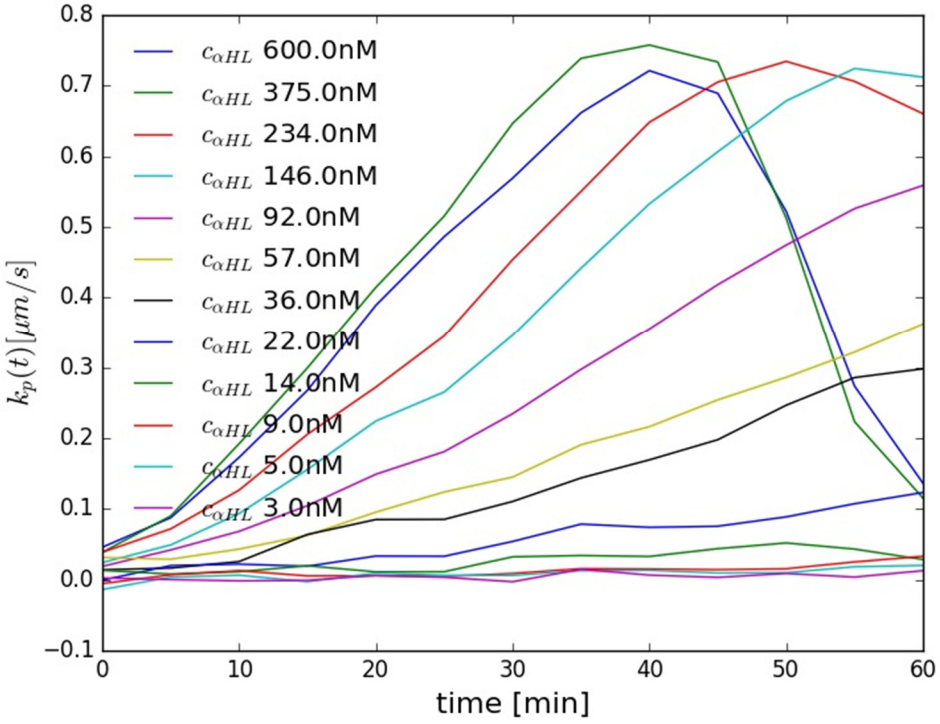

Figure 56 Permeability coefficient of membrane as a function of time.

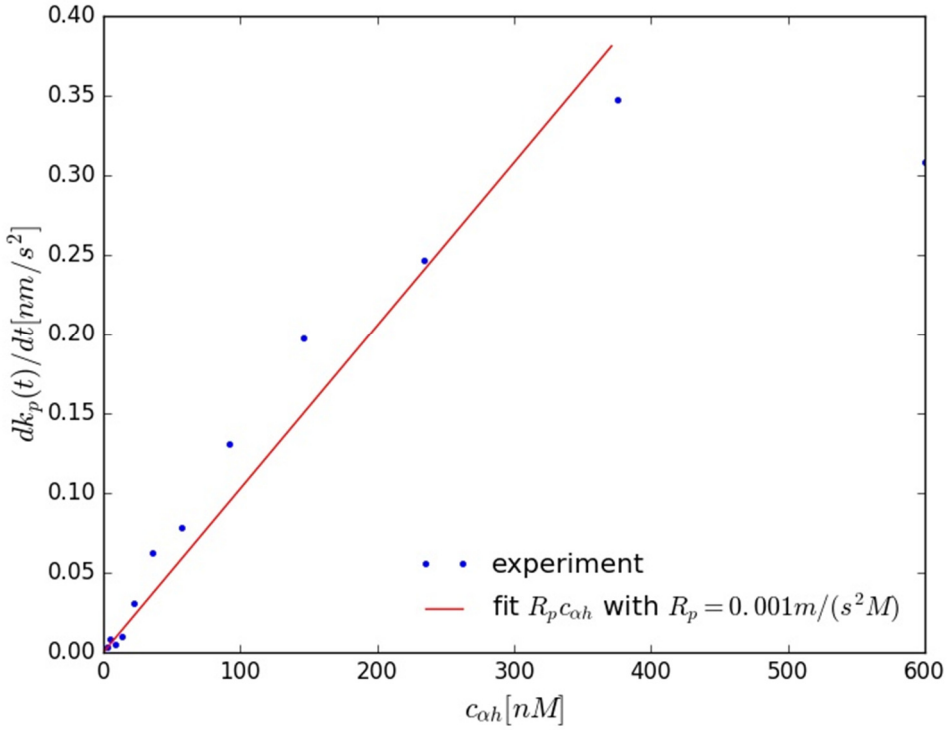

Figure 57 Rate of change of permeability for different concentration of αHL.

6.2.6.5. Estimation of number of pores

To estimate the number of pores we adopt the following approximations:

- we model the membrane by a set of N channels. Each nanopore (alpha-hemolysin) is a tube-shape of diameter d = 1.8 nm (average of the stem) and the length l = 5.2 nm [8]. The area occupied by a single nanopore is estimated from the radius of a single molecule and equals $s_{\alpha HL} = 2.54 * 10^{-6}$ μm².
- for the purpose of this estimation, we assume that there is a simple diffusion process inside the nanopore and that the diffusion coefficient of Ca ions is estimated by the self-diffusion of water molecules in 25°C, characterized by diffusion coefficient $D = 2.3 * 10^{-9}$ m²/s [177].
- moreover, for a given concentration of calcium ions in a donor and acceptor droplets we assume the stationary state inside the nanopore: the concentration profile inside the channel is linear with the position along the channel. There is a gradient inside the channel: $(c_d - c_a)/l$.

The current of ions J inside the nanopore is described by (following from diffusion equation):

$$J = D\frac{c_d - c_a}{l} \qquad \text{Eq. 26}$$

In the whole membrane, the summarized flux of ions (number of ions per second – Φ) is given by the current in a single channel J multiplied by the cross-section area of a single channel $\pi d^2/4$ and then multiplied by the number of channels N,

$$\phi = \frac{JN\pi d^2}{4} = D\frac{c_d - c_a}{4l} N\pi d^2. \qquad \text{Eq. 27}$$

The total flux of ions through the bilayer is also given by $\Phi = jS$. From Eq. 11, $j = k_p(t)(c_d - c_a)$, applied in the case under consideration we get $\phi = Sk_p(c_d - c_a)$. From combining this expression with the above Equation 27, we receive:

$$Sk_p = \frac{DN\pi d^2}{4l}. \qquad \text{Eq. 28}$$

It leads to an estimation of number of nanopores at any time as follows:

$$N(t) = \frac{4Sl}{D\pi d^2} k_p(t). \qquad \text{Eq. 29}$$

The time dependence of the estimated number of pores in the experiment is derived from utilizing the above equation in the Eq. 25:

$$N(t) = \frac{4Sl}{D\pi d^2} R_p c_{\alpha h} t. \quad \text{Eq. 30}$$

Additionally, we calculate the pore fraction area φ which is defined by the ratio of the surface of all pores to the surface of the membrane:

$$\varphi(t) \equiv \frac{N(t)\pi d^2}{4S}. \quad \text{Eq. 31}$$

The combination of the last two equations gives:

$$\varphi(t) = \frac{l}{D} R_p c_{\alpha h} t. \quad \text{Eq. 32}$$

For the pair of droplets where highest concentration of alpha-hemolysin was used, $c_{\alpha h}$ = 600 nM, after 40 minutes of the experiment the above formula gives the fraction of the number of pores to be 3.3 x 10^{-6}, which gives $N(40min) = \varphi(40\ min)S/s_{\alpha HL}$ = 1.2 x 10^4 pores.

6.3. Chapter summary and conclusions

We demonstrate a simple-to-use microfluidic device which opens the possibility of generation of multiple lipid bilayers from very small samples of the lipid (ca. 30 µL) and the protein solutions (sample can be as small as 5 µL). We aimed at obtaining a format that would be easy to fabricate and operate. We fulfill these demands by utilizing microfluidic modules for development of a device in which formation of bilayers will require neither a skilled operator nor sophisticated equipment. 12 bilayers are formed at the interface of droplets, which are metered in special microfluidic modules from a random sequence of liquid plugs. The volumes of droplets, and hence the area of the bilayers formed between 2 droplets, are uniform. We did not observe malformation of bilayers or coalescence events. We confirm that formed membranes are functional lipid bilayers with experiments showing the passive transport of small fluorescent molecules and with insertion of protein molecules into the bilayer.

The further increase of the number of bilayers can be achieved by parallelization, realistically by the factor of 8, giving the number of 96 droplet pairs [178]. Motorized microscope or automated imaging plate reader can be employed for the imaging. However, more precise CNC micromilling machine would be required, along with careful design and adjustment of channel resistances in parallel dilution modules (e.g. by implementation of flow resistors) and finally the need of smart sample deposition strategy

e.g. similar to 3D-printed lids sealing the inlet for the sample [179]. It is worth noting that it was not trivial to down-scale the structure of Meter&Store trap – both in terms of difficulty in microfabrication and adjusting the dimensions of trap structures for particular choice of fluids and the scale of the chambers. The solution of phospholipids in hexadecane has a very low (<1 mN/m) [25] interfacial tension with water – the value is much lower in comparison to fluorocarbon oils (3–14 mN/m) [180–182] used in the study of Meter&Store traps published by Derzsi *et al* [102]. The low surface tension results in many problems such as facilitates formation of small, unwanted satellite droplets at the steps and barriers in the traps or premature breaking of droplets at the barrier. Therefore, we needed to carefully choose the dimensions and aspect ratios of the traps, mainly: the depth of bypasses, the height of the barrier and the length of the trap needed to be optimized. In ca. 10 iterations we decreased the height of the bypass in the metering trap and adjusted the height of the bypasses and barriers located around the storage well to the 50% of the depth of the main channel (previously the depth of this area was 33% of the main channel). This change was necessary to speed up the derailing of the small droplets from the metering trap to the bottom of the wells. In this work for the first time the trap-based system for formation of lipid bilayers combined the ability of facile preparing on-chip dilutions of a sample with passive positioning of droplets. Thanks to this feature we tested various concentrations coming from one protein sample. However, comparing to original design, the precision of the performance of the dilutor is lower, which can be explained by the use of smaller volume of droplets and the presence of phospholipids in the continuous phase (mean RSD 14% and 4%, respectively). Droplets have to merge during dilution in the metering trap but later they have to remain unfused and separated by the bilayer in the side well of the trap. The merging during dilution is facilitated by squeezing of droplets ad then pulling them apart – this phenomenon was previously described by Bremond *et al*. [97]. However, the reproducibility and precision of dilution might be higher for decreased phospholipid concentration in the oil - an approach that cannot be applied in the current design due to the need of formation of bilayer in the side well in the next step of the protocol. However, in the future applications one can consider sequential using of two supplies of oil. First low concentration of surfactant can be injected for metering of buffer droplets and for the dilution and then surfactant-rich oil can be supplies for formation of the droplet interface bilayer in the side well.

We chose micromilling for fabrication of devices over the standard soft lithography methods because of the need for the three-dimensional structures of the traps, i.e. continuous slope of the floor of storage well. Additionally the chemical composition of continuous phase did not allow for the use of PDMS (polymer common in fabrication of microfluidic devices, which structure gets swollen by hexadecane and other alkane oils widely used for dissolving the lipids [103]). For faster and precise reproduction of chips, mass production schemes such as injection molding could be employed [183–185]. Contrary to the systems presented in Chapter 3 - 5, the described device does not require complex actuation (e.g. valves, piezoelectric modules) neither optical sensors for feedback-triggered control of microflows of fluids. It is rather based on the use of commercial syringe pumps, and we hope that in the future simpler sources of flow can be adopted for execution of operation on this passive system – e.g. a pipette [102], pumping lids [179] or passive pumping method [123,186].

One of the aims of the project was to measure the passive permeation rate of small molecules through the lipid bilayer. Transport of fluorescein between droplets connected via lipid bilayer was shown as a proof of the correct formation of membranes, however rarely it was followed by the quantitative description of the process. Droplets are a perfect tool to study transport phenomena, as they provide containers of well-defined volumes and, when immobilized in traps, result in a stable area of contact. The investigated small molecule – fluorescein – does not leak from droplets into the surrounding hexadecane, therefore the transport through a lipid membrane is the only route. We calculated the permeability coefficient of fluorescein through the DOPC bilayer to be equal to 5.4×10^{-8} m/s in pH 7.3, a value very close to the results obtained by Nisisako *et al.* (5.1×10^{-8} m/s in pH 7.5) [134]. Slightly higher coefficient value results from using lower pH (7.3 instead of 7.5) at which more species of fluorescein become uncharged and able to permeate. The presence of silicone oil in continuous phase, that affects the properties of bilayer, might influence the difference between the obtained results. Interestingly the calculated permeability coefficient value through DOPC bilayer is very close to a value measured in an endothelial cells culture (5.8×10^{-8} m/s) [187].

Electrophysiological methods to study single-channel behavior are a gold-standard, yet the fluorescence imaging creates new possibilities in studying of the activity of membrane proteins. Monitoring the flux of ions associated with excitation of fluorescent dye is a non-invasive method, which can be easily automated for collection of data from parallel

compartments. The fluorescence read-out is usually widely accessible among researchers and cheaper than electrophysiology measurements systems. Again, as a biologically relevant demonstration, we measured the ion flux through αHL nanopores incorporated in the DPhPC bilayer. The measurements of Ca^{2+} flow through αHL nanopores confirmed the data from similar experiments conducted in non-microfluidic system by Castell *et al*. showing an increase of fluorescent dye sensitive to the presence of calcium ions [156]. Most studies so far focused on showing the transport through alpha-hemolysin on a single-channel level. Here we take a different approach. Based on the available literature data and by creating a model which allows us to calculate the permeability rates we estimate the number of nanopores present in the bilayer.

The small volume of droplets and stable surface area of bilayers allow for data collection in over a period of ca. 60 minutes. We calculated the characteristic time for diffusion of fluorescein to be 33 seconds in 9 nL droplets, allowing for assumption of uniform distribution of molecules within the compartments. For the sizes of droplets used in the original work presenting Meter&Store traps, the time for diffusion would be 447 seconds. Even smaller droplets would be possible to obtain using different fabrication strategy e.g. multilayer soft lithography [188]. However, because the derailing of droplets to wells is not completely uniform in time, there is a variation between each pair of droplets in the exact moment of formation of bilayer. Differences at the level of few seconds do not significantly affect final results of experiments lasting ~60 min. but could be problematic in the case of very short experiments. In addition, due to the limited imaging area, the acquisition of images of multiple points using motorized microscope cannot be done at once. For 12 pairs of droplets it took 30 seconds to acquire images of all of them. Therefore, we did not aim to miniaturize the system to the further extend, due to the limitations in the rate of detection.

CHAPTER 7.

Summary and Conclusions

In the Chapter 7 general conclusions stemming from research projects described in Chapters 3-6 are provided. The approaches undertaken in this dissertation to construct microfluidic systems for formation of lipid bilayers are compared. Results of research on alpha-hemolysin are summarized. Finally, the directions of future development of droplet microfluidics systems to form lipid bilayers are indicated.

7.1. Research overview

This dissertation describes and discusses different approaches towards development of microfluidic systems dedicated to formation of model lipid bilayers. Microfluidic techniques aid research in fields of biochemistry and biophysics by offering manipulation of liquids at microscales, which results in possibility of formation of multiple nanoscale compartments from a small volume of a sample. Importantly, new microfluidic tools allow not only for more efficient performance of assays, but also enable addressing research questions from cell-scale perspective. Droplet Interface Bilayers emerged as an alternative approach for formation of artificial lipid bilayers in comparison to well established methods, such as assays on liposomes or Black Lipid Membrane. Microfluidic techniques have been proven to provide new approaches available for characterisation of lipid bilayers and membrane proteins. Here we employ a variety of droplet microfluidic techniques focused on controlled, automated and efficient preparation of DIBs.

The major advantage of formation of lipid bilayers at the interface of droplets is the exceptional mechanical and electrical stability of the obtained membrane. Bilayers obtained at the interface of droplets are stable during incubation lasting days, whereas this period is reduced to few hours for membranes obtained using BLM method. What is even more important, DIBs encased in a microfluidic device withstand mechanical stress caused e.g. by shaking of experimental setup. In the devices described in this dissertation, we were able to incubate pairs of droplets for longer than 24 h. Contrary to Supported Lipid Bilayer method that also provides mechanically stable membranes, microdroplets allow for the access to the bilayer from both sides. Here we demonstrate that within a pair or a network of few droplets individual droplets can be extracted without the cross-contamination between the droplet content, even when constant voltage of +/- 50 mV was applied. The streams of oil were used to separate bilayer leaflets and precisely manipulate the location of droplets within microfluidic channels. In addition, we demonstrated the control over the bilayer area with the application of flow of oil perpendicular to bilayer plane. Both reorganisation of droplet pairs or networks and defining the size of bilayer by changing position of droplets were performed manually in previous studies. Results described in this thesis show that the use of microfluidics allows for construction of robust experimental systems, where forming a lipid bilayer is independent from manual skills of the operator.

Below the most important findings presented in the dissertation are summarised and discussed.

7.1.1. Droplet microfluidic assays in biochemistry and biophysics

The growing interest in using droplet microfluidics in biological research was accompanied with the development of systems dedicated for high-throughput formation of monodisperse droplets. Assays that include encapsulation of DNA, bacteria or cells in aqueous droplets usually rely on fluorinated oils as continues phase, containing triblock copolymers as surfactants. It is worth noting that in comparison to these well-established droplet assays, the chemistry of continues phase (oil) used in this thesis is different and created challenges in handling of the droplets. The interfacial tensions of aqueous droplets with hexadecane with dispersed phospholipids is much lower in comparison to water with fluorinated oil. Low interfacial tension creates a risk of small satellite droplets being pinched off during droplet generation and splitting, resulting in the lack of reproducibility and cross-contamination between droplets. Therefore, a greater care was taken when designing microfluidic channels with the emphasis on the trapping structures.

Additional challenge in forming lipid bilayers in microfluidic channels is that the oils required for phospholipid dispersion are not compatible with standard materials used for fabrication of microfluidic devices, mostly with PDMS elastomer. This thesis describes the use of polycarbonate as a material suitable for handling and incubation of aqueous droplets submerged in hexadecane. Contrary to PDMS, polycarbonate is inert to hexadecane and does not get swollen. We chose polycarbonate for its good transparency – a characteristic crucial for microscope imaging of droplets, and for the ability to process the material with CNC micromilling machine. CNC milling proves to be especially useful for obtaining channels of continuously changing dimensions, a feature not being possible to fabricate using soft lithography.

7.1.2. Comparison of automated and passive approaches

Two approaches for lipid membrane formation are distinguished in this thesis. First, we focused on building a system in which generation of droplets and their flow within channels on microfluidic chip was controlled with programmable external valves. Coupled with the optical feedback, this system proven to be useful for automated, unsupervised and cyclic formation of lipid membranes. We achieved relatively high

throughput of stable bilayer formation and protein measurement - one bilayer formed every 3 minutes - a frequency limited by the time required for bilayer zipping at the interface of droplets and the time needed for incorporation of protein molecule into the membrane. Even more complex operations on droplets i.e. extraction on demand a droplet from a network was demonstrated. Importantly the construction of the experimental set-up was designed with respect to the presence of electrodes for single channel measurements. We collected electrophysiological measurements that exhibited satisfactory signal-to-noise ratio and were not hampered by the presence of surrounding electrical equipment. Using the automated system, we were able to quantify the inhibition of alpha-hemolysin nanopore with gamma-cyclodextrin molecules within 3 hours of continuous operation of the system.

However, when we consider the accessibility of the described system in laboratories not specialised in microfluidics, we need to admit that valve-based technology is not straightforward to implement. On the other hand, the number of laboratories that aim at using ready microfluidic devices operated by commercial pumping systems is growing. Therefore, we decided to propose a system in which processing of a sample would be executed on-chip in a manner depending on geometries of microfluidic channels. We aimed at constructing a simple to operate microfluidic chip that will be able to produce model lipid bilayers with high efficiency. We used hydrodynamic traps for parallel trapping of pairs of droplets coupled with dilution of a sample directly on a chip. We measured the transport of small molecules: passive leakage through a membrane and transport facilitated by nanopores. The proposed system is similar in functionality to commercially available artificial bilayer systems that are used for testing of permeability of various compounds through membranes.

In conclusion, both approaches for droplet formation and location in microfluidic chip – valve-controlled and defined by geometry of microfluidic channels – possess advantages in building a microfluidic platform dedicated for formation of model membranes. In the future, the development of the system may include equipping the traps described in Chapter 6 with electrodes for easy handling of droplets and for more complex characterisation of protein function.

7.1.3. Characterization of alpha-hemolysin activity in microfluidic devices

In this thesis the capabilities of the proposed microfluidic devices in membrane protein research are demonstrated using bacterial toxin – alpha-hemolysin. The formation of a well-defined channel – assembly of 7 subunits into a nanopore in the presence of a bilayer – is a property commonly used to test the quality of the artificial lipid membrane (e. g. the lamellarity).

Chapter 3 describes determination of kinetics of inhibition of alpha-hemolysin with gamma-cyclodextrin based on high-throughput measurements on microfluidic chip. A similar type of study was performed manually using droplets arranged into a static array of droplets containing inhibitors and a droplet with protein solution placed on a movable electrode. When designing a microfluidic system for automated exchange of droplets we were particularly concerned about the stability of droplets and contamination of electrodes. The final design of a trapping structure described in the Chapter 3 with electrodes was achieved through iterations starting from a design proposed by prof. H. Bayley [22]. Gradually we developed a unique design in which we achieved robust routing of droplets and efficient flushing out of droplets from electrodes. To avoid the coalescence of droplets while removing one of the droplets from a pair it was crucial to include a narrow channel from which a flow of oil was applied to gently separate two leaflets of a bilayer. The angle at which the electrodes were positioned was adjusted for the streams of oil to remove the droplet completely and washing efficiency was confirmed with electrical measurements. We conducted a high-throughput screening experiments on exposing alpha-hemolysin channels embedded in the bilayer to gamma-cyclodextrin molecules. The temporary docking of cyclodextrins inside of the protein pore and resulting block of flow of ions is a well characterised process. We compared the calculated K_d value to the literature data [155]. From the results of electrophysiological measurements it can be concluded that the proposed microfluidic device provides a good quality data not affected by artefacts coming from the system.

The ability to sense small molecules (notably DNA) by using alpha-hemolysin nanopores increased the interest in the use of this protein in biotechnology. In Chapter 4 we demonstrate that a high concentration of nanopores allows for a transmission of electric signal by transporting ions through the barrier of lipid bilayer. Droplets containing high

concentration of protein were excluded from being directly exposed to a sample of interest. So far droplets containing various types of molecules were used to functionalise lipid bilayers in an attempt to build networks of communicating compartments regarded as simple models for tissue structures. We constructed a system in which components of the network can be extracted and replaced on demand, and in which we tune the level of transmission of signal by varying the concentration of nanopores.

The focus on the transport processes through alpha-hemolysin nanopores, especially single-channel studies, allowed researchers to precisely establish the rates of transport of various ions. Combining the literature data of calcium ions leakage and mathematical modelling we were able to estimate the number of pores present in a bilayer based on a fluorescence signal increase corresponding to the levels of calcium ions transported between compartments by alpha-hemolysin protein. This study presented a new approach towards quantification of permeation of lipid membranes induced by presence of proteins.

7.2. Future applications of microfluidics in studies of model bilayers

This thesis provides examples of how the use of droplet microfluidics contributes to the development of research methods for studying the activity of membrane proteins reconstituted into artificial lipid bilayers. Droplet interface bilayer technique is currently being mastered towards better resemblance of natural membranes. The focus lies in controlling the properties of the artificial membrane by adjusting composition of lipids to be complex. For example one of the recent reports demonstrated direct delivery of sterol molecules to the lipid bilayer in order to induce changes in bilayer tension and thus affect the activity of potassium channels present in the membrane [36]. In another study changes in bilayer tension were obtained by axial withdrawal and compression of two droplets resulting in activation of mechanically gated bacterial channel MscL [46]. In the view of these studies the microfluidic system described in Chapter 3 that allows for precisely controlled separation of droplets with the flow of oil could be potentially used both to control the tension and to deliver components dissolved in oil to be built into the structure of the membrane.

Further improvements of the presented microfluidic systems might include increasing the performance throughput. The screening of activity of membrane proteins in the presence of active compounds requires both high efficiency and easy-to-operate experimental

setup. In the context of electrophysiological measurements, a multiplexed amplifier that allows for parallel recordings at a single-channel level would be necessary for multiplexed measurements from a microfluidic device. A desired solution would be to arrange electrodes (obtained for example by printing or by nanofabrication techniques) to be combined with the versatile droplet trapping structures described in this dissertation (Figure 58). The use of passive traps for formation of lipid bilayers allows to take the advantage of droplet microfluidics i.e. low sample consumption and manipulation with droplet position and content directly on chip. Simultaneous electrical recordings and monitoring fluorescence level within the compartments would allow for comprehensive understanding of the pore formation within the membrane.

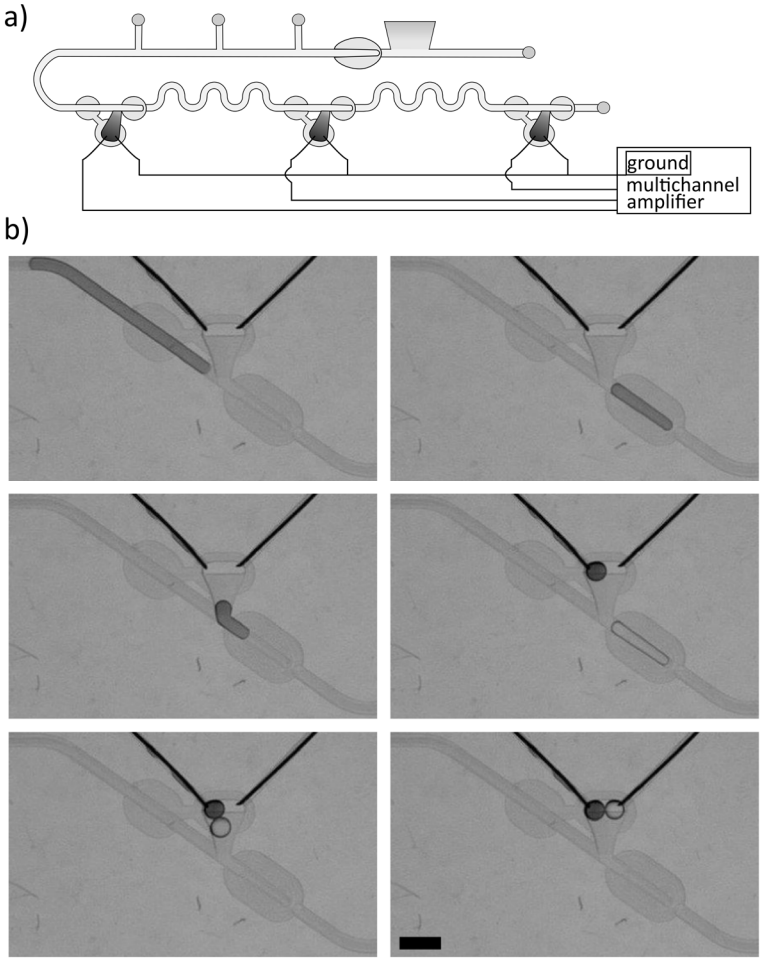

Figure 58 Implementation of electrodes into a well in Meter&Store module. a) A schematic of a device comprising passive traps and electrodes. b) We performed initial trials of combining silver wire electrodes with the trapping structure. A sequence of snapshots depicts passive operations of merging and trapping of droplets in pairs on two electrodes. The scale bar is 1 mm.

One of the most interesting emerging applications is the application of droplets for DNA nanopore sequencing, the field being currently explored by the Oxford Nanopore

company [189]. So far, the company offers a device dedicated for manipulation with droplets with electric field for the automatic preparation of libraries for sequencing. As a future perspective they envision to use automated manipulation with droplets for forming membranes as a support for nanopores for sequencing.

In addition to above mentioned improvements there is still a lot of potential to explore in the use of droplet microfluidics for the studies on interactions of proteins with lipid membranes. The knowledge about the interplay between proteins and cell membranes is important in the context of understanding mechanism of many diseases. The size of droplets can be controlled providing compartments of defined volume – an important feature when processes such as pathological aggregation of proteins in the presence of membranes are considered [190]. Moreover, the overall small volume of the sample suggests that temperature changes can be easily induced – both for the control of membrane fluidity, and for possibility of direct expression of proteins in droplets using in vitro transcription and translation.

Literature

1. Drews, J. Drug Discovery: A Historical Perspective. *Science* **2009**, *287*, 1960–1964.
2. Saliba, A.E.; Vonkova, I.; Gavin, A.C. The systematic analysis of protein-lipid interactions comes of age. *Nat. Rev. Mol. Cell Biol.* **2015**, *16*, 753–761.
3. Coskun, Ü.; Simons, K. Cell membranes: The lipid perspective. *Structure* **2011**, *19*, 1543–1548.
4. Lombard, J. Once upon a time the cell membranes: 175 years of cell boundary research. *Biol. Direct* **2014**, *9*, 32.
5. Brewer, P.D.; Habtemichael, E.N.; Romenskaia, I.; Mastick, C.C.; Coster, A.C.F. Insulin-regulated Glut4 translocation: Membrane protein trafficking with six distinctive steps. *J. Biol. Chem.* **2014**, *289*, 17280–17298.
6. Peraro, M.D.; Van Der Goot, F.G. Pore-forming toxins: Ancient, but never really out of fashion. *Nat. Rev. Microbiol.* **2016**, *14*, 77–92.
7. Song, L.; Hobaugh, M.R.; Shustak, C.; Cheley, S.; Bayley, H.; Gouaux, J.E. Structure of Staphylococcal alpha-Hemolysin, a Heptameric Transmembrane Pore. *Science* **1996**, *30701*.
8. Gouaux, E. alpha-Hemolysin from Staphylococcus aureus : An Archetype of beta-Barrel , Channel-Forming Toxins. *J. Struct. Biol.* **1998**, *122*, 110–122.
9. Giovanni Maglia; Heron, A.; Stoddart, D.; Japrung, D.; Bayley, H. Analysis of Single Nucleotide With Protein Nanopore. *Methods Enzymol.* **2010**, *475*, 591–623.
10. Bayley, H.; Braha, O.; Gu, L.Q. Stochastic sensing with protein pores. *Adv. Mater.* **2000**, *12*, 139–142.
11. Stoddart, D.; Heron, A.J.; Mikhailova, E.; Maglia, G.; Bayley, H. Single-nucleotide discrimination in immobilized DNA oligonucleotides with a biological nanopore. *Proc. Natl. Acad. Sci.* **2009**, *106*, 7702–7707.
12. Gu, L.Q.; Shim, J.W. Single molecule sensing by nanopores and nanopore devices. *Analyst* **2010**, *135*, 441–451.
13. Winterhalter, M.; Lasic, D.D. Liposome stability and formation: Experimental parameters and theories on the size distribution. *Chem. Phys. Lipids* **1993**, *64*, 35–43.
14. Hodgkin, A.L.; Huxley, A.F. A quantitative description of membrane current and its application to conduction and escitation in nerve. *J. Physiol.* **1952**, *117*, 500–544.
15. Dunlop, J.; Bowlby, M.; Peri, R.; Vasilyev, D.; Arias, R. High-throughput electrophysiology: An emerging paradigm for ion-channel screening and physiology. *Nat. Rev. Drug Discov.* **2008**, *7*, 358–368.
16. Ries, R.S.; Choi, H.; Blunck, R.; Bezanilla, F.; Heath, J.R. Black lipid membranes: Visualizing the structure, dynamics, and substrate dependence of membranes. *J. Phys. Chem. B* **2004**, *108*, 16040–16049.
17. White, S.H. Analysis of the Torus Surrounding Planar Lipid Bilayer Membranes. *Biophys. J.* **1972**, *12*, 432–445.
18. Tien, H. Black Lipid Membranes at Bifaces: Formation characteristics, optical and some thermodynamic properties. *J. Gen. Physiol.* **2004**, *52*, 125–144.

19. Montal, M.; Mueller, P. Formation of Bimolecular Membranes from Lipid Monolayers and a Study of Their Electrical Properties. *Proc. Natl. Acad. Sci. U. S. A.* **1972**, *69*, 3561–3566.
20. Tamm, L.K.; McConnell, H.M. Supported phospholipid bilayers. *Biophys. J.* **1985**, *47*, 105–113.
21. Tsofina, L.M.; Liberman, E.A.; Babakov, A. V. Production of bimolecular protein-lipid membranes in aqueous solution. *Nature* **1966**, *2*, 407–408.
22. Bayley, H.; Cronin, B.; Heron, A.; Holden, M.A.; Hwang, W.L.; Syeda, R.; Thompson, J.; Wallace, M. Droplet interface bilayers. *Mol. Biosyst.* **2008**, *4*, 1191.
23. Leptihn, S.; Castell, O.K.; Cronin, B.; Lee, E.-H.; Gross, L.C.M.; Marshall, D.P.; Thompson, J.R.; Holden, M.; Wallace, M.I. Constructing droplet interface bilayers from the contact of aqueous droplets in oil. *Nat. Protoc.* **2013**, *8*, 1048–1057.
24. Thutupalli, S.; Fleury, J.B.; Steinberger, A.; Herminghaus, S.; Seemann, R. Why can artificial membranes be fabricated so rapidly in microfluidics? *Chem. Commun.* **2013**, *49*, 1443–1445.
25. Taylor, G.J.; Venkatesan, G.A.; Collier, C.P.; Sarles, S.A. Direct in situ measurement of specific capacitance, monolayer tension, and bilayer tension in a droplet interface bilayer. *Soft Matter* **2015**, *11*, 7592–7605.
26. Freeman, E.C.; Najem, J.S.; Sukharev, S.; Philen, M.K.; Leo, D.J. The mechanoelectrical response of droplet interface bilayer membranes. *Soft Matter* **2016**, *12*, 3021–3031.
27. Barriga, H.M.G.; Booth, P.; Haylock, S.; Bazin, R.; Templer, R.H.; Ces, O. Droplet interface bilayer reconstitution and activity measurement of the mechanosensitive channel of large conductance from Escherichia coli. *J. R. Soc. Interface* **2014**, *11*.
28. Hwang, W.L.; Chen, M.; Cronin, B.; Holden, M.A.; Bayley, H. Asymmetric droplet interface bilayers. *J. Am. Chem. Soc.* **2008**, *130*, 5878–5879.
29. Taylor, G.; Nguyen, M.A.; Koner, S.; Freeman, E.; Collier, C.P.; Sarles, S.A. Electrophysiological interrogation of asymmetric droplet interface bilayers reveals surface-bound alamethicin induces lipid flip-flop. *Biochim. Biophys. Acta - Biomembr.* **2019**, *1861*, 335–343.
30. Syeda, R.; Holden, M.A.; Hwang, W.L.; Bayley, H. Screening Blockers Against a Potassium Channel with a Droplet Interface Bilayer Array. *J. Am. Chem. Soc.* **2008**, *130*, 15543–15548.
31. Booth, M.J.; Restrepo Schild, V.; Box, S.J.; Bayley, H. Light-patterning of synthetic tissues with single droplet resolution. *Sci. Rep.* **2017**, *7*, 1–10.
32. Huang, J.; Lein, M.; Gunderson, C.; Holden, M. a Direct Quantitation of Peptide-Mediated Protein Transport across a Droplet-Interface Bilayer. *J. Am. Chem. Soc.* **2011**, *133*, 15818–15821.
33. Lein, M.; Huang, J.; Holden, M.A. Robust reagent addition and perfusion strategies for droplet-interface bilayers. *Lab Chip* **2013**, *13*, 2749–2753.
34. Taylor, G.J.; Sarles, S.A. Heating-enabled formation of droplet interface bilayers using escherichia coli total lipid extract. *Langmuir* **2015**, *31*, 325–337.
35. Danial, J.S.H.; Cronin, B.; Mallik, C.; Walllace, M.I. On demand modulation of lipid composition in an individual bilayer. *Soft Matter* **2017**, *13*, 1788–1793.
36. Iwamoto, M.; Oiki, S. Constitutive boost of a K+ channel via inherent bilayer tension and a unique tension-dependent modality. *Proc. Natl. Acad. Sci.* **2018**, *115*, 13117–13122.
37. de Wit, G.; Danial, J.S.H.; Kukura, P.; Wallace, M.I. Dynamic label-free imaging of lipid

nanodomains. *Proc. Natl. Acad. Sci.* **2015**, *112*, 12299 LP-12303.

38. Rojko, N.; Cronin, B.; Danial, J.S.H.; Baker, M.A.B.; Anderluh, G.; Wallace, M.I. Imaging the Lipid-Phase-Dependent Pore Formation of Equinatoxin II in Droplet Interface Bilayers. *Biophys. J.* **2014**, *106*, 1630–1637.
39. Boreyko, J.B.; Mruetusatorn, P.; Sarles, S.A.; Retterer, S.T.; Collier, C.P. Evaporation-induced buckling and fission of microscale droplet interface bilayers. *J. Am. Chem. Soc.* **2013**, *135*, 5545–5548.
40. Mruetusatorn, P.; Boreyko, J.B.; Venkatesan, G.A.; Sarles, S.A.; Hayes, D.G.; Collier, C.P. Dynamic morphologies of microscale droplet interface bilayers. *Soft Matter* **2014**, *10*, 2530–2538.
41. Heron, A.J.; Thompson, J.R.; Cronin, B.; Bayley, H.; Wallace, M.I. Simultaneous Measurement of Ionic Current and Fluorescence from Single Protein Pores. *J. Am. Chem. Soc.* **2009**, *131*, 1652–1653.
42. Sengel, J.T.; Wallace, M.I. Imaging the dynamics of individual electropores. *Proc. Natl. Acad. Sci.* **2016**, *113*, 5281–5286.
43. Leptihn, S.; Thompson, J.R.; Ellory, J.C.; Tucker, S.J.; Wallace, M.I. In vitro reconstitution of eukaryotic ion channels using droplet interface bilayers. *J. Am. Chem. Soc.* **2011**, *133*, 9370–9375.
44. Heron, A.J.; Thompson, J.R.; Mason, A.E.; Wallace, M.I. Direct detection of membrane channels from gels using water-in-oil droplet bilayers. *J. Am. Chem. Soc.* **2007**, *129*, 16042–16047.
45. Fischer, A.; Holden, M.A.; Pentelute, B.L.; Collier, R.J. Ultrasensitive detection of protein translocated through toxin pores in droplet-interface bilayers. *Proc. Natl. Acad. Sci.* **2011**, *108*, 16577–16581.
46. Najem, J.S.; Dunlap, M.D.; Rowe, I.D.; Freeman, E.C.; Grant, J.W.; Sukharev, S.; Leo, D.J. Activation of bacterial channel MscL in mechanically stimulated droplet interface bilayers. *Sci. Rep.* **2015**, *5*, 1–11.
47. Gross, L.C.M.; Heron, A.J.; Baca, S.C.; Wallace, M.I. Determining Membrane Capacitance by Dynamic Control of Droplet Interface Bilayer Area. *Langmuir* **2011**, *27*, 14335–14342.
48. Gross, L.C.M.; Castell, O.K.; Wallace, M.I. Dynamic and Reversible Control of 2D Membrane Protein Concentration in a Droplet Interface Bilayer. *Nano Lett.* **2011**, *11*, 3324–3328.
49. Najem, J.S.; Freeman, E.C.; Yasmann, A.; Sukharev, S.; Leo, D.J. Mechanics of Droplet Interface Bilayer "Unzipping" Defines the Bandwidth for the Mechanotransduction Response of Reconstituted MscL. *Adv. Mater. Interfaces* **2017**, *4*.
50. Rosholm, K.R.; Baker, M.A.B.; Ridone, P.; Nakayama, Y.; Rohde, P.R.; Cuello, L.G.; Lee, L.K.; Martinac, B. Activation of the mechanosensitive ion channel MscL by mechanical stimulation of supported Droplet-Hydrogel bilayers. *Sci. Rep.* **2017**, *7*, 1–10.
51. Coste, B.; Xiao, B.; Santos, J.S.; Syeda, R.; Grandl, J.; Spencer, S.; Kim, S.E.; Schmidt, M.; Mathur, J.; Dubin, A.E.; et al. Piezos are pore-forming subunits of mechanically actived channels. *Nature* **2012**, *483*, 176–181.
52. Booth, M.J.; Restrepo Schild, V.; Downs, F.G.; Bayley, H. Functional aqueous droplet networks.

Mol. Biosyst. **2017**, *13*, 1658–1691.

53. Elani, Y.; Ces, O.; Friddin, M.; Law, R. V.; Brooks, N.J.; Seddon, J.M.; Trantidou, T. Engineering Compartmentalized Biomimetic Micro- and Nanocontainers. *ACS Nano* **2017**, *11*, 6549–6565.
54. Thutupalli, S.; Herminghaus, S.; Seemann, R. Bilayer membranes in micro-fluidics: From gel emulsions to soft functional devices. *Soft Matter* **2011**, *7*, 1312–1320.
55. Maglia, G.; Heron, A.J.; Hwang, W.L.; Holden, M.A.; Mikhailova, E.; Li, Q.; Cheley, S.; Bayley, H. Droplet networks with incorporated protein diodes show collective properties. *Nat. Nanotechnol.* **2009**, *4*, 437–440.
56. Villar, G.; Heron, A.J.; Bayley, H. Formation of droplet networks that function in aqueous environments. *Nat. Nanotechnol.* **2011**, *6*, 803–808.
57. Villar, G.; Graham, A.D.; Bayley, H. A tissue-like printed material. *Science* **2013**, *340*, 48–52.
58. Ahrberg, C.D.; Manz, A.; Chung, B.G. Polymerase chain reaction in microfluidic devices. *Lab Chip* **2016**, *16*, 3866–3884.
59. Murphy, T.W.; Zhang, Q.; Naler, L.B.; Ma, S.; Lu, C. Recent advances in the use of microfluidic technologies for single cell analysis. *Analyst* **2018**, *143*, 60–80.
60. Li, L.; Ismagilov, R.F. Protein Crystallization Using Microfluidic Technologies Based on Valves, Droplets, and SlipChip. *Annu. Rev. Biophys.* **2010**, *39*, 139–158.
61. Squires, T.M.; Quake, S.R. Microfluidics: Fluid physics at the nanoliter scale. *Rev. Mod. Phys.* **2005**, *77*, 977–1026.
62. Song, H.; Chen, D.L.; Ismagilov, R.F. Reactions in Droplets in Microfluidic Channels. *Angew. Chemie Int. Ed.* **2006**, *45*, 7336–7356.
63. Casadevall i Solvas, X.; deMello, A. Droplet microfluidics: recent developments and future applications. *Chem. Commun.* **2011**, *47*, 1936–1942.
64. Balagaddé, F.K.; You, L.; Hansen, C.L.; Arnold, F.H.; Quake, S.R. Long-Term Monitoring of Bacteria Undergoing Programmed Population Control in a Microchemostat. *Science* **2005**, *309*, 137 LP-140.
65. Regehr, K.J.; Domenech, M.; Koepsel, J.T.; Carver, K.C.; Ellison-Zelski, S.J.; Murphy, W.L.; Schuler, L.A.; Alarid, E.T.; Beebe, D.J. Biological implications of polydimethylsiloxane-based microfluidic cell culture. *Lab Chip* **2009**, *9*, 2132–2139.
66. Thorsen, T.; Roberts, R.W.; Arnold, F.H.; Quake, S.R. Dynamic Pattern Formation in a Vesicle-Generating Microfluidic Device. *Phys. Rev. Lett.* **2001**, *86*, 4163–4166.
67. Anna, S.L.; Bontoux, N.; Stone, H.A. Formation of dispersions using “flow focusing” in microchannels. *Appl. Phys. Lett.* **2003**, *82*, 364–366.
68. Umbanhowar, P.B.; Prasad, V.; Weitz, D.A. Monodisperse Emulsion Generation via Drop Break Off in a Coflowing Stream. *Langmuir* **2000**, *16*, 347–351.
69. Utada, A.S.; Lorenceau, E.; Link, D.R.; Kaplan, P.D.; Stone, H.A.; Weitz, D.A. Monodisperse Double Emulsions Generated from a Microcapillary Device. *Science* **2005**, *308*, 537 LP-541.
70. Sugiura, S.; Nakajima, M.; Iwamoto, S.; Seki, M. Interfacial Tension Driven Monodispersed Droplet Formation from Microfabricated Channel Array. *Langmuir* **2001**, *17*, 5562–5566.

71. Opalski, A.S.; Kaminski, T.S.; Garstecki, P. Droplet Microfluidics as a Tool for the Generation of Granular Matters and Functional Emulsions. *KONA Powder Part. J.* **2018**, 1–22.
72. Yadavali, S.; Jeong, H.-H.; Lee, D.; Issadore, D. Silicon and glass very large scale microfluidic droplet integration for terascale generation of polymer microparticles. *Nat. Commun.* **2018**, *9*, 1222.
73. Agresti, J.J.; Antipov, E.; Abate, A.R.; Ahn, K.; Rowat, A.C.; Baret, J.-C.; Marquez, M.; Klibanov, A.M.; Griffiths, A.D.; Weitz, D.A. Ultrahigh-throughput screening in drop-based microfluidics for directed evolution. *Proc. Natl. Acad. Sci.* **2010**, *107*, 4004 LP-4009.
74. Pekin, D.; Skhiri, Y.; Baret, J.-C.; Le Corre, D.; Mazutis, L.; Ben Salem, C.; Millot, F.; El Harrak, A.; Hutchison, J.B.; Larson, J.W.; et al. Quantitative and sensitive detection of rare mutations using droplet-based microfluidics. *Lab Chip* **2011**, *11*, 2156–2166.
75. Frenz, L.; Blank, K.; Brouzes, E.; Griffiths, A.D. Reliable microfluidic on-chip incubation of droplets in delay-lines. *Lab Chip* **2009**, *9*, 1344–1348.
76. Schmitz, C.H.J.; Rowat, A.C.; Köster, S.; Weitz, D.A. Dropspots: a picoliter array in a microfluidic device. *Lab Chip* **2009**, *9*, 44–49.
77. Huebner, A.; Bratton, D.; Whyte, G.; Yang, M.; deMello, A.J.; Abell, C.; Hollfelder, F. Static microdroplet arrays: a microfluidic device for droplet trapping, incubation and release for enzymatic and cell-based assays. *Lab Chip* **2009**, *9*, 692–698.
78. Bai, Y.; He, X.; Liu, D.; Patil, S.N.; Bratton, D.; Huebner, A.; Hollfelder, F.; Abell, C.; Huck, W.T.S. A double droplet trap system for studying mass transport across a droplet-droplet interface. *Lab Chip* **2010**, *10*, 1281–1285.
79. Toprakcioglu, Z.; Challa, P.K.; Levin, A.; Knowles, T.P.J. Observation of molecular self-assembly events in massively parallel microdroplet arrays. *Lab Chip* **2018**, *18*, 3303–3309.
80. Brouzes, E.; Medkova, M.; Savenelli, N.; Marran, D.; Twardowski, M.; Hutchison, J.B.; Rothberg, J.M.; Link, D.R.; Perrimon, N.; Samuels, M.L. Droplet microfluidic technology for single-cell high-throughput screening. *Proc. Natl. Acad. Sci.* **2009**, *106*, 14195 LP-14200.
81. Baret, J.-C.; Miller, O.J.; Taly, V.; Ryckelynck, M.; El-Harrak, A.; Frenz, L.; Rick, C.; Samuels, M.L.; Hutchison, J.B.; Agresti, J.J.; et al. Fluorescence-activated droplet sorting (FADS): efficient microfluidic cell sorting based on enzymatic activity. *Lab Chip* **2009**, *9*, 1850–1858.
82. Churski, K.; Kaminski, T.S.; Jakiela, S.; Kamysz, W.; Baranska-Rybak, W.; Weibel, D.B.; Garstecki, P. Rapid screening of antibiotic toxicity in an automated microdroplet system. *Lab Chip* **2012**, *12*, 1629–1637.
83. Dolega, M.E.; Jakiela, S.; Razew, M.; Rakszewska, A.; Cybulski, O.; Garstecki, P. Iterative operations on microdroplets and continuous monitoring of processes within them; determination of solubility diagrams of proteins. *Lab Chip* **2012**, *12*, 4022–4025.
84. Makulska, S.; Jakiela, S.; Garstecki, P. A micro-rheological method for determination of blood type. *Lab Chip* **2013**, *13*, 2796–2801.
85. Kant, K.; Abalde-Cela, S. Surface-Enhanced Raman Scattering Spectroscopy and Microfluidics: Towards Ultrasensitive Label-Free Sensing. *Biosensors* 2018, *8*, 62.
86. Chen, D.; Du, W.; Liu, Y.; Liu, W.; Kuznetsov, A.; Mendez, F.E.; Philipson, L.H.; Ismagilov,

R.F. The chemistrode: A droplet-based microfluidic device for stimulation and recording with high temporal, spatial, and chemical resolution. *Proc. Natl. Acad. Sci.* **2008**, *105*, 16843 LP-16848.

87. Fidalgo, L.M.; Whyte, G.; Ruotolo, B.T.; Benesch, J.L.P.; Stengel, F.; Abell, C.; Robinson, C.V.; Huck, W.T.S. Coupling Microdroplet Microreactors with Mass Spectrometry: Reading the Contents of Single Droplets Online. *Angew. Chemie Int. Ed.* **2009**, *48*, 3665–3668.
88. Smith, C.A.; Li, X.; Mize, T.H.; Sharpe, T.D.; Graziani, E.I.; Abell, C.; Huck, W.T.S. Sensitive, High Throughput Detection of Proteins in Individual, Surfactant-Stabilized Picoliter Droplets Using Nanoelectrospray Ionization Mass Spectrometry. *Anal. Chem.* **2013**, *85*, 3812–3816.
89. Gu, S.; Lu, Y.; Ding, Y.; Li, L.; Song, H.; Wang, J.; Wu, Q. A droplet-based microfluidic electrochemical sensor using platinum-black microelectrode and its application in high sensitive glucose sensing. *Biosens. Bioelectron.* **2014**, *55*, 106–112.
90. Baroud, C.N.; Robert de Saint Vincent, M.; Delville, J.-P. An optical toolbox for total control of droplet microfluidics. *Lab Chip* **2007**, *7*, 1029–1033.
91. Franke, T.; Braunmüller, S.; Schmid, L.; Wixforth, A.; Weitz, D.A. Surface acoustic wave actuated cell sorting (SAWACS). *Lab Chip* **2010**, *10*, 789–794.
92. Abate, A.R.; Agresti, J.J.; Weitz, D.A. Microfluidic sorting with high-speed single-layer membrane valves. *Appl. Phys. Lett.* **2010**, *96*, 203509.
93. Mazutis, L.; Griffiths, A.D. Preparation of monodisperse emulsions by hydrodynamic size fractionation. *Appl. Phys. Lett.* **2009**, *95*, 204103.
94. Hatch, A.C.; Patel, A.; Beer, N.R.; Lee, A.P. Passive droplet sorting using viscoelastic flow focusing. *Lab Chip* **2013**, *13*, 1308–1315.
95. Niu, X.; Gielen, F.; Edel, J.B.; deMello, A.J. A microdroplet dilutor for high-throughput screening. *Nat. Chem.* **2011**, *3*, 437.
96. Sun, M.; Vanapalli, S.A. Generation of Chemical Concentration Gradients in Mobile Droplet Arrays via Fragmentation of Long Immiscible Diluting Plugs. *Anal. Chem.* **2013**, *85*, 2044–2048.
97. Bremond, N.; Thiam, A.R.; Bibette, J. Decompressing emulsion droplets favors coalescence. *Phys. Rev. Lett.* **2008**, *100*, 1–4.
98. Link, D.R.; Anna, S.L.; Weitz, D.A.; Stone, H.A. Geometrically Mediated Breakup of Drops in Microfluidic Devices. *Phys. Rev. Lett.* **2004**, *92*, 54503.
99. Korczyk, P.M.; Derzsi, L.; Jakieła, S.; Garstecki, P. Microfluidic traps for hard-wired operations on droplets. *Lab Chip* **2013**, *13*, 4096–4102.
100. Narayanamurthy, V.; Nagarajan, S.; Firus Khan, A.Y.; Samsuri, F.; Sridhar, T.M. Microfluidic hydrodynamic trapping for single cell analysis: mechanisms, methods and applications. *Anal. Methods* **2017**, *9*, 3751–3772.
101. Bai, Y.; He, X.; Liu, D.; Patil, S.N.; Bratton, D.; Huebner, A.; Hollfelder, F.; Abell, C.; Huck, W.T.S. A double droplet trap system for studying mass transport across a droplet-droplet interface. *Lab Chip* **2010**, *10*, 1281–1285.
102. Derzsi, L.; Kaminski, T.S.; Garstecki, P. Antibiograms in five pipetting steps: Precise dilution assays in sub-microliter volumes with a conventional pipette. *Lab Chip* **2016**, *16*, 893–901.

103. Dangla, R.; Gallaire, F.; Baroud, C.N. Microchannel deformations due to solvent-induced PDMS swelling. *Lab Chip* **2010**, *10*, 2972–2978.
104. Kawano, R.; Osaki, T.; Sasaki, H.; Takeuchi, S. A polymer-based nanopore-integrated microfluidic device for generating stable bilayer lipid membranes. *Small* **2010**, *6*, 2100–2104.
105. Stimberg, V.C.; Bomer, J.G.; Van Uitert, I.; Van Den Berg, A.; Le Gac, S. High yield, reproducible and quasi-automated bilayer formation in a microfluidic format. *Small* **2013**, *9*, 1076–1085.
106. Shoji, K.; Kawano, R. Microfluidic Formation of Double-Stacked Planar Bilayer Lipid Membranes by Controlling the Water-Oil Interface. *Micromachines* **2018**, *9*, 253.
107. Suzuki, H.; Tabata, K.; Kato-Yamada, Y.; Noji, H.; Takeuchi, S. Planar lipid bilayer reconstitution with a micro-fluidic system. *Lab Chip* **2004**, *4*, 502.
108. Le Pioufle, B.; Suzuki, H.; Tabata, K. V.; Noji, H.; Takeuchi, S. Lipid bilayer microarray for parallel recording of transmembrane ion currents. *Anal. Chem.* **2008**, *80*, 328–332.
109. Suzuki, H.; Pioufle, B.L.; Takeuhci, S. Ninety-six-well planar lipid bilayer chip for ion channel recording Fabricated by hybrid stereolithography. *Biomed. Microdevices* **2009**, *11*, 17–22.
110. Osaki, T.; Suzuki, H.; Le Pioufle, B.; Takeuchi, S. Multichannel simultaneous measurements of single-molecule translocation in α-hemolysin nanopore array. *Anal. Chem.* **2009**, *81*, 9866–9870.
111. Ota, S.; Suzuki, H.; Takeuchi, S. Microfluidic lipid membrane formation on microchamber arrays. *Lab Chip* **2011**, *11*, 2485–2487.
112. Kusters, I.; Van Oijen, A.M.; Driessen, A.J.M. Membrane-on-a-chip: Microstructured silicon/silicon-dioxide chips for high-throughput screening of membrane transport and viral membrane fusion. *ACS Nano* **2014**, *8*, 3380–3392.
113. Urban, M.; Kleefen, A.; Mukherjee, N.; Seelheim, P.; Windschiegl, B.; Vor der Brüggen, M.; Tampé, R.; Koçer, A. Highly Parallel Transport Recordings on a Membrane-on-Nanopore Chip at Single Molecule Resolution. *Nano Lett.* **2014**, *14*, 1674–1680.
114. Watanabe, R.; Soga, N.; Yamanaka, T.; Noji, H. High-throughput formation of lipid bilayer membrane arrays with an asymmetric lipid composition. *Sci. Rep.* **2014**, *4*, 1–6.
115. Watanabe, R.; Soga, N.; Fujita, D.; Tabata, K. V.; Yamauchi, L.; Asanuma, D.; Hyeon Kim, S.; Kamiya, M.; Urano, Y.; Suga, H.; et al. Arrayed lipid bilayer chambers allow single-molecule analysis of membrane transporter activity. *Nat. Commun.* **2014**, *5*, 1–8.
116. Baaken, G.; Sondermann, M.; Schlemmer, C.; Rühe, J.; Behrends, J.C. Planar microelectrode-cavity array for high-resolution and parallel electrical recording of membrane ionic currents. *Lab Chip* **2008**, *8*, 938–944.
117. Baaken, G.; Ankri, N.; Schuler, A.-K.; Rühe, J.; Behrends, J.C. Nanopore-Based Single-Molecule Mass Spectrometry on a Lipid Membrane Microarray. *ACS Nano* **2011**, *5*, 8080–8088.
118. Funakoshi, K.; Suzuki, H.; Takeuchi, S. Lipid Bilayer Formation by Contacting Monolayers in a Microfluidic Device for Membrane Protein Analysis. *Anal. Chem.* **2006**, *78*, 8169–8174.
119. Zagnoni, M.; Sandison, M.E.; Marius, P.; Morgan, H. Bilayer lipid membranes from falling droplets. *Anal. Bioanal. Chem.* **2009**, *393*, 1601–1605.
120. Poulos, J.L.; Portonovo, S.A.; Bang, H.; Schmidt, J.J. Automatable lipid bilayer formation and

ion channel measurement using sessile droplets. *J. Phys. Condens. Matter* **2010**, *22*.

121. Thapliyal, T.; Poulos, J.L.; Schmidt, J.J. Automated lipid bilayer and ion channel measurement platform. *Biosens. Bioelectron.* **2011**, *26*, 2651–2654.
122. El-Arabi, A.M.; Salazar, C.S.; Schmidt, J.J. Ion channel drug potency assay with an artificial bilayer chip. *Lab Chip* **2012**, *12*, 2409–2413.
123. Saha, S.C.; Powl, A.M.; Wallace, B.A.; de Planque, M.R.R.; Morgan, H. Screening ion-channel ligand interactions with passive pumping in a microfluidic bilayer lipid membrane chip. *Biomicrofluidics* **2015**, *9*.
124. Acharya, S.A.; Portman, A.; Salazar, C.S.; Schmidt, J.J. Hydrogel-stabilized droplet bilayers for high speed solution exchange. *Sci. Rep.* **2013**, *3*.
125. Lu, B.; Kocharyan, G.; Schmidt, J.J. Lipid bilayer arrays: Cyclically formed and measured. *Biotechnol. J.* **2014**, *9*, 446–451.
126. Tsuji, Y.; Kawano, R.; Osaki, T.; Kamiya, K.; Miki, N.; Takeuchi, S. Droplet Split-and-Contact Method for High-Throughput Transmembrane Electrical Recording. *Anal. Chem.* **2013**, *85*, 10913–10919.
127. Barlow, N.E.; Bolognesi, G.; Flemming, A.J.; Brooks, N.J.; Barter, L.M.C.; Ces, O. Multiplexed droplet Interface bilayer formation. *Lab Chip* **2016**, *16*, 4653–4657.
128. Nguyen, M.A.; Srijanto, B.; Collier, C.P.; Retterer, S.T.; Sarles, S.A. Hydrodynamic trapping for rapid assembly and: In situ electrical characterization of droplet interface bilayer arrays. *Lab Chip* **2016**, *16*, 3576–3588.
129. Tonooka, T.; Sato, K.; Osaki, T.; Kawano, R.; Takeuchi, S. Lipid bilayers on a picoliter microdroplet array for rapid fluorescence detection of membrane transport. *Small* **2014**, *10*, 3275–3282.
130. Stanley, C.E.; Elvira, K.S.; Niu, X.Z.; Gee, A.D.; Ces, O.; Edel, J.B.; Demello, A.J. A microfluidic approach for high-throughput droplet interface bilayer (DIB) formation. *Chem. Commun.* **2010**, *46*, 1620–1622.
131. Elani, Y.; Demello, A.J.; Niu, X.; Ces, O. Novel technologies for the formation of 2-D and 3-D droplet interface bilayer networks. *Lab Chip* **2012**, *12*, 3514–3520.
132. Elani, Y.; Solvas, X.C.I.; Edel, J.B.; Law, R. V.; Ces, O. Microfluidic generation of encapsulated droplet interface bilayer networks (multisomes) and their use as cell-like reactors. *Chem. Commun.* **2016**, *52*, 5961–5964.
133. Walsh, E.; Feuerborn, A.; Cook, P.R. Formation of droplet interface bilayers in a Teflon tube. *Sci. Rep.* **2016**, *6*, 1–9.
134. Nisisako, T.; Portonovo, S.A.; Schmidt, J.J. Microfluidic passive permeability assay using nanoliter droplet interface lipid bilayers. *Analyst* **2013**, *138*, 6793–6800.
135. King, P.H.; Jones, G.; Morgan, H.; De Planque, M.R.R.; Zauner, K.P. Interdroplet bilayer arrays in millifluidic droplet traps from 3D-printed moulds. *Lab Chip* **2014**, *14*, 722–729.
136. Schlicht, B.; Zagnoni, M. Droplet-interface-bilayer assays in microfluidic passive networks. *Sci. Rep.* **2015**, *5*, 1–8.
137. Kang, X.F.; Cheley, S.; Rice-Ficht, A.C.; Bayley, H. A storable encapsulated bilayer chip

containing a single protein nanopore. *J. Am. Chem. Soc.* **2007**, *129*, 4701–4705.

138. Jeon, T.J.; Poulos, J.L.; Schmidt, J.J. Long-term storable and shippable lipid bilayer membrane platform. *Lab Chip* **2008**, *8*, 1742–1744.
139. Jung, S.H.; Choi, S.; Kim, Y.R.; Jeon, T.J. Storable droplet interface lipid bilayers for cell-free ion channel studies. *Bioprocess Biosyst. Eng.* **2012**, *35*, 241–246.
140. Sarles, S.A.; Leo, D.J. Regulated attachment method for reconstituting lipid bilayers of prescribed size within flexible substrates. *Anal. Chem.* **2010**, *82*, 959–966.
141. Bayoumi, M.; Bayley, H.; Maglia, G.; Sapra, K.T. Multi-compartment encapsulation of communicating droplets and droplet networks in hydrogel as a model for artificial cells. *Sci. Rep.* **2017**, *7*, 1–11.
142. Baxani, D.K.; Morgan, A.J.L.; Jamieson, W.D.; Allender, C.J.; Barrow, D.A.; Castell, O.K. Bilayer Networks within a Hydrogel Shell: A Robust Chassis for Artificial Cells and a Platform for Membrane Studies. *Angew. Chemie Int. Ed.* **2016**, *55*, 14240–14245.
143. Venkatesan, G.A.; Sarles, S.A. Droplet immobilization within a polymeric organogel improves lipid bilayer durability and portability. *Lab Chip* **2016**, *16*, 2116–2125.
144. Challita, E.J.; Najem, J.S.; Monroe, R.; Leo, D.J.; Freeman, E.C. Encapsulating networks of droplet interface bilayers in a thermoreversible organogel. *Sci. Rep.* **2018**, *8*, 1–11.
145. Aghdaei, S.; Sandison, M.E.; Zagnoni, M.; Green, N.G.; Morgan, H. Formation of artificial lipid bilayers using droplet dielectrophoresis. *Lab Chip* **2008**, *8*, 1617–1620.
146. Poulos, J.L.; Nelson, W.C.; Jeon, T.J.; Kim, C.J.; Schmidt, J.J. Electrowetting on dielectric-based microfluidics for integrated lipid bilayer formation and measurement. *Appl. Phys. Lett.* **2009**, *95*, 95–97.
147. Dixit, S.S.; Kim, H.; Vasilyev, A.; Eid, A.; Faris, G.W. Light-driven formation and rupture of droplet bilayers. *Langmuir* **2010**, *26*, 6193–6200.
148. Friddin, M.S.; Bolognesi, G.; Elani, Y.; Brooks, N.J.; Law, R. V.; Seddon, J.M.; Neil, M.A.A.; Ces, O. Optically assembled droplet interface bilayer (OptiDIB) networks from cell-sized microdroplets. *Soft Matter* **2016**, *12*, 7731–7734.
149. Cheley, S.; Gu, L.-Q.; Bayley, H. Stochastic Sensing of Nanomolar Inositol 1,4,5-Trisphosphate with an Engineered Pore. *Chem. Biol.* **2002**, *9*, 829–838.
150. Churski, K.; Nowacki, M.; Korczyk, P.M.; Garstecki, P. Simple modular systems for generation of droplets on demand. *Lab Chip* **2013**, *13*, 3689–3697.
151. Jakiela, S.; Kaminski, T.S.; Cybulski, O.; Weibel, D.B.; Garstecki, P. Bacterial Growth and Adaptation in Microdroplet Chemostats. *Angew. Chemie Int. Ed.* **2013**, *52*, 8908–8911.
152. Zagnoni, M.; Cooper, J.M. A microdroplet-based shift register. *Lab Chip* **2010**, *10*, 3069–3073.
153. Churski, K.; Korczyk, P.; Garstecki, P. High-throughput automated droplet microfluidic system for screening of reaction conditions. *Lab Chip* **2010**, *10*, 816–818.
154. Kaminski, T.S.; Jakiela, S.; Czekalska, M.A.; Postek, W.; Garstecki, P. Automated generation of libraries of nL droplets. *Lab Chip* **2012**, *12*, 3995–4002.
155. Mantri, S.; Tanuj Sapra, K.; Cheley, S.; Sharp, T.H.; Bayley, H. An engineered dimeric protein pore that spans adjacent lipid bilayers. *Nat. Commun.* **2013**, *4*, 1725.

156. Castell, O.K.; Berridge, J.; Wallace, M.I. Quantification of membrane protein inhibition by optical ion flux in a droplet interface bilayer array. *Angew. Chemie - Int. Ed.* **2012**, *51*, 3134–3138.
157. https://www.nanion.de/en/products/orbit-16.html accessed 31/03/2019.
158. Holden, M.A.; Needham, D.; Bayley, H. Functional bionetworks from nanoliter water droplets. *J. Am. Chem. Soc.* **2007**, *129*, 8650–8655.
159. Yasuga, H.; Kawano, R.; Takinoue, M.; Tsuji, Y.; Osaki, T.; Kamiya, K.; Miki, N.; Takeuchi, S. Logic Gate Operation by DNA Translocation through Biological Nanopores. *PLoS One* **2016**, *11*, e0149667.
160. Carreras, P.; Elani, Y.; Law, R. V.; Brooks, N.J.; Seddon, J.M.; Ces, O. A microfluidic platform for size-dependent generation of droplet interface bilayer networks on rails. *Biomicrofluidics* **2015**, *9*, 0–7.
161. http://www.oxsybio.com accessed 31/03/2019.
162. Holden, M.A. *Building interconnected membrane networks*; Elsevier Ltd, 2015; Vol. 128;.
163. Elani, Y.; Gee, A.; Law, R. V.; Ces, O. Engineering multi-compartment vesicle networks. *Chem. Sci.* **2013**, *4*, 3332–3338.
164. Tomoike, F.; Tonooka, T.; Osaki, T.; Takeuchi, S. Repetitive formation of optically-observable planar lipid bilayers by rotating chambers on a microaperture. *Lab Chip* **2016**, *16*, 2423–2426.
165. Kawano, R.; Tsuji, Y.; Sato, K.; Osaki, T.; Kamiya, K.; Hirano, M.; Ide, T.; Miki, N.; Takeuchi, S. Automated Parallel Recordings of Topologically Identified Single Ion Channels. *Sci. Rep.* **2013**, *3*, 1995.
166. Hwang, W.L.; Holden, M.A.; White, S.; Bayley, H. Electrical behavior of droplet interface bilayer networks: Experimental analysis and modeling. *J. Am. Chem. Soc.* **2007**, *129*, 11854–11864.
167. Krishnan, S.; Ziegler, D.; Arnaut, V.; Martin, T.G.; Kapsner, K.; Henneberg, K.; Bausch, A.R.; Dietz, H.; Simmel, F.C. Molecular transport through large-diameter DNA nanopores. *Nat. Commun.* **2016**, *7*, 12787.
168. Burns, J.R.; Göpfrich, K.; Wood, J.W.; Thacker, V. V; Stulz, E.; Keyser, U.F.; Howorka, S. Lipid-Bilayer-Spanning DNA Nanopores with a Bifunctional Porphyrin Anchor. *Angew. Chemie Int. Ed.* **2013**, *52*, 12069–12072.
169. Damean, N.; Olguin, L.F.; Hollfelder, F.; Abell, C.; Huck, W.T.S. Simultaneous measurement of reactions in microdroplets filled by concentration gradients. *Lab Chip* **2009**, *9*, 1707–1713.
170. Cai, L.-F.; Zhu, Y.; Du, G.-S.; Fang, Q. Droplet-Based Microfluidic Flow Injection System with Large-Scale Concentration Gradient by a Single Nanoliter-Scale Injection for Enzyme Inhibition Assay. *Anal. Chem.* **2012**, *84*, 446–452.
171. Miller, O.J.; Harrak, A. El; Mangeat, T.; Baret, J.-C.; Frenz, L.; Debs, B. El; Mayot, E.; Samuels, M.L.; Rooney, E.K.; Dieu, P.; et al. High-resolution dose–response screening using droplet-based microfluidics. *Proc. Natl. Acad. Sci.* **2012**, *109*, 378 LP-383.
172. Ahn, K.; Agresti, J.; Chong, H.; Marquez, M.; Weitz, D.A. Electrocoalescence of drops synchronized by size-dependent flow in microfluidic channels. *Appl. Phys. Lett.* **2006**, *88*,

264105.

173. Szymborski, T.; Korczyk, P.M.; Hołyst, R.; Garstecki, P. Ionic polarization of liquid-liquid interfaces; dynamic control of the rate of electro-coalescence. *Appl. Phys. Lett.* **2011**, *99*, 94101.

174. Gielen, F.; van Vliet, L.; Koprowski, B.T.; Devenish, S.R.A.; Fischlechner, M.; Edel, J.B.; Niu, X.; deMello, A.J.; Hollfelder, F. A Fully Unsupervised Compartment-on-Demand Platform for Precise Nanoliter Assays of Time-Dependent Steady-State Enzyme Kinetics and Inhibition. *Anal. Chem.* **2013**, *85*, 4761–4769.

175. Postek, W.; Kaminski, T.S.; Garstecki, P. A precise and accurate microfluidic droplet dilutor. *Analyst* **2017**, *142*, 2901–2911.

176. Rani, S.A.; Pitts, B.; Stewart, P.S. Rapid Diffusion of Fluorescent Tracers into Staphylococcus epidermidis Biofilms Visualized by Time Lapse Microscopy. *Antimicrob. Agents Chemother.* **2005**, *49*, 728 LP-732.

177. Mills, R. Self-diffusion in normal and heavy water in the range 1-45.deg. *J. Phys. Chem.* **1973**, *77*, 685–688.

178. Guzowski, J.; Korczyk, P.M.; Jakiela, S.; Garstecki, P. Automated high-throughput generation of droplets. *Lab Chip* **2011**, *11*, 3593–3595.

179. Begolo, S.; Zhukov, D. V; Selck, D.A.; Li, L.; Ismagilov, R.F. The pumping lid: investigating multi-material 3D printing for equipment-free, programmable generation of positive and negative pressures for microfluidic applications. *Lab Chip* **2014**, *14*, 4616–4628.

180. Leung, K.; Zahn, H.; Leaver, T.; Konwar, K.M.; Hanson, N.W.; Pagé, A.P.; Lo, C.-C.; Chain, P.S.; Hallam, S.J.; Hansen, C.L. A programmable droplet-based microfluidic device applied to multiparameter analysis of single microbes and microbial communities. *Proc. Natl. Acad. Sci.* **2012**, *109*, 7665 LP-7670.

181. Mazutis, L.; Griffiths, A.D. Selective droplet coalescence using microfluidic systems. *Lab Chip* **2012**, *12*, 1800–1806.

182. Lee, M.; Collins, J.W.; Aubrecht, D.M.; Sperling, R.A.; Solomon, L.; Ha, J.-W.; Yi, G.-R.; Weitz, D.A.; Manoharan, V.N. Synchronized reinjection and coalescence of droplets in microfluidics. *Lab Chip* **2014**, *14*, 509–513.

183. Lee, U.N.; Su, X.; Guckenberger, D.J.; Dostie, A.M.; Zhang, T.; Berthier, E.; Theberge, A.B. Fundamentals of rapid injection molding for microfluidic cell-based assays. *Lab Chip* **2018**, *18*, 496–504.

184. Kan, C.W.; Rivnak, A.J.; Campbell, T.G.; Piech, T.; Rissin, D.M.; Mösl, M.; Peterça, A.; Niederberger, H.-P.; Minnehan, K.A.; Patel, P.P.; et al. Isolation and detection of single molecules on paramagnetic beads using sequential fluid flows in microfabricated polymer array assemblies. *Lab Chip* **2012**, *12*, 977–985.

185. Hindson, B.J.; Ness, K.D.; Masquelier, D.A.; Belgrader, P.; Heredia, N.J.; Makarewicz, A.J.; Bright, I.J.; Lucero, M.Y.; Hiddessen, A.L.; Legler, T.C.; et al. High-Throughput Droplet Digital PCR System for Absolute Quantitation of DNA Copy Number. *Anal. Chem.* **2011**, *83*, 8604–8610.

186. Walker, G.M.; Beebe, D.J. A passive pumping method for microfluidic devices. *Lab Chip* **2002**,

2, 131–134.

187. Simon, M.J.; Kang, W.H.; Gao, S.; Banta, S.; Iii, B.M. TAT is not capable of transcellular delivery across an intact endothelial monolayer in vitro. *Ann. Biomed. Eng.* **2011**, *39*, 394–401.

188. Jeong, H.-H.; Lee, B.; Jin, S.H.; Jeong, S.-G.; Lee, C.-S. A highly addressable static droplet array enabling digital control of a single droplet at pico-volume resolution. *Lab Chip* **2016**, *16*, 1698–1707.

189. https://nanoporetech.com accessed 31/03/2019.

190. Galvagnion, C. The Role of Lipids Interacting with α-Synuclein in the Pathogenesis of Parkinson's Disease. *J. Parkinsons. Dis.* **2017**, *7*, 433–450.